Interface Modification of Carbon Fiber Reinforced SiC Composites Prepared by Polycarbosilane Impregnation-Pyrolysis Method

December 1998
Graduate School of Marine Science and
Engineering, Nagasaki University

Guobin Zheng

Contents

Chapter 1 General Introduction

1.1 Current state of researches on fiber/ceramic composites

Continuous fiber reinforced ceramic matrix (fiber/ceramic) composites have been studied and developed in the past three decades as structural materials for potential applications in high temperature environments. These applications include components of vehicle and aircraft. engines, internal combustion engine parts, wear-resistant materials, heat exchanger, etc. In these service conditions, properties of high strength, high toughness, low density, low thermal expansion and high-temperature stability are required [1-4]. Although monolithic ceramics offer many of these properties, they generally lack toughness, damage-tolerance and thermal shock resistance. Many efforts have been made to improve toughness of ceramic materials by applying phase-transformation and microcracks toughening, particle dispersion, or reinforcement of short or long fibers. Works on these fields have shown that the highest toughness is obtained by continuous fiber reinforced ceramic composites [5,6].

Fiber/ceramic composite is regarded as one of key materials in the next century and will be used in various industrial fields of transportation, electric power generation, oil industry, chemical process industry, industrial process equipment, environmental equipment, etc. However, there are many unsolved problems such as high cost and unreliability of the composites. The high cost of fiber/ceramic composites is due to the complicated fabrication process. The unreliability is due to the complicated relations among the mechanical properties of fiber/ceramic composites, microstructure, fabrication conditions and service conditions. The properties of fiber/ceramic composites depend on the properties of their components, such as elastic modulus, strength and strength distribution of the reinforcing fibers, elastic modulus and strength of the matrix, and the interface characteristics between the fibers and the matrix [7,8]. The interface characteristics depend on structures of the fibers and the matrix, and also on the processing conditions.

At present, many fiber/ceramic systems of CF/SiC, SiC/SiC, CF/Si_3N_4, SiC/ Si_3N_4, C/C and fiber/oxide composites are under development.

1.2 Potential of carbon fiber reinforced SiC composites

The properties of a fiber/ceramic composite are firstly dependent upon the reinforcing fiber. There are many kinds of commercially available ceramic fibers, such as carbon fibers, SiC fibers (Nicalon, Hi-Nicalon), Si-C-Ti-O (Tyranno) fibers, Si_3N_4 fibers, BN fibers, and Al_2O_3 fibers. Since fiber/ceramic composites are fabricated and used at high temperatures, it is important for the reinforcing fibers to stand such severe conditions for long time. The most widely used fibers in fiber/ceramic composites are carbon fibers and SiC-based fibers. Among these fibers, carbon fibers exhibit unparalleled thermal resistance. They can retain their strength at temperatures as high as 2500℃ [9], while SiC-based fibers (including Nicalon, Hi-Nicalon, Tyranno fiber) exhibit much lower thermal stability than carbon fibers [10,11].

Carbon fibers possess excellent properties, such as low density, high strength and high stiffness, thus they are widely used for various composite materials. Various types of carbon fibers from high strength ones to high modulus ones, which depend on their precursors and processing conditions, are available. The main precursors utilized for production of carbon fibers are polyacrylonitrile (PAN) and pitch. In order to fabricate carbon fibers, precursor fibers of PAN or pitch are stabilized by oxidation in air at about 200-300°C, and then carbonized at temperatures between 1000°C-1500°C. If they are further heat-treated at temperatures above 2000°C, graphite fibers are obtained with higher graphitization degree and higher elastic modulus [9]. Because of the variety of carbon fibers, they provide many choices for designing a fiber/ceramic system. The variety in characteristics of carbon fibers also gives rise to the complexity of the carbon fiber reinforced composites, since a minor change in the structure of carbon fibers may lead to a significant influence on the properties of the composites in some cases. The main shortcoming of carbon fibers is that they are gasified at temperatures above 500°C in environments containing oxygen. However, this shortcoming can be overcome by protective surface coatings [12].

Silicon carbide is one of the best refractory materials. SiC ceramic materials possess good high-temperature strength, low thermal expansion coefficient, good heat

conductivity, as well as abrasion resistance and low density. Moreover, they possess good chemical stabilility for oxidation by formation of a protective glassy or partially crystallized SiO_2 layer on the surface of the material.

Therefore, carbon fiber reinforced SiC (CF/SiC) composites are widely studied and developed as structural materials for applications at high temperature [13]. However, Many problems have to be solved yet before the composites acquire wide applications These problems include high cost of production and complicated fracture behavior which depends on interface, fiber architecture, etc. Particularly, fabrication processes have a great effect on the properties and cost of the composites.

1.3 Fabrication methods of CF/SiC composites

There are several methods to fabricate CF/SiC composites, such as chemical vapor infiltration (CVI) [14-21], reaction-bonding, slurry infiltration followed by hot-pressing, and preceramic polymer impregnation. The characteristics of the methods are described as follows.

1. 3. 1 CVI method

CVI technique was originally developed by researchers in the United States, Germany and France. CVI technique was evolved from CVD that was generally used to obtain uniform coatings or films with tailored composition by decomposition of gaseous compounds. CVI technique is used to form entire ceramic matrices by infiltrating fiber preforms with low molecular gaseous organometallic compounds, e.g. CH_3SiCl_3, and depositing ceramic on fiber surfaces. With the densification of the composites, pores in the composites become so small that it is difficult to let gaseous species diffuse through these thin pores. In order to obtain composites with high density, the deposition temperature must be very low (for example, 1100°C for SiC matrix) to decrease the reaction rate, so that the entire deposition rate is controlled by chemical reaction, rather than the diffusion of gas species [22]. As a result, it takes extremely long time, ranged from several weeks to several months, to obtain composites with an acceptable density. The advantages of CVI technique are described as follows.

- The processing temperature is low so that damage to reinforcing fibers is minimal.

- The process can be applied to complex shape with near-net-shape feature.
- The process can be employed to fabrication of matrix with tailored compositions or functional-gradient structures by co-deposition, for example, co-deposition of C-SiC [18], SiC-other carbides [4].

The main shortage of the CVI technique is long processing time of several hundred hours, thus causing high cost and low productivity. To overcome these problems, temperature-gradient and force-flow CVI techniques were developed to shorten the processing time [14, 15]. However, these techniques are limited in complex shapes.

1.3.2 Slurry infiltration and hot-pressing method

Sintering is a conventional method to fabricate monolithic ceramic materials. If sintering is employed for fabrication of fiber/ceramic, pressure is required since the existence of fibers inhibits the shrinkage of ceramic and thus it is difficult to obtain dense materials. With this method, carbon fibers are first impregnated with a slurry consisting of SiC powder, organic solvent and binder, and they are then dried and laminated to form prepregs. Finally, the prepregs are hot-pressed at high. temperatures [23-26]. The advantages of the slurry technique include short processing time, low cost and high productivity.

The main drawbacks of this method are described as follows.

- The fibers are severely damaged at high mechanical pressure and high temperatures.
- The process is only applied to simple shapes with one or two dimensional reinforcing fibers

In fact, this technique is more likely used for fabrication of glass or glass-ceramic matrix than for ceramic-matrix composite, because the glass or glass-ceramic can be easily consolidated at low temperature about 1000℃ with viscous flow [27].

1.3.3 Polymer impregnation pyrolysis (PIP) method

Since silicon polymers can be decomposed to inorganic materials, many preceramic polymers were developed as precursors of ceramic fibers of SiC, Si_3N_4, BN, Al_2O_3, etc.

The polymer precursor of SiC, polycarbosilane, was first successfully synthesized by Yajima [28, 29], then it was commercialized to fabricate SiC fibers by Nippon Carbon Company. Since then, various preceramic polymers were developed such as polysilazilane and polycarbosilane. Some polymers are shown in Table 1-1 [30]. These polymers can be melted at low temperature from room temperature to about 300°C or dissolved in organic solvents. Therefore, they exhibit excellent shaping feature, and are used not only to fabricate fibers [31-33], but also to prepare coatings or films [34].

With PIP method, the polymers in liquid or solution are infiltrated into fiber preforms, and then the preform is pyrolysed to form matrix [35-38]. The polymers decompose to inorganic materials at low temperatures about 1200°C [33, 39]. As decomposition of polymer causes significant volume shrinkage, several cycles of infiltration is required to obtain an appreciably dense composite.

Table 1 Some polymer precursors and their pyrolytic products. [30]

Polymer precursor	Temperature(°C)/atmosphere	Products
Polymethylsilane	950/Ar	SiC
Polymethyvinylsilane	1000/Ar	SiC
Polycarbosilane	1400/N_2	SiC
Polytitanocarbosilane	1300/ N_2	$SiC_xO_yTi_z$
Polysilaethylene	1000/ N_2	SiC
Polyhydridosilazane	1200/ N_2	Si_3N_4
Polymethyisilazane	800/NH_3	Si_3N_4
Polyvinylsilazane	1200/ N_2	SiC_xN_y/C
Polyvinylphenylsilazane	1000/ N_2	Si_3N_4
Polycyclomethylsilazane	1000/ Ar	Si_3N_4/SiC
Polyboronsiliconimide	1250/ NH_3	BN/ Si_3N_4
Polymethylsiloxane	1000/He	SiO_xC_y
Polyphenylsilsesquioxane	1400/Ar	SiC_xO_y

The advantages of this technique are as follows:

- It can be applied to complex shape with near-net-shape feature.

- The processing temperature is low so that damage to fibers was minimul.
- The microstructure and composition can be tailored by mixing polymers.
- The processing time is shorter than that of the currently-used CVI technique.

The shortages are as follows.

- Polymer-derived matrix is generally sub-stable. It may degrade at temperatures above 1500℃.
- It takes relatively long time for processing in comparison with slurry technique

Some efforts have been made to shorten the processing time. For example, fiber preform was first impregnated with slurry of ceramic powder, polymer and solvent, to decrease impregnation cycles. They were further densified by polymer impregnation/pyrolysis process [40,41].

Greil also developed a technique called active-filler densification. Fibers were infiltrated by slurry consisting of active filler powders and solvent and pressed to form a prepreg. The prepreg was heat-treated so that active filler reacted with polymer or atmosphere to cause volume expansion to counteract the volume shrinkage due to decomposition of polymer [30]. Greil calculated the possible volume expansion of various active fillers. Among these active fillers, boron reacted with nitrogen, causing very large volume expansion [42].

1.3.4 Reaction bonding method

Although reaction-bonded silicon carbide ceramics exhibit moderate strength and toughness in comparison with the hot-pressed materials, they can be fabricated at relatively low temperatures. The reaction bonding method used to fabricate CF/SiC has two routes. The first route is that carbon fibers are impregnated with resin or pitch and silicon powder, then heat-treated at about 1400℃, near the melting point of silicon, to allow the reaction between carbon and silicon [43-46]. The composites made by this route possess a high porosity. The other route is that porous C/C composites are infiltrated with melt silicon and the reaction between carbon and silicon results in SiC. The problem of this route is incomplete reaction between carbon and silicon [13].

Table 1-2 Some properties of fiber/SiC composites.

Composites	Preparation method	Fiber configuration	Vf %	Porosity %	Bending strength MPa	Toughness MPa m1/2	Tensile strength MPa	Ref
Cf/SiC	CVI		42-47	10,15	450-500		270-300	3
SiC/SiC	CVI		40-50	10,15	500-600		250-300	3
SiCf/SiC	CVI	cloth	41.6	10	437			14
CF/SiC	PCS+slurry	3D	36		185	7.3		26
CF/Si3N4	PSZ	3D	36	8	260	6		26
CF/CSiC	CVI	cloth			139-266		192-216	19
SiCf/SiC	CVI	2D	35	15	326	16.2		18
SiCf/SiC	CVI	3D	32	11	692	29.8		18
CF/SiC	CVI	1D			700			13
SiCf/SiC	CVI	2D			350			13
Si-C-Ti-O/SiC	PCS	3D	39	17	410	11.5		35
SiCf/SiC	PCS+SiCw	2D	33	27	300			38
C/SiC	SiCp+PCS	1D	40		350			40
CF/SiC	reactionbonding	1D	55	>20	530			43-45
Hi-Ni/SiC	Slurry	1D			900	30		24
CF/SiC	Slurry	1D	56		950	30		25
CF/SiC	Slurry	1D	32		420	13		23

1.3.5 Properties of the CF/SiC composites

Different fabrication methods lead to the different microstructure of matrix, resulting to different properties of the composites. Up to now, the highest mechanical properties are achieved with the composites fabricated by CVI method. Table 1-2 lists some properties of fiber/SiC composites fabricated by the above methods. However, the composites fabricated by CVI technique is limited to very special applications and is unlikely to be used in common products because of its high cost. The composites fabricated by polymer impregnation-pyrolysis are expected to gain wide applications.

1.4 Factors influencing the mechanical properties of fiber/SiC composites

1.4.1 Coatings on the fibers

Fiber/ceramic composites can possess high toughness due to the presence of the interface between fiber and matrix, although both the fiber and matrix are completely brittle [47]. Because the interface is so important, many efforts have been made to tailor the interface between fiber and matrix. The most frequently used method to tailor the interface is surface coatings on the fiber, among which coatings of pyrolytic carbon and boron nitride were found to be most effective [15, 16, 48-51]. These coatings decrease the interface bonding, so that the next equation could be satisfied to allow the interface debonding.

$$\Gamma_i \leq (1/4)\Gamma_f \qquad (1\text{-}1)$$

where Γ_i is the debonding energy, Γ_f is the fiber fracture energy [52].

Many researchers have found that the interface failure occurred in the coatings [50]. For a certain fiber/ceramic system, the mechanical properties of the composite are largely controlled by the interface characteristics. The coating made the interface properties more stable, thus resulted in a composite with more stable properties. Hi-Nicalon SiC fibers with C coating or BN coating are provided by Nippon Carbon Co. in aim to the applications in ceramic matrix composites [53]. Naslain *et al* used a multi-layer coating by pulse-CVI technique to increase the toughness of the composites [54]. However, these coating are susceptible to oxidation in high temperatures, it is a severe task to find a coating that can stand high temperature in oxidation environment [55].

Some other coatings like SiC are generally used to inhibit the reactions between fiber and matrix. These coatings are combined with C coating and BN coating to exhibit a more stable interface [56].

The coatings on fibers are generally prepared by CVD, because of the uniformity and easiness of tailoring compositions. The technique is convenient if the composite is prepared by CVI technique. Other methods for coatings include sol-gel and polymer pyrolyse etc, which show poor uniformity in comparison with CVD [57].

It was also reported that in some fiber/ceramic systems, interlayer C between fiber and matrix can be formed during processing of the composites because the reaction in matrix precipitate carbon [58].

1.4.2 Microstructure of fibers

For many fiber/ceramic systems without fiber coatings, the surface properties of fibers directly affect the interface. The surface properties of fibers depend strongly on the structure of the fibers in most cases. In fiber/resin composites where strong interface bonding is required, the surfaces of fibers generally are treated by oxidation to enhance the interface bonding. Weak interface bonding is required in fiber/ceramic composites, as described in eq.(1-1). The interface sliding stresses play a key role in the properties of composites after debonding. The toughness of composites increases with increasing radius of the fibers and decreases with increasing interface sliding stresses [7]. The interface sliding stresses are depended upon the residual thermal stresses and surface roughness of fibers. For most commercial ceramic fibers, there are few chances to modify the structures of the fibers. On the other hand, carbon fibers possess a wide range of structures and properties so that tailoring the interface is possible by selecting adequate carbon fibers for desirable composite.

1.4.3 Microstructure of matrix

Many research efforts are conducted to tailor the microstructure of matrix in C/C composites. There are relatively few reports to discuss the effect of the matrix microstructure change in CF/SiC composites. The composites fabricated by CVI have

been demonstrated to possess better properties than those fabricated by other methods, such as polymer impregnation and reaction-bonding, as stated in 1.3.5. Kim et al reported CF/SiC with multiple layers of C and SiC in the matrix [59]. Liu *et al* reported that the codeposition of C-SiC controlled the structure of the matrix [19]. However, there exist other factors which may have a more significant effect on the properties of the composites, so it is difficult to identify how the structure of a certain matrix affects the properties of the composites. Porosity of the composites and residual stresses are two important factors to affect the properties of the composites. Porosity of the CF/SiC composites ranged from 10% to 20%. It has not been known how the porosity affects the properties of the composites.

1.5 Purpose of the Present Research

Applications of CF/SiC composites are largely dependent on how to obtain high performance composites with low cost. As described in 1.3, all the methods to fabricate CF/SiC have their intrinsic advantages and shortages. The composites prepared by polymer method seems to have potentially high performance and low cost, so this method will be a promising method to fabricate CF/SiC composites for wide applications. The preceramic polymer impregnation/pyrolysis method that is used to fabricate CF/SiC has not been well established, since a new fabrication method results in composites with different microstructure. Especially, the characteristics of the interface between carbon fiber and polymer-derived matrix have not well understood. The first aim of the present study is to investigate the fabrication technique of CF/SiC by polycarbosilane impregnation-pyrolysis method.

In addition, there are various carbon fibers with different structures, and they are expected to have different behavior in composites. The second aim of this research is to understand how the structure of carbon fibers affect the mechanical behavior of CF/SiC composites, using various commercial carbon fibers or the carbon fibers heat-treated at different temperatures.

The interface characteristics between carbon fiber and matrix, which play key roles in the mechanical behavior of the composites, are also dependent upon the microstructure

of the matrix. The third aim of this study is to study how the mechanical properties of composites were affected by controlling the microstructure of the matrix. The methods that are used to control the microstructure of the matrix include heat-treatment, boron or BN addition in matrix.

The outline of this research is as follows.

Chapter 1 is an introduction of the recent researches about the CF/SiC composites and the objectives of this research.

Chapter 2 is devoted to the preparation process of CF/SiC by polycarbosilane impregnation-pyrolysis, the microstructure of the matrix, and effect of different commercial carbon fibers on the properties of the composites. Basic preparation process was established in this chapter, and the different mechanical behavior of composites was discussed here.

Chapter 3 is concerned with the change of the microstructure of the polycarbosilane-derived matrix by heat treatment and its effect on the mechanical behavior of CF/SiC composites.

Chapter 4 is devoted to the change of the structure of PAN-based and pitch-based carbon fibers by heat-treatment at the temperature ranged from 1400°C to 2000°C, and its effect on the interface characteristics and the mechanical behavior of CF/SiC composites.

Chapter 5 is concerned with the effect of boron addition on the mechanical behavior CF/SiC. The oxidation-resistance of CF/SiC with boron addition is also investigated.

Chapter 6 is devoted to the effect of BN addition on the mechanical properties of CF/SiC.

Chapter 7 is the summary of this research.

References

1. J. J. Mecholsky, Ceramic Bulletin, **65**, 315 (1986).
2. J. A. Cornie, Y-T. Chiang, D. R. Uhlmann, A. Mortensen and J. M. Collins, **65**, 293 (1986).
3. M. H. Van de Voodrde and M. R. Nedele, Ceram. Sic. & Eng. **17**, 1 (1996).
4. L. J. Schioler and J.J. Stiglich, Jr., Ceramic Bulletin, **65**, 289 (1986).
5. Gilbert Fantozzi and Christian Olagnon, in "Materials Science and Technology: vol.13 Structure and Properties of Composites" (VCH, Germany, 1993), p. 183.
6. 香川　豊，八田　博志，セラミックス基複合材料，1989
7. A. G. Evans and F.W. Zok, J. Mater. Sci. **29**, 3857 (1994).
8. A. G. Evans and D. B. Marshall, Acta Metall. **37**, 2567 (1989).
9. S. Otani, K. Okuda and S. Matsuda, in "Tanso Seni" (Kindai Hensyu Sya,Japan, 1983) p. 701.
10. G. Chollon, R. Pailler, R. Naslain, F. Laanani, M. Monthioux and P. Olry, J. Mater. Sci. **32**, 327 (1997).
11. M. Shibuya, S. Kajii, and T. Yamamura, J. Ceram. Soc. Japan, **102**, 1022 (1994).
12. M. E. Westwood, J. D. Webster, R. J. Day, F. H. Hayes and R. Taylor, J. Mater. Sci. **31**,1389 (1996).
13. E. Fitzer and R. Gadow, Ceramic Bulletin, **65**, 326 (1986).
14. D. P. Stinton, A. J. Caputo and R. A. Lowden, Ceram. Bullitin, **65**, 347 (1986).
15. D. P. Stinton, T. M. Besmann, and R. A. Lowden, Ceram. Bullitin, **67**, 350 (1988).
16. A. J. Caputo, D. P. Stinton, R. A. Lowden and T. M. Besmann, Ceram. Bullitin. **66**, 368 (1987).
17. F. Lamouroux, X. Bourrat, R.Nasalain and J. Sevely, Carbon, **33,** 1273 (1993).
18. J. M. Yang, W. Lin, C. J. Shin, W. Kai, S. M. Jeng and C.V. Burkland, J. Mater. Sci. **26,** 2954 (1991).
19. W. Liu, Y. Wei and J. Deng, Carbon, **33,** 441 (1995).
20. S. Goujard, L. Vandenbucke and H. Tawil, J. Mater. Sci. **29**, 6212 (1994).
21. A. J. Eckel and R. C. Bradt, J. Am. Ceram. Soc., 72, 455 (1989).
22. M. Wang and C. Laird, J. Mater. Sci. **31**, 2065 (1996).
23. K. Nakano, A. Kamiya, H. Ogawa, and Y. Nishino, J. Ceram. Soc. of Japan, **100**, 472 (1992).
24. A. Kamiya, K. Nakano, N. Terazawa, Y. Nishino and H. Ichikawa, J. Ceram. Soc. of Japan, **103**, 191 (1995).
25. H. Yoshida, N, Miyata, K, Naito, S.Ishikawa and C. Yamagashi, J. Ceram. Soc. of Japan, **102**, 1016 (1994).

26. K. Nakano, A. Kamiya, Y. Nishino, T. Imura, and T-W. Chou, J. Am. Ceram. Soc. **78**, 2811 (1995).
27. I. W. Donald, Key Engineering Materials, **108-110,** 123 (1995).
28. S. Yajima, Y. Hasegawa, K. Okamura and T. Matsuzawa, Nature **273**, 525 (1978).
29. S. Yajima, Am. Ceram. Soc. Bull., **62**, 893 (1983).
30. P. Greil, *J. Am. Ceram. Soc.*, **78,** 835 (1995).
31. Y. Hasegawa, J. Mater. Sci., **24,** 1177 (1989).
32. E. Bouillon, F. Langłais, R. Pailler, R. Naslain, F. Cruege, P.V. Huong, J.C. Sarthou, A. Delpuech, C. Laffon, P. Lagarde, M. Monthioux and A. Oberlin, J. Mater. Sci. **26**, 1333 (1991).
33. Y. Hasegawa, and K. Okamura, J. Mater. Sci., **18**, 3633 (1983).
34. Y. Hasegawa, and K. Okamura, J. Mater. Sci., **21**, 321 (1986).
35. T. Tanaka, N. Tamari, I. Kondoh and M. Iwasa, J. Ceram. Soc. of Japan, **103,** 1 (1995).
36. M. Shibuya, FC Report, **11**, 240 (1993).
37. W. J. Sherwood, C. K. Whitmarsh, and J. M. Jacobs, Ceram. Eng. &.Sci. Proc. **17** (3) 174 (1996).
38. K. Sato, T. Suzuki, O. Funayama, and T. Isoda, J. Ceram. Soc. of Japan, **100,** 444 (1992).
39. M. R. Mucalo, N. B. Milestone, I. C. Vickridge and M. V. Swan, J. Mater. Sci., **29,** 4487 (1994).
40. D. W. Shin and H. Tanaka, J. Am. Ceram. Soc., **77,** 97 (1994).
41. H. Yoshida, N. Miyata, M. Sagawa, S. Ishikawa, K. Naito, N. Enomoto and C. Yamagishi, J. Ceram. Soc. of Japan, **100,** 454 (1992).
42. D. Suttor, T. Erny, and P. Greil, J. Am. Ceram. Soc., **80,**1831 (1997).
43. E. Tani, and K. Shobu, J. Ceram. Soc. of Japan, **103,** 401 (1995).
44. E. Tani, K. Shobu and T. Watanabe, J. Ceram. Soc. of Japan, **100,** 596 (1992).
45. E. Tani, K. Shobu and T. Watanabe, J. Ceram. Soc. of Japan, **102,** 210 (1994).
46. S. Suyama, T. Kameda, N. Amiji, M. Umezawa, and H. Ichikawa, Ceram. Eng. & Sci. **17**, 118 (1996).
47. M. D. Thouless, O. Sbaizero, L. S. Sigl, and A. G. Evans, J. Am. Ceram. Soc., **72,** 525 (1989).
48. G. N. Morscher, J. Am. Ceram. Soc., **80,** 2029 (1997).
49. D. Singh, J. P. Singh, and M. J. Wheeler, J. Am. Ceram. Soc., **79,** 591 (1997).
50. E. Y. Sun, S. R. Nutt and J. J. Brennan, J. Am. Ceram. Soc., **79,** 1521 (1996).
51. P. F. Tortorelli, C. A. Wjayawardhana and L. Riester, Ceram. Eng. & Sci. Proc. **15,**

133 (1994).
52. M. Y. He and J. W. Hutchinson, Int. J. Solids Struct. **25**, 1 (1989).
53. A. Kamiya, K. Nakano, S. Moribe, T. Imura and H. Ichikawa, J. Ceram. Soc. Japan, **102**, 957 (1994).
54. R. Naslain, Ceramic symposium, Nov. 1997, Kurume, Japan.
55. M. Backhaus-Ricoult, and N. Mozdzierz, J. Mater. Sci. **30**, 3487 (1995).
56. D. Dierich, P. W. Martin, K. Nestler, S. Stockel, K. Weise and G. Marx, J. Mater. Sci. **31**, 5979 (1996).
57. M. K. Cinibulk, Ceram. Eng. Sci. Proc. **17**, 241 (1996).
58. M. Y. Cheng, J. M. Battison and T. Mah, J. Mater. Sci., **24**, 3213 (1987).
59. Y-W. Kim, J. G. Lee, M-S Kim, and J-H. Park, J. Mater. Sci. **31**, 335 (1996).

Chapter 2 Preparation of CF/SiC Composites by Polycarbosilane Impregnation-Pyrolysis Method and Effect of Different Types of Carbon Fibers on the Mechanical Properties of the Composites

2. 1 Introduction

The polymer impregnation-pyrolysis method for fabrication of CF/SiC is gaining an increasing attention in recent years because of the balance between the mechanical properties of the composites and fabrication cost of this technique [1]. The polymer method provides the essential features such as applicability to complex shapes and near-net-shape. The preceramic polymer liquid with low viscosity can be obtained by dissolving in organic solvent or melting at elevated temperature, and it can be easily infiltrated into the fiber preform by using vacuum impregnation or pressure impregnation.

Polycarbosilane, as a precursor for SiC, is generally used for fabrication of SiC fiber. The typical structure of polycarbosilane is shown as following [2].

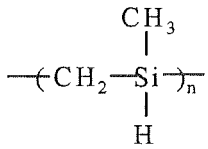

Some polycarbosilane can be melted at about 200-300°C, and some do not completely melt, depending on their structure and molecular weight. Tanaka *et al* reported the fabrication of Tyranno/SiC using molten polycarbosilane [3]. Yoshida *et al* prepared CF/SiC composites using polycarbosilane solution [4]. In these researches, the microstructure of matrix and the infiltration behavior of polycarbosilane were not described.

There are various commercially available carbon fibers from PAN-based high strength carbon fibers to pitch-based high modulus carbon fibers which show very different structures [5]. However, these carbon fibers are produced mainly for resin matrix composites in which strong interfacial bonding is preferred. It can be expected that these carbon fibers may show different behavior in ceramic matrix composites. There are still relatively few reports about the effect of different types of carbon fibers on the

mechanical properties and fracture behavior of CF/SiC prepared from preceramic polymers. In this chapter, the preparation process of CF/SiC by impregnation-pyrolysis of polycarbosilane (PCS) and the effect of different types of carbon fibers on the mechanical properties of CF/SiC composite materials are investigated.

2. 2 Experimental Procedure

2.2.1 Raw materials

Four types of continuous carbon fibers, PAN-based high strength carbon fiber (HSCF), pitch-based high modulus carbon fiber (HMCF) and ultra-high modulus carbon fiber CF50 (E=500 GPa) and CF70 (E=700 GPa), were used as the reinforcements. Some properties of these carbon fibers are shown in Table 2-1. HSCF and HMCF which were fabricated at temperatures below 1500°C had relatively low modulus, while CF50 and CF70 which were fabricated at temperatures above 2000°C showed much higher modulus than the other two types of carbon fibers. They were immersed in acetone to remove the sizing from the surface of fibers before being used for the preparation of the composites.

Table 2-1 Properties of as-received carbon fibers

Types of carbon fibers	Precursors of fibers	Density g/cm^3	Diameter μm	Tensile strength MPa	Tensile Modulus GPa
HSCF	PAN	1.76	7.0	3830	240
HMCF	pitch	1.90	9.8	3350	277
CF50	pitch	2.14	9.4	3950	519
CF70	pitch	2.18	9.4	4200	700

Polycarbosilane (Type-UH, Nippon Carbon Co.) was used as the precursor of the SiC matrix, whose properties are shown in Table 2-2 (data by the maker). It can be directly pyrolysed to ceramic with a yield of about 74% without curing. Behavior of PCS pyrolysis in N_2 was clarified by using thermogravimetry analysis (TGA).

Table 2-2 Properties of polycarbosilane (Type-UH)

Mean molecular	m.p.*	Chemical compositions wt%					SiC yield
weight	°C	Si	C	H	O	N	%
5000	partial ~350	49.4	39.5	8.1	1.35	1.65	74

*only partially melting at about 350°C

2.2.2 Preparation process of CF/SiC composites

The preparation process of CF/SiC is illustrated in Fig. 2-1. The carbon fibers were wound unidirectionally on a metal frame and placed in a metal die. 50wt% PCS toluene solution was poured into the metal die and infiltrated into the fiber preform. The preform infiltrated with PCS was then pressed to remove excess solution. After being dried at 80°C, the prepregs were pyrolysed at 1200°C in N_2 with a heating rate of 5°C/min to 300°C, 1°C/min to 800°C and 5°C/min to 1200°C, holding at 1200°C for 1 hour. The prepregs were then impregnated with 50wt% PCS solution in vacuum, dried at 80°C, and pyrolysed at 1200°C in N_2 with the same heating program as described above. The impregnation-pyrolysis process was repeated for 5-9 cycles to increase the density of the composite samples. The samples after those treatments were named as HSCF/SiC, HMCF/SiC, CF50/SiC and CF70/SiC, respectively. CF50/SiC and CF70/SiC were also prepared through 12 cycles of impregnation/pyrolysis process to obtain a higher density. The sizes of the as-prepared composites were approximately 80mm×37mm×1mm.

2.2.3 Characterization

Apparent densities of the composite samples were measured from their mass and sizes. The volume fractions of fiber (V_f) were measured from SEM photographs of the polished transverse sections of the samples. The values of porosity of the composites were then calculated from the apparent density of the composites, the density of the carbon fiber and the SiC matrix, and V_f according to the following expression,

$$V_p = V_f(d_f/d_c-1)+V_m(d_m/d_c-1) \qquad (2\text{-}1)$$

where V_p is the porosity of the composite, d_f, d_m and d_c are the density of the fiber, the matrix and the composite.

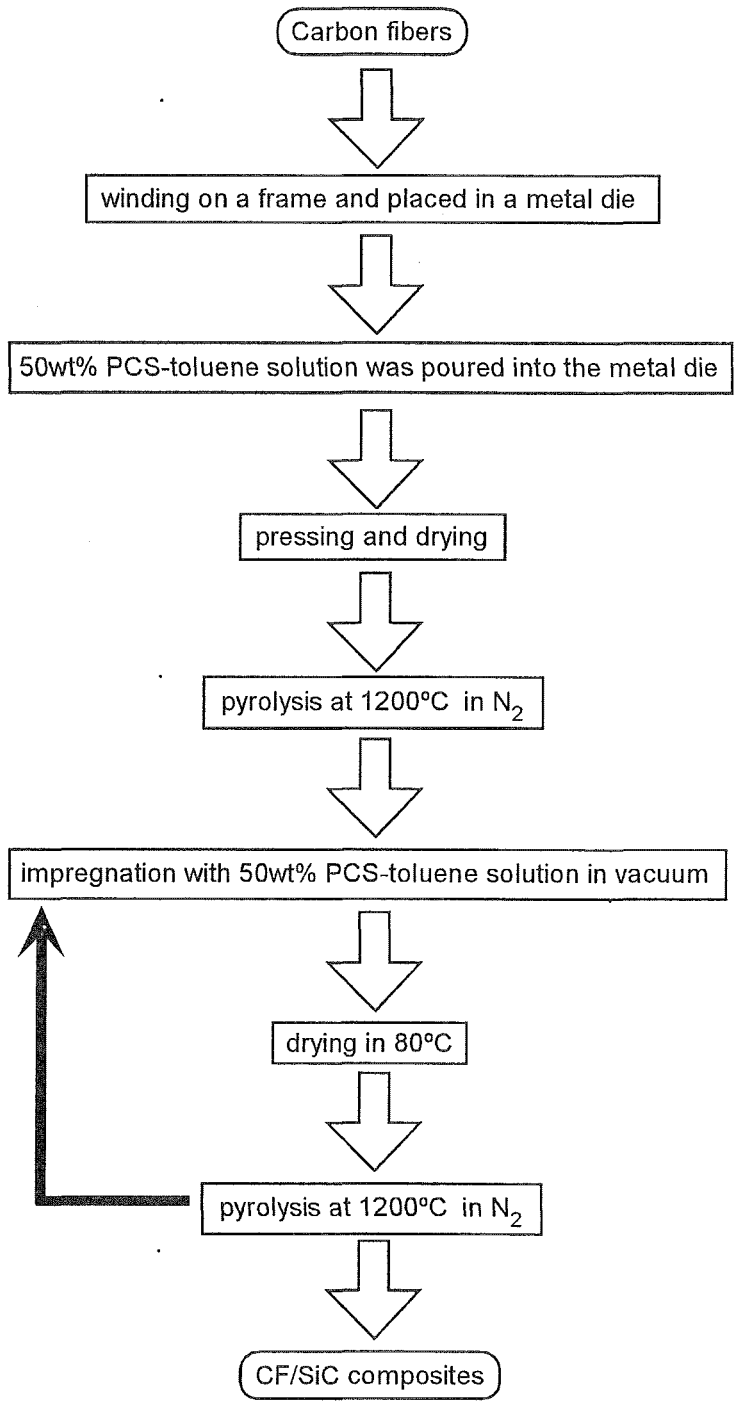

Fig. 2-1 Preparation process of CF/SiC by impregnation-pyrolysis of polycarbosilane.

Four-point flexural strength of the samples was measured with a crosshead speed of 0.5 mm/min, a support span of 30 mm and a loading span of 10 mm. The load-displacement curves were recorded simultaneously by using load cell and laser extensometer during the flexural test. The sizes of samples for bending test were about 3.5 mm in width, 1 mm in thickness and 40 mm in length.

The flexural strength is calculated according to the following equation.

$$\sigma_{UTS} = \frac{3P(L-l)}{2wt^2} \qquad (2\text{-}2)$$

where P is the highest load, L is the support span, l is the loading span, w is the width of the specimen, and t is the thickness of the specimen.

The composite samples were incorporated in resin, and were polished with SiC paper and diamond slurry, and then they were observed by scanning electronic microscopy (SEM). Fracture surfaces of the specimens after flexural test were also observed by SEM. The crystallinity of the PCS-derived SiC was analyzed by X-ray diffraction (XRD).

TEM specimens were prepared by polishing CF/SiC samples with a thickness of 0.5 mm down to 40-50 μm. · Molybdenum meshes with a hole of 1 mm in diameter were then stuck on the two sides of the specimen with epoxy resin to prevent CF/SiC samples from being damaged during ion milling, because the specimens were very low in transverse strength. The specimens were then thinned by ion-milling at an angle of 25° for four hours and then 15° at 5 kV until perforation. The specimens were not rotated during ion-milling, and the direction of ion beam were vertical to the alignment of carbon fiber in CF/SiC specimens, to prevent the matrix from separating as the specimens were thinned. TEM observation was conducted with a JEOL 2010 operated at 200 kV. The matrix was also analyzed by electron diffraction.

2. 3 Results

2.3.1 Pyrolysis behavior of polycarbosilane

Figure 2-2 shows TGA curve of PCS pyrolysed in N_2. It was observed that PCS lost about 6% of its mass between 100-300°C, due to the evaporation of small molecules

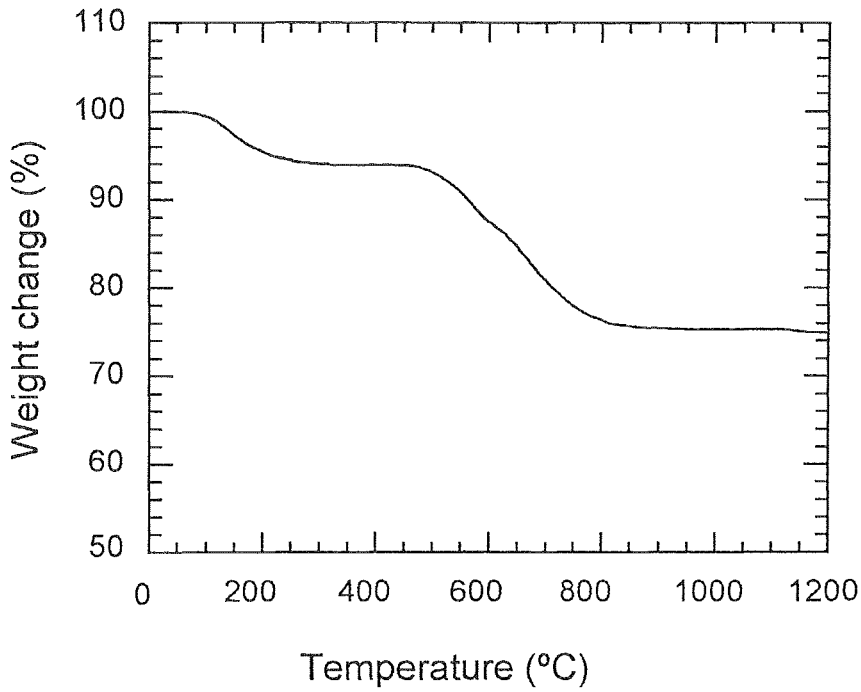

Fig. 2-2 TGA curve of polycarbosilane in N_2.

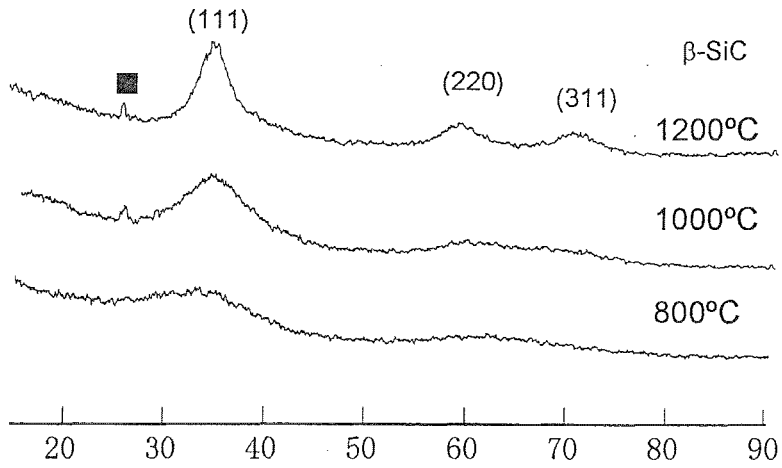

Fig. 2-3 XRD profiles of PCS-derived products pyrolysed at different temperatures.

in PCS. From 300 to 440°C, PCS had almost no change in mass. PCS began to decompose at about 440°C, and the weight decreased rapidly until about 800°C. The mass of PCS residue had almost no change above 800°C. This indicated the decomposition of PCS had almost been finished at 800°C. The ultimate pyrolytic yield at 1200°C was about 76%. The pyrolysis of PCS powders in a tubular furnace showed also about 75% yield, which was similar to the TGA results. Since the decomposition of PCS takes place between 440-800°C, the low heating rate was set in this temperature range when composites were prepared.

XRD profiles of pyrolytic product of PCS at 800°C, 1000°C and 1200°C are shown in Fig. 2-3. The pyrolytic product of PCS at 800°C was completely amorphous, while the product at 1000°C exhibited a broad peak at about 35.6°, which was identified to be (111) peak of β-SiC, and the product at 1200°C exhibited three broad peaks which were identified to be (111), (220) and (311) peaks of β-SiC. The broad peaks indicate that the crystallites of SiC were very small. The L_{111}, crystalline size of SiC obtained at 1200°C, was measured to be 1.95 nm. The peak at 26.6° was probably caused by silica. It still appeared in 1400°C-heat-treated samples. However, it was not detected in the 1600°C-heat-treated samples which showed some weight loss, as stated in the next chapter. These phenomena suggested that there were silica and free carbon in pyrolytic product of PCS, which were also verified by other researchers [2, 6].

2.3.2 Microstructure of CF/SiC composites with impregnation

Figure 2-4 shows the morphology of the CF/SiC after first time impregnation-pyrolysis cycle. Severe shrinkage of the matrix, due to the vaporization of the solvent and the decomposition of PCS, was observed. HMCF appeared to have good bonding with the matrix, while CF70 showed relatively poor bonding with the matrix.

Figure 2-5 shows SEM micrographs of the polished cross surfaces of HSCF/SiC, HMCF/SiC and CF70/SiC samples with 9 cycles impregnation. It was observed that the carbon fibers in HSCF/SiC sample were densely distributed in the matrix, so it had very high V_f value. HMCF/SiC had a relatively low V_f, and CF70/SiC had the lowest V_f among the three composites. The average V_f values of HSCF/SiC, HMCF/SiC and

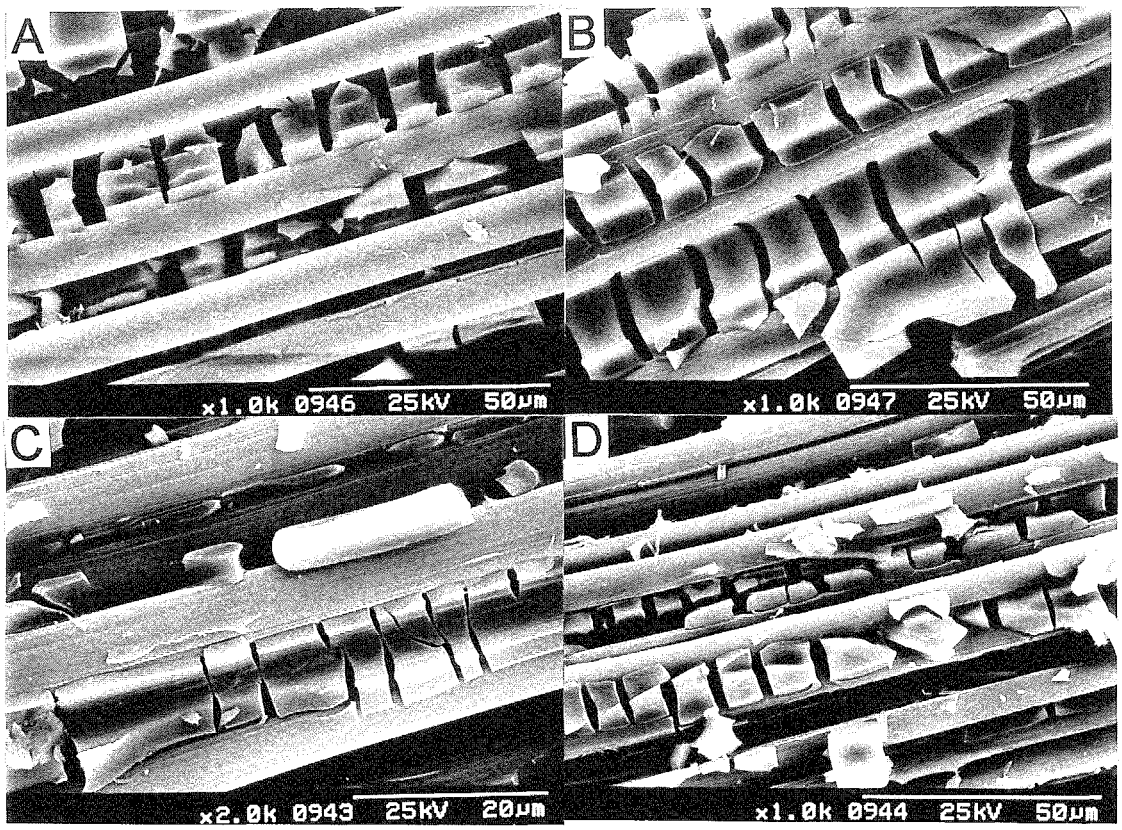

Fig. 2-4 Morphology of HMCF/SiC (A, B) and CF70/SiC (C, D) after first impregnation-pyrolysis process.

CF70/SiC were measured to be 63%, 56% and 42%, respectively. The apparent difference among the values of V_f of these CF/SiC composites were related to the multiple-impregnation process, which will be explained a little later.

Figure 2-6 shows the change of the density and the porosity of HSCF/SiC, HMCF/SiC and CF70/SiC samples with impregnation cycles of polycarbosilane. As being expected, the density of all the composites increased with the increase of the impregnation cycles. It was noted that there were some differences in the increasing trend of density with impregnation cycles among these composites. The density of HSCF/SiC and HMCF/SiC increased up to 7 cycles impregnation, then showed almost no increase. As the composites became dense and their porosity decreased, the pores, especially near the surface of the composites, became small or were filled, it was difficult for PCS to infiltrate further. On the other hand, the density of CF70/SiC

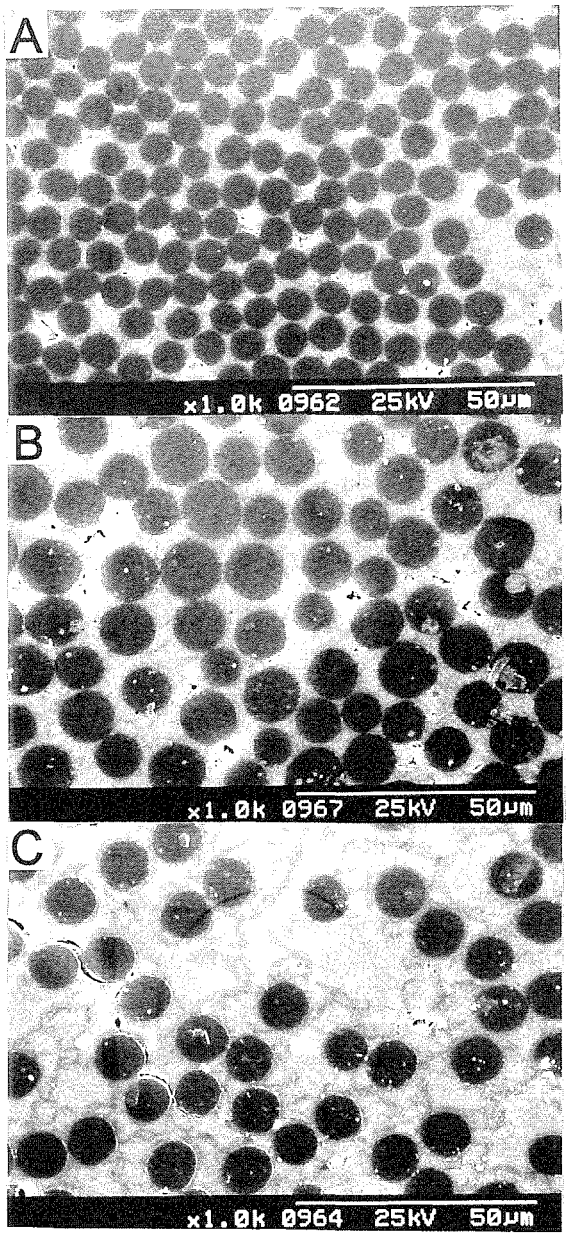

Fig. 2-5 SEM micrographs of polished transverse sections of HSCF/SiC (A), HMCF/SiC (B) and CF70/SiC (C).

increased up to the 9th cycle of impregnation. As known from Fig. 2-5, CF70/SiC had low fiber volume fraction, thus it had higher porosity from beginning than HSCF/SiC and HMCF/SiC. Another reason is involved the impregnation process of PCS, and will be discussed a little later. The values of the final porosity of these composites with 9 impregnation cycles were about 12-13%.

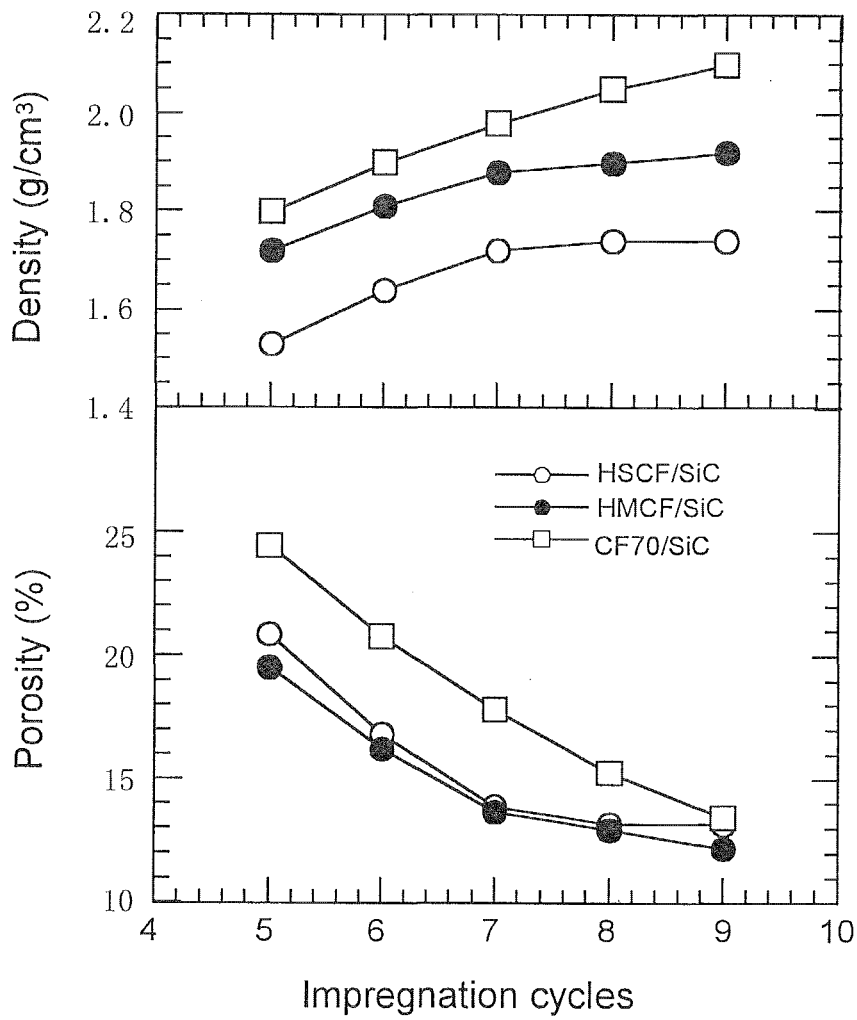

Fig. 2-6. Changes of density and porosity of HSCF/SiC, HMCF/SiC and CF70/SiC with impregnation cycles of polycarbosilane.

2. 3. 3 The mechanical properties of CF/SiC composites

The flexural strengths of the composite samples after more than 5 impregnation cycles were measured. Figure 2-7 shows the change of four-point flexural strength of HSCF/SiC, HMCF/SiC and CF70/SiC samples with impregnation cycles of PCS. As being expected from the density of these composites, the strength of HSCF/SiC and HMCF/SiC samples increased after 5-7 impregnation cycles. After 8-9 impregnation cycles, the strength of HSCF/SiC and HMCF/SiC samples showed almost no increase, because there was no increase in density. On the other hand, the strength of CF70/SiC samples increased steadily up to 9 cycles impregnation, corresponding with the increase of the density in Fig. 2-6.

Fig. 2-8 shows the apparent stress-strain curves of CF70/SiC with 5-9 impregnation cycles and typical apparent stress-strain curves of HSCF/SiC and HMCF/SiC. HSCF/SiC and HMCF/SiC failed in a brittle mode, whereas CF70/SiC exhibited non-brittle failure. When the density of CF70/SiC was low, they failed in a shear way. With the increase of the density, the shear strength increased, resulting in higher flexural strength.

The density of CF70/SiC continued to increase up to 9 cycles impregnation as shown in Fig. 2-6, so CF70/SiC and CF50/SiC were prepared through 12 impregnation-pyrolysis cycles. The mechanical properties of the composites are shown in Table 2-3. The matrix cracking stress was determined from the load at which deviation from linearity in the load-displacement curves occurred. The matrix cracking stresses of HSCF/SiC and HMCF/SiC are not listed in Table 2-3, because these two composites failed in a brittle mode. The ultimate flexural strength was obtained from the peak load. The four kinds of CF/SiC composites in Table 2-3 can be classified into two groups. The first group of HSCF/SiC and HMCF/SiC failed in a brittle mode with flexural strength of 210 MPa and 275 MPa, respectively. The other group of CF50/SiC and CF70/SiC failed in a non-brittle fracture mode with ultimate flexural strength of 624 MPa and 967 MPa, respectively. Figure 2-9 shows the load-displacement behavior of CF50/SiC and CF70/SiC. The fracture behavior of CF50/SiC and CF70/SiC was markedly non-linear.

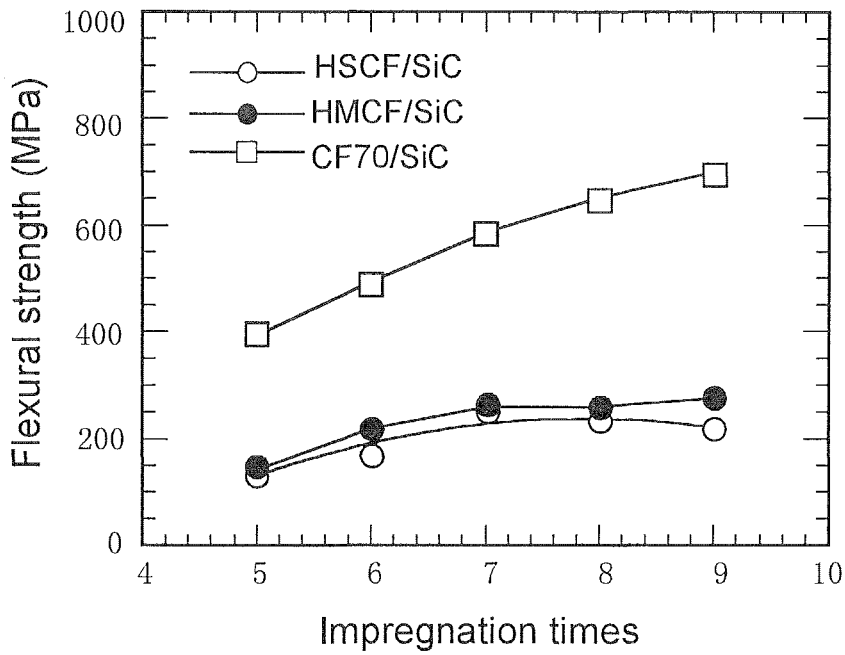

Fig. 2-7. Changes of the values of flexural strength of HSCF/SiC, HMCF/SiC and CF70/SiC samples with impregnation times of polycarbosilane.

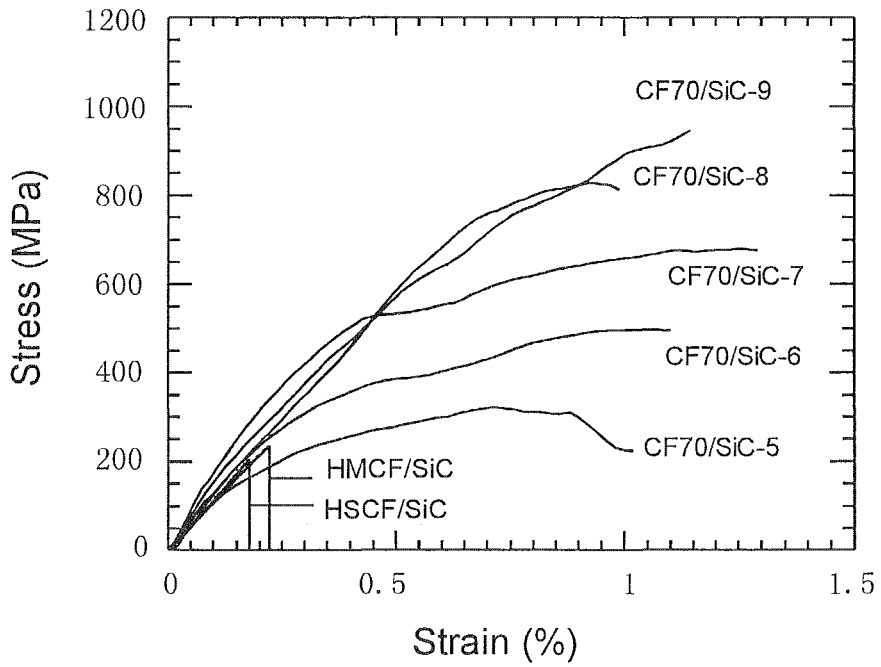

Fig. 2-8. Typical Stress-strain curves of CF70/SiC samples with 5-9 times impregnation of polycarbosilane and typical ones of HSCF/SiC and HMCF/SiC.

Table 2-3 Mechanical properties of the composites

Composites	Apparent density (g/cm^3)	V_f (%)	Total porosity (%)	Matrix cracking stress (MPa)	Flexural strength (MPa)	Modulus (GPa)	Fracture mode
HSCF/SiC	1.74	67	13	–	220±38	105	brittle
HMCF/SiC	1.92	58	12	–	275±51	121	brittle
CF50/SiC	2.20	43	10.2	242±50	624±123	188	non-brittle
CF70/SiC	2.28	33	9.6	268±43	967±62	207	non-brittle

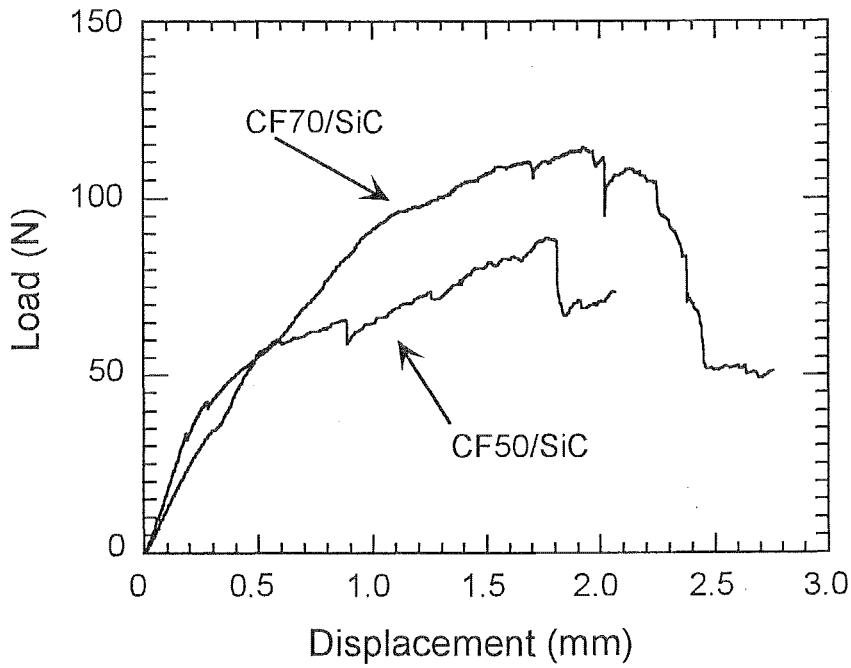

Fig. 2-9 Load-displacement curves CF50/SiC and CF70/SiC in four-point bending test.

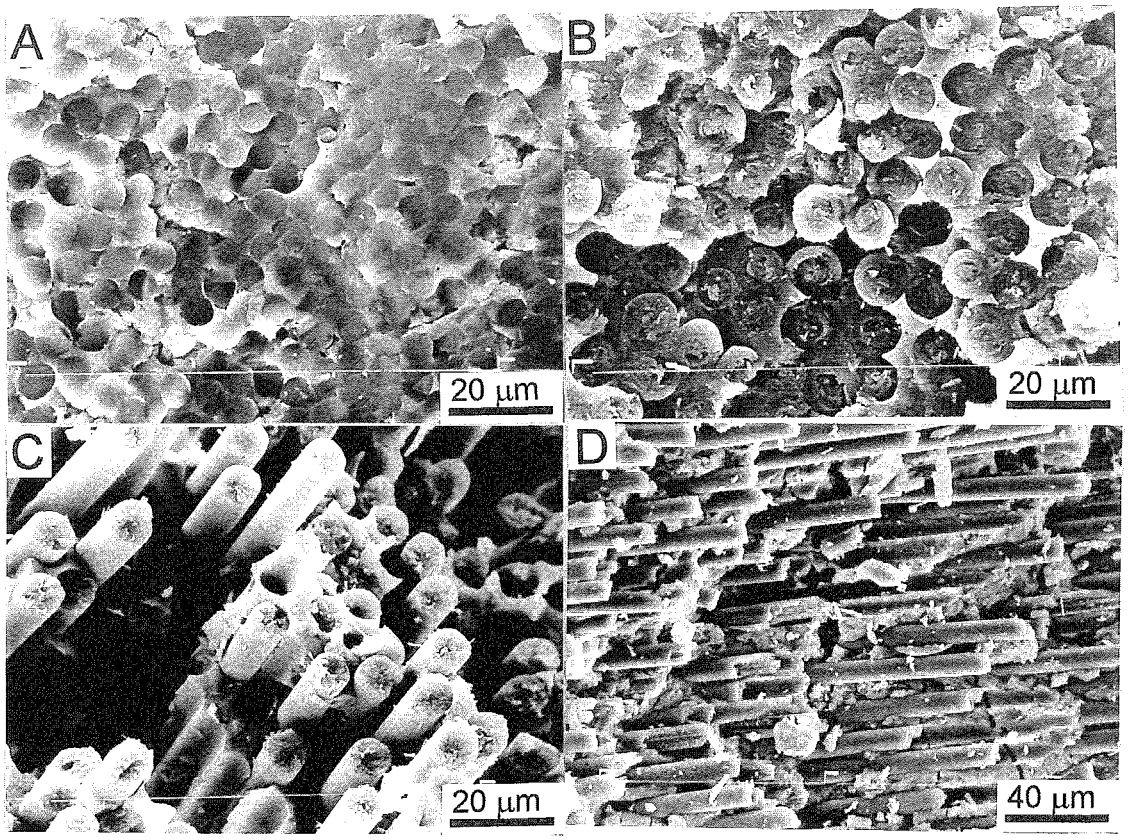

Fig. 2-10 Fracture surfaces of HSCF/SiC (A), HMCF/SiC (B), CF50/SiC (C) and CF70/SiC (D) after bending test.

To elucidate the failure behaviors of the composites, the specimens after the bending tests were observed by SEM. Figure 2-10 shows the fracture surfaces of HSCF/SiC, HMCF/SiC, CF50/SiC and CF70/SiC. Both of HSCF/SiC and HMCF/SiC exhibited flat fracture surfaces with very short fiber pullout. Among them, HSCF/SiC showed a completely flat fracture surface. It has been well demonstrated that these phenomena were caused by strong interfacial bonding between carbon fiber and matrix. On the contrary, the fracture surfaces of CF50/SiC and CF70/SiC showed extensive fiber pullout which was caused by weak interfacial bonding of CF/matrix. It was also observed that there were many matrix cracks normal to the fiber axis direction on the tensile surface of the CF50/SiC and CF70/SiC after bending tests. Figure 2-11 shows the matrix crackings on the surface and inside CF70/SiC. CF50/SiC also exhibited

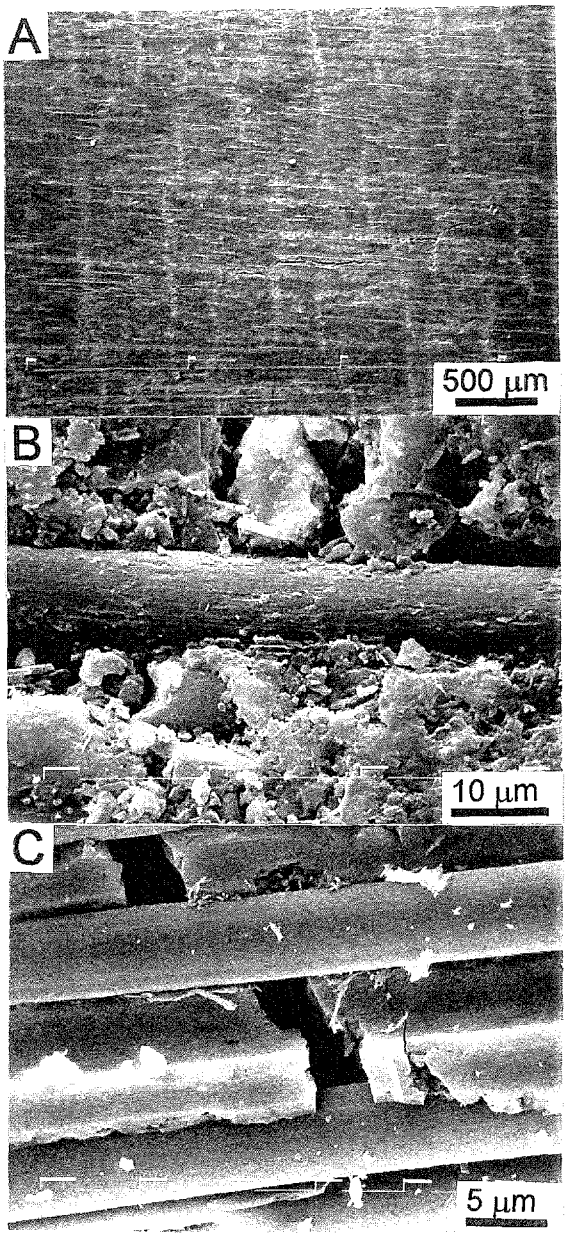

Fig. 2-11 Matrix cracks in CF70/SiC after bending tests. On the surface (A, B) and inside the sample (C).

similar phenomena. Formation of matrix crackings has been also reported on many continuous fiber reinforced ceramic composites with high strength, and the phenomena have been treated theoretically by many researchers [7,8].

The ultimate tensile strength of ceramic matrix composites which exhibited matrix crackings and fiber pullout was deduced theoretically by Curtin [9], as shown by the following formula,

$$\sigma_{UTS} = V_f \sigma_c \left(\frac{2}{m+2}\right)^{1/(m+1)} \left(\frac{m+1}{m+2}\right) \qquad (2\text{-}3)$$

where V_f represents the fiber volume fraction, σ_c is the characteristic strength of fiber, m is the Weibull modulus of fiber strength distribution. The m of CF50 and CF70 were measured to be 3.53 and 4.06, respectively, by testing the mono-filament strength of as-received fibers. Here the ultimate tensile strength values of CF50/SiC and CF70/SiC were estimated approximately, by assuming that σ_c was equal to the average strength of the fibers. The ultimate tensile strengths of CF50/SiC and CF70/SiC were then calculated to be 1176 MPa and 930 MPa, respectively.

It was reported that the flexural strengths are approximately 1.4 times greater than tensile strengths of continuous fiber reinforced ceramic matrix composites [10]. Therefore the predicted ultimate flexural strength of CF50/SiC and CF70/SiC were obtained as 1646 MPa and 1300 MPa, respectively. Compared with the measured values in Table 2-3, it can be noted that the measured flexural strength of CF70/SiC was about 75% of the predicted value. On the other hand, the flexural strength of CF50/SiC was only approximately 38% of the predicted value. The main reason was that CF50/SiC failed in a shear way before tensile failure.

2.4. Discussion

It has been well demonstrated that interfacial properties between fiber and matrix play an important role in properties of ceramic matrix composites. In order to obtain high-performance ceramic matrix composites, weak interface bonding is necessary to resist catastrophic failure through interfacial debonding [11,12]. Interfacial strength can be evaluated by the morphology of the fracture surface, that is, long fiber pullout indicates

weak interfacial strength. The interfacial properties in composites are considered to have close relationships with the surface characteristic of the fibers, microstructure of the matrix and processing conditions of the composites. Since all four kinds of CF/SiC composites were prepared from the same processing conditions, it was reasonable to consider that the differences of interfacial strength in these composites were caused by the difference of the surface characteristics of the carbon fibers.

2.4.1 Interface of carbon fiber/SiC and impregnation mechanism

Two kinds of composites, HMCF/SiC and CF70/SiC, were observed by TEM. The interfaces of CF70/SiC and HMCF/SiC were shown in Fig. 2-12. In the matrix of CF70/SiC, many micropores, which were smaller than 200 nm, were observed (Fig. 2-12A). These pores were formed due to the decomposition of PCS, and they were mainly distributed in the boundaries of particles. The interface between CF70 and the matrix was separated as shown in Fig. 2-12A. Although the separation might be caused during ion-milling, the phenomenon was an evidence of weak interface of CF70/SiC. Furthermore, matrix near the interface consisted of several layers, which were separated by many micropores. The layer near the interface was thinner. TEM by high magnification clearly showed the layers (Fig. 2-12B). In Fig. 2-4, it was shown that CF70 bonded weakly or even separated with PCS after first time impregnation of PCS. The result in Fig. 2-4 is consistent with the observation by TEM. Therefore, a model was proposed to explain the impregnation process of PCS into CF70, as shown in Fig.2-13A. After first time of impregnation and pyrolysis, SiC matrix was poorly bonded or even separated from CF70. In the following impregnation, PCS infiltrated into the spacing between previously-formed SiC and CF70, and a thinner layer was formed after pyrolysis. Such a process was repeated until the spacing became too small for further impregnation. One direct result of this process was the enlargement of the spacing between carbon fibers, thus it decreased the fiber volume fraction in CF70/SiC as described in 2.3.2. One advantage of this process was that a path between fiber and matrix formed, and it allowed further PCS impregnation. This was beneficial for the densification of CF70/SiC samples.

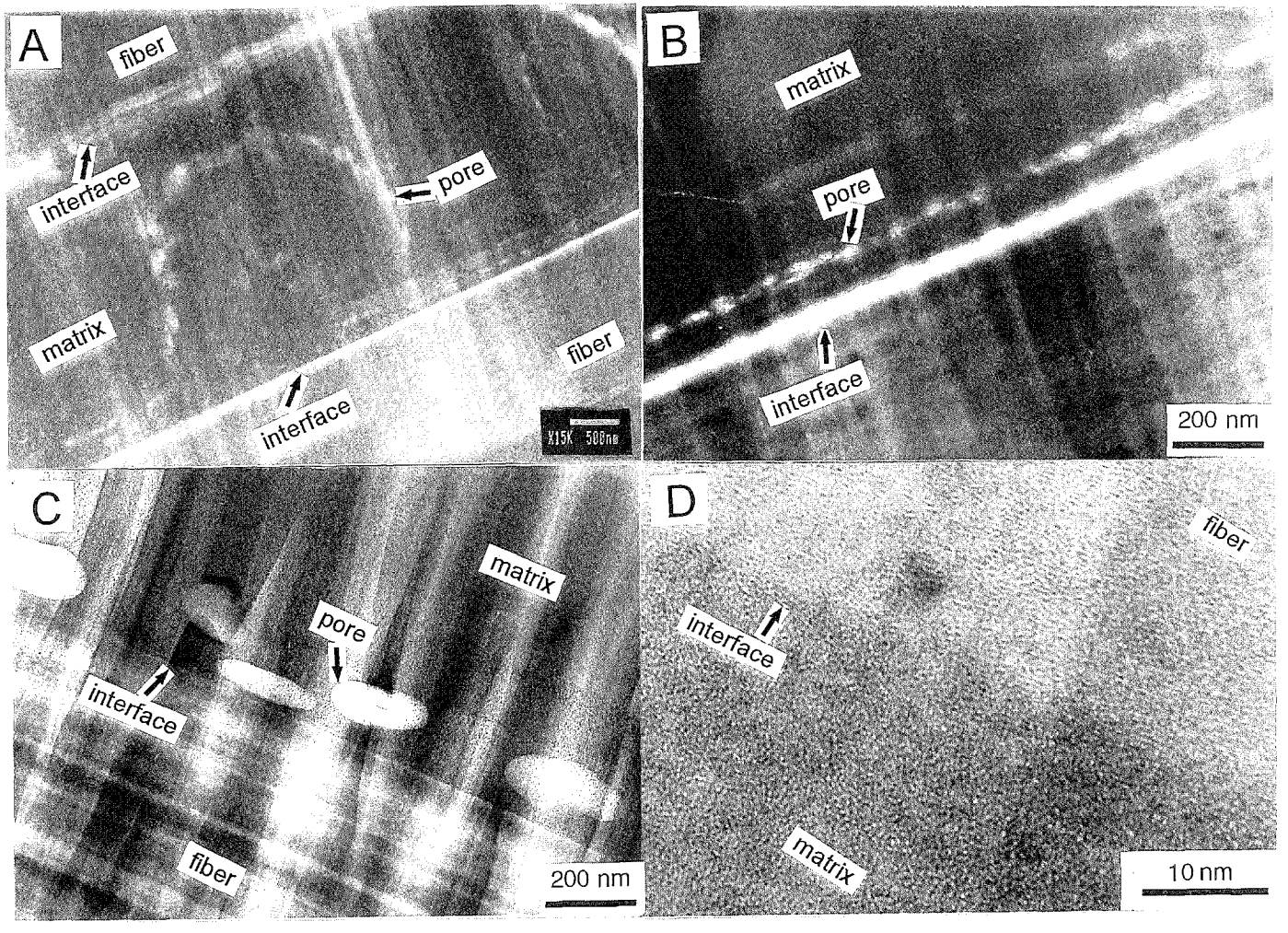

Fig. 2-12 TEM images of the interface of CF70/SiC (A, B) and HMCF/SiC (C, D).

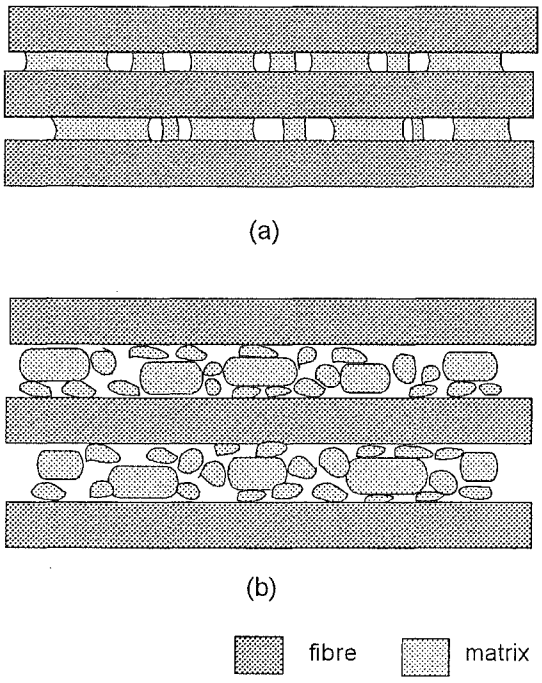

Fig. 2-13 The impregnation model of polycarbosilane into fibre tows: HSCF and HMCF (a), CF50 and CF70 (b). Large particles were formed in the first impregnation, and small particles were formed in the subsequent impregnations.

The interface between HMCF and the matrix appeared to be bonded strongly as shown in Fig. 2-12C and D. The multi-layered matrix and pores as observed in CF70/SiC were not observed in HMCF/SiC. The pores distributed in matrix particles were also observed in the vicinity of interface of HMCF/SiC. The high resolution image of the interface between HMCF and the matrix showed a complete interface bonding. In Fig. 2-4, HMCF was shown to bond well with PCS after initial impregnation. An impregnation model of PCS into HMCF was proposed, as shown in Fig. 2-13. The impregnation process of PCS in HMCF/SiC was different from that in CF70/SiC. Matrix tended to bond strongly with HMCF after first time of impregnation and pyrolysis, therefore, shrinkage of the matrix after pyrolysis of PCS made the fiber spacing small. In following impregnation, PCS infiltrated into the space between matrix particles, thus, the fiber volume fraction of HMCF/SiC was higher than that of CF70/SiC. CF50 /SiC showed similar behavior to CF70/SiC, while HSCF/SiC was

similar to HMCF/SiC.

The above results suggested that the difference of the interfaces started from the first impregnation-pyrolysis process. The carbon fibers showed different behavior toward impregnation of PCS solution and the subsequent pyrolysis process, because of the differences in their microstructures and their surface activities. They resulted in the difference in matrix microstructures and interface between fiber and matrix.

From above discussion, it was found that the wettability of PCS solution to fibers was essential to the preparation of CF/SiC. The good wettability and the weak interface seem self-contradictory. In the four types of carbon fibers used in the experiments, graphitized CF50 and CF70 were found to have adequate wettability and weak bond with the matrix.

2.4.2 The structure of the carbon fibers

It has been shown that the difference of interface was due to the structure of carbon fibers. Since HSCF and HMCF were fabricated below 1500°C and CF50 and CF70 were fabricated above 2000°C, it was expected that their crystallinity and microstructures differed remarkably between the two groups of fibers. The XRD profiles of these carbon fibers are shown in Fig. 2-14. It was known that CF50 and CF70 exhibited much better crystallinity than HSCF and HMCF. The lattice spacing d_{002} and the crystallite size of L_{c002} calculated according to the Gakushiho are shown in Table 2-4. It was confirmed that the crystallinities of HSCF and HMCF were not well-developed with less stacking layers and bigger d_{002} spacing, whereas CF50 and CF70 were apparently highly-graphitized with large crystallite size and small d_{002} spacing.

Table 2-4 The d_{002} and L_{c002} of carbon fibers

carbon fibers	d_{002} (Å)	L_{c002} (Å)
HSCF	3.479	15
HMCF	3.476	22
CF50	3.418	200
CF70	3.395	230

The difference in the crystallinities of the carbon fibers may give rise to the difference in the surface structure and activity of the carbon fibers. Moreover, the carbon fibers fabricated below 1500°C have more impurity elements such as N and O, which originated from the precursors or

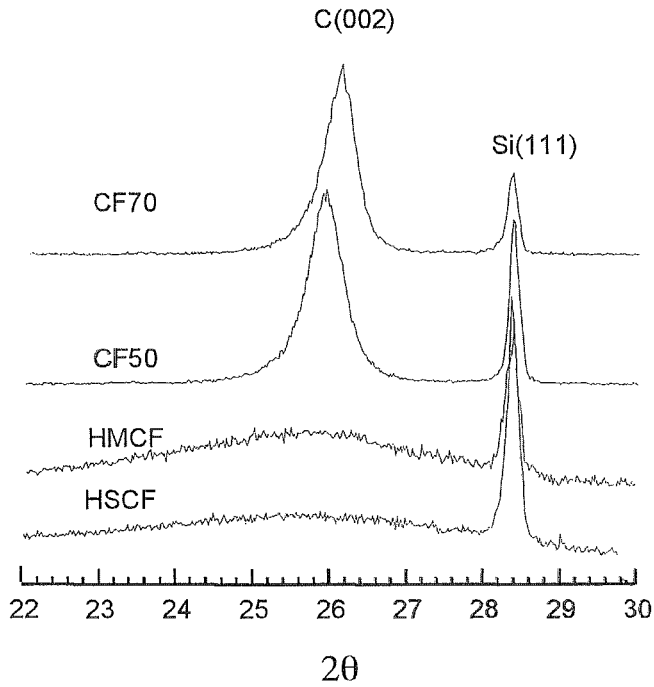

Fig. 2-14 (002) XRD profiles of carbon fibers.

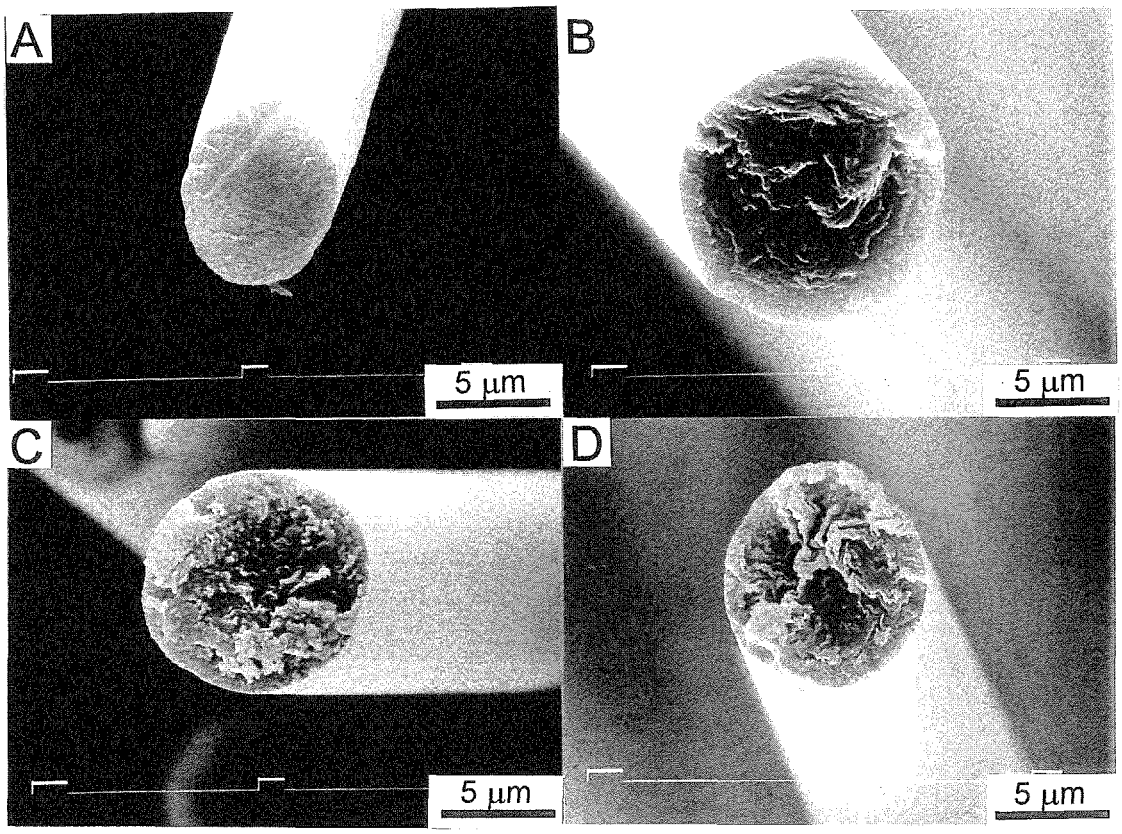

Fig. 2-15 Transverse sections of HSCF (A), HMCF (B), CF50 (C) and CF70 (D).

formed by adsorbing moleculars in atmosphere [16]. Therefore, HSCF and HMCF were generally thought to have more functional groups on their surfaces than CF50 and CF70 which were fabricated above 2000°C.

SEM micrographs of the texture of the carbon fibers are shown in Fig. 2-15. It was noted that HSCF had a relatively random structure, and HMCF had an onion-like structure in its inner core and a radial structure in the outer layer, while both CF50 and CF70 had a radial structure.

The observation of CF70 by HRTEM revealed that the structure of skin of CF70 is not the same as the structure of inner core. Fig. 2-16 shows that the (002) images from skin to core. The core of CF70 exhibits large, parallel 002 planes, while the skin shows relatively poor crystallinity. The reason about the difference of the structure between the skin and the core of CF70 is not clearly known, because the processing conditions of CF70 are unclear. Fig. 2-17 shows the (002) image of the core of HMCF. The (002) planes in HMCF are not stacked very well, but showed a good orientation along the fiber axis. The image of the skin of HMCF can be seen in Fig. 2-12D. No apparent difference between the skin and the core in HMCF was observed. But the crystallinity of the skin of CF70 was still much better than that of HMCF.

From these results and observation about the structure of the carbon fibers, the crystallinty (d_{002} and $L_c(002)$) of the carbon fibers obtained by XRD only gives the average information, which is not accurate information about the skin or surface of carbon fibers, while TEM observation gives more accurate information. In the present four types of carbon fibers, the graphitized carbon fibers, CF50 and CF70, were more suitable as the reinforcement of CF/SiC.

2.4.3 Fracture behavior of CF/SiC

Because HSCF/SiC and HMCF/SiC had strong interface bonding, cracking in the matrix could easily propagate across the interface between the carbon fiber and matrix, and this resulted in failure at low strain. On the other hand, the weak interfacial bonding in CF50/SiC and CF70/SiC resisted propagation of matrix cracks into the carbon fibers by debonding of the interface, although the cracks propagated throughout the matrix.

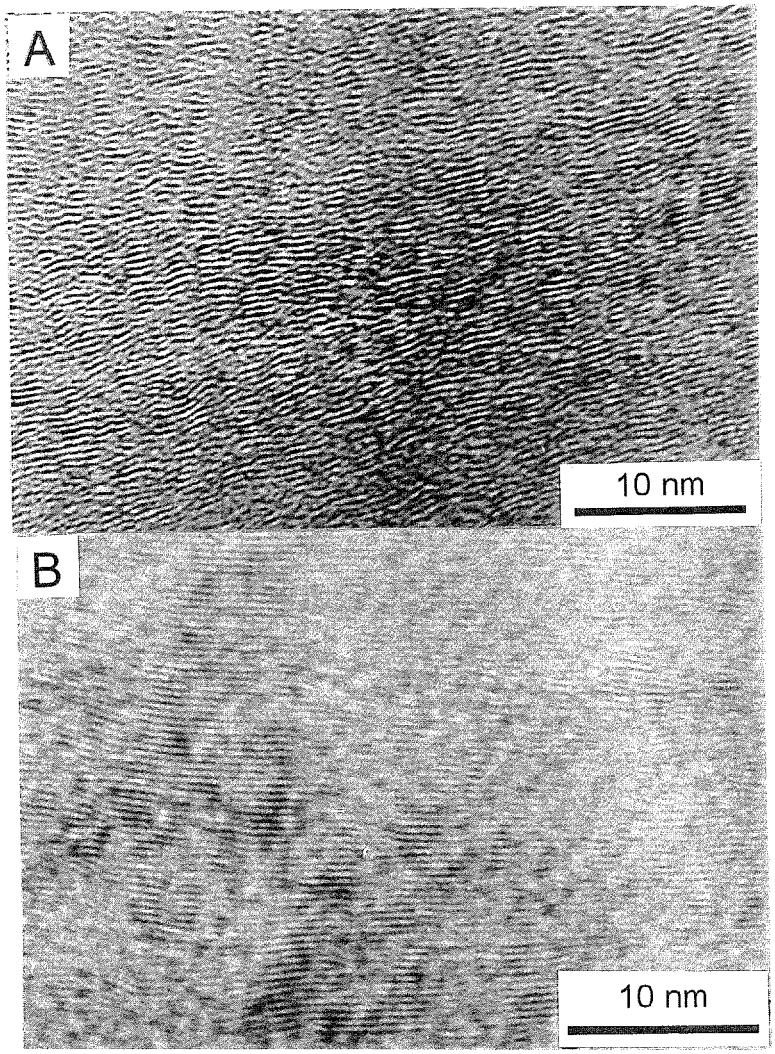

Fig. 2-16 HRTEM images of skin (A) and core (B) in CF70.

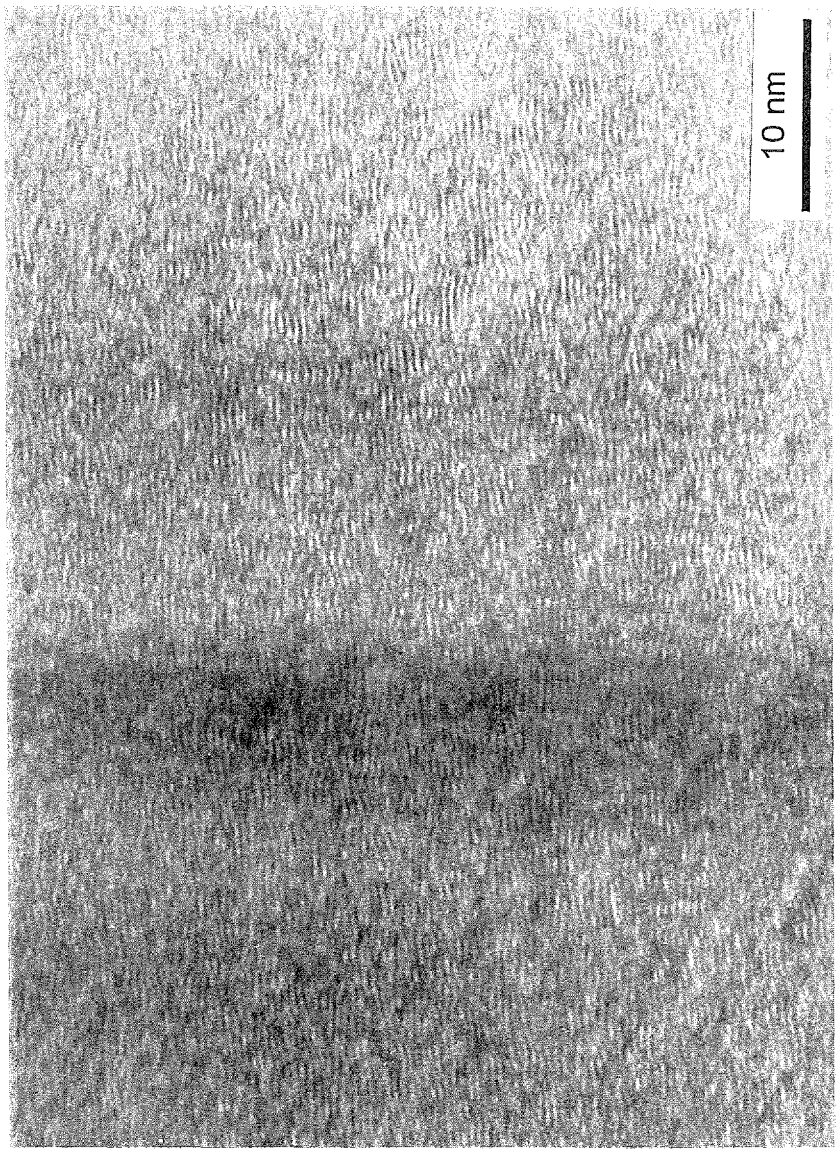

Fig. 2-17 HRTEM image of HMCF.

After that, carbon fibers still supported the load by friction between fiber and matrix.

The four types of CF/SiC were divided into two groups. HSCF and HMCF belonged to strong interfacial bonding group, and CF50 and CF70 belonged to weak interfacial bonding group. Although HSCF/SiC and HMCF/SiC exhibited similar mechanical behavior in the present conditions, there was some difference between HSCF/SiC and HMCF/SiC. From the fracture surfaces of HSCF and HMCF in Fig. 2-10, it is noted that the HSCF/SiC showed almost completely flat fracture surface, while HMCF/SiC showed some short fiber pullout although it could not resist the propagation of the matrix cracks. This difference indicated that HMCF/SiC had relatively weak bonding interface compared with HSCF/SiC, and it can be explained by their differences of crystallinity and microstructures as described above.

The differences of interfacial properties of CF50/SiC and CF70/SiC, both of which exhibited multiple matrix cracking and extensive fiber pullout, had not been well understood here, because fiber pullout length and distribution had not been precisely measured in the present experiments. Moreover, the shear failure of CF50/SiC during bending test made it difficult to compare the CF50/SiC and CF70/SiC.

2.5 Conclusions

Four types of carbon fibers, PAN-based HSCF and pitch-based HMCF which had low graphitization degree, and pitch-based CF50 and CF70 which had a high graphitization degree, were used to prepare carbon fiber reinforced SiC composites by multiple impregnation of polycarbosilane and subsequent pyrolysis. The microstructure of the matrix, the infiltration behavior of PCS and the flexural behavior of the composites were investigated. From the above results and discussion, the following conclusions were drawn out.

(1) Pyrolytic product of polycarbosilane at 1200°C in N_2 consisted of nearly amorphous β-SiC and some impurity oxygen.

(2) CF70/SiC exhibited different impregnation behavior of polycarbosilane from HSCF/SiC and HMCF/SiC. Matrix shrank away from the fiber during pyrolysis in CF70/SiC, and the following impregnation allowed polycarbosilane infiltrate into

the space between fiber and matrix. Matrices in HSCF/SiC and HMCF/SiC strongly bonded with the fibers, polycarbosilane infiltrated the space between matrix particles at the following impregnation.

(3) Density of the composites increased with impregnation times. It took 9 times for HSCF/SiC and HMCF/SiC, and 12 times for CF50/SiC and CF70/SiC to achieve high density.

(4) Among the four types unidirectional CF/SiCs, CF50/SiC and CF70/SiC showed non-brittle fracture behavior with multiple matrix cracking and extensive fiber pullout, while HSCF/SiC and HMCF/SiC exhibited brittle fracture behavior, by four-point bending tests. The graphitized carbon fibers (CF50 and CF70) were more adequate to be used as reinforcement of the CF/PCS-derived-SiC than the carbon fibers (HSCF and HMCF) treated below 1500°C.

(5) CF70/SiC exhibited high flexural strength of approximately 967 MPa which was about 75% of predicted strength. On the other hand, the flexural strength of CF50/SiC was 624 MPa, which was about 38% of predicted strength, because CF50/SiC failed in a shear way during bending tests.

References

1. M. H. Van de Voodrde and M. R. Nedele, Ceram. Sci. & Eng. **17**, 1(1996).
2. Y. Hasegawa, and K. Okamura, J. Mater. Sci., **18**, 3633 (1983).
3. T. Tanaka, N. Tamari, I. Kondoh and M. Iwasa, J. Ceram. Soc. of Japan, **103,** 1 (1995).
4. H. Yoshida, N. Miyata, M. Sagawa, S. Ishikawa, K. Naito, N. Enomoto and C. Yamagishi, J. Ceram. Soc. of Japan, **100,** 454 (1992).
5. S. Otani, K. Okuda and S. Matsuda, In "Tanso Seni" (Kindai Hensyu Sya,Japan, 1983) pp. 205-217.
6. M. R. Mucalo, N. B. Milestone, I. C. Vickridge and M. V. Swan, J. Mater. Sci., **29,** 4487 (1994).
7. J. Aveston, G. A. Cooper and A. Kelly, in "The Properties of Fiber Composites", (Conf. Proc. National Physical Laboratory, IPC Science and Technology Press, 1971) p. 15.
8. D. B. Marshall, B. N. Cox, and A. G. Evans, Acta Metall., 33, 2013 (1985).
9. W. A. Curtin, J. Am. Ceram. Soc. **74,** 2837 (1991).
10. P. S. Steif and A. Trojnacki, J. Am. Ceram. Soc. 77, 221 (1994).
11. A. G. Evans and F. W. Zok, J. Mater. Sci., **29**, 3857 (1994).
12. M. D. Thouless, O. Sbaizero, L. S. Sigl, and A. G. Evans, J. Am. Ceram. Soc., **72,** 525 (1989).

Chapter 3 Microstructure and Mechanical Properties of CF/SiC Composites after Heat-Treatment

3.1 Introduction

The preparation of ceramic matrix composites from preceramic polymers, such as polycarbosilane (PCS), has been gaining increasing interest in recent years. This method can be applied to fabricate complex shape with near-net-shape feature, and carried out at relatively low temperatures [1,2]. The preceramic polymers were originally used as precursors for ceramic fibers. The structures of polymer-derived ceramics are different from the structures of those obtained by CVI or sintering method [3,4]. As ceramic materials can be obtained at relatively low temperatures, most of polymer-derived ceramic materials are nearly amorphous and nonstoichiometric. When they are heat-treated at higher temperatures, they may crystallise and give rise to internal reaction due to the existence of oxygen. Many efforts to obtain a more stoichiometric polymer-derived-ceramics with low oxygen content have been made by many researchers [5,6]. The aim may be achieved either by controlling pyrolysis conditions, e.g. for fabrication of Hi-Nicalon [7], or by synthesizing polymers with different structure [2].

Since CF/SiC composites will be mainly used for applications at high temperatures, it is important to know structural change of the composites at high temperatures and its effect on the mechanical properties. For PCS-derived SiC fiber, its instability at high temperature leads to a significant degradation of the fiber properties, so it is generally used at temperatures below 1200°C. For CF/SiC composites, the load of the composites is mainly sustained by the carbon fibers, and the matrix plays a role to transfer the load. The instability of the matrix at high temperature may not lead to a significant degradation of CF/SiC. On the other hand, the properties of the composites also depend on the interface between the fiber and matrix. The change in the structure of matrix affects not only the properties of matrix but also the interface properties of the composites. In the present chapter, the effect of heat treatment on the microstructure and mechanical properties of CF/SiC was investigated.

3.2 Experimental procedure

PCS powder was pyrolysed at 1200°C in nitrogen for 1 hour. The pyrolysed powder was placed in graphite boats and then heat-treated at 1400°C, 1600°C and 1800°C for 1 hour, respectively. The heat-treatment at 1400°C was conducted in a tubular furnace, while the heat-treatments at 1600°C and 1800°C were conducted in a graphite-resistance furnace. The crystallinity of the heat-treated SiC powders was analyzed by x-ray diffraction (XRD), and the crystallite size, L_{111}, was measured according to the Scherrera equation.

Two kinds of carbon fibers, PAN-based carbon fibers (HSCF) and pitch-based carbon fibers (HMCF), were used as reinforcements. Their properties were described in Chapter 2. CF/SiC composites were prepared by impregnation-pyrolysis of PCS, as described in Chapter 2. They were cut to the size of $36 \times 3.5 \times 1$ mm^3, and then heat-treated at 1400°C, 1600°C and 1800°C, respectively. The heat-treatment conditions were the same as those for powder samples as stated above. When heat-treated at 1600°C and 1800°C, the specimens were embedded in graphite powders. The weight of the specimens before and after HTT was measured to know the weight change. The four-point bending test of these specimens was performed with a cross speed of 0.5 mm/min, a support span of 30 mm and a loading span of 10 mm. The crystallinity of the samples was evaluated by XRD. The microstructure and fracture surfaces of the specimens were observed by scanning electron microscope (SEM).

The structure of matrix was also analyzed by TEM and electron diffraction. The preparation method of the specimen for TEM observation and the observation method were described in Chapter 2.

3.3 Results and discussion

3.3.1 Behavior of PCS-derived SiC matrix with HTT

Figure 3-1 shows HRTEM (High Resolution TEM) micrograph, dark field micrograph and electron diffraction pattern of SiC matrix. Many microcrystals distributed in the matrix. The electron diffraction pattern of the matrix showed three rings, corresponding to the (111), (220) and (311) Bragg reflections of β-SiC. These diffraction rings ranged

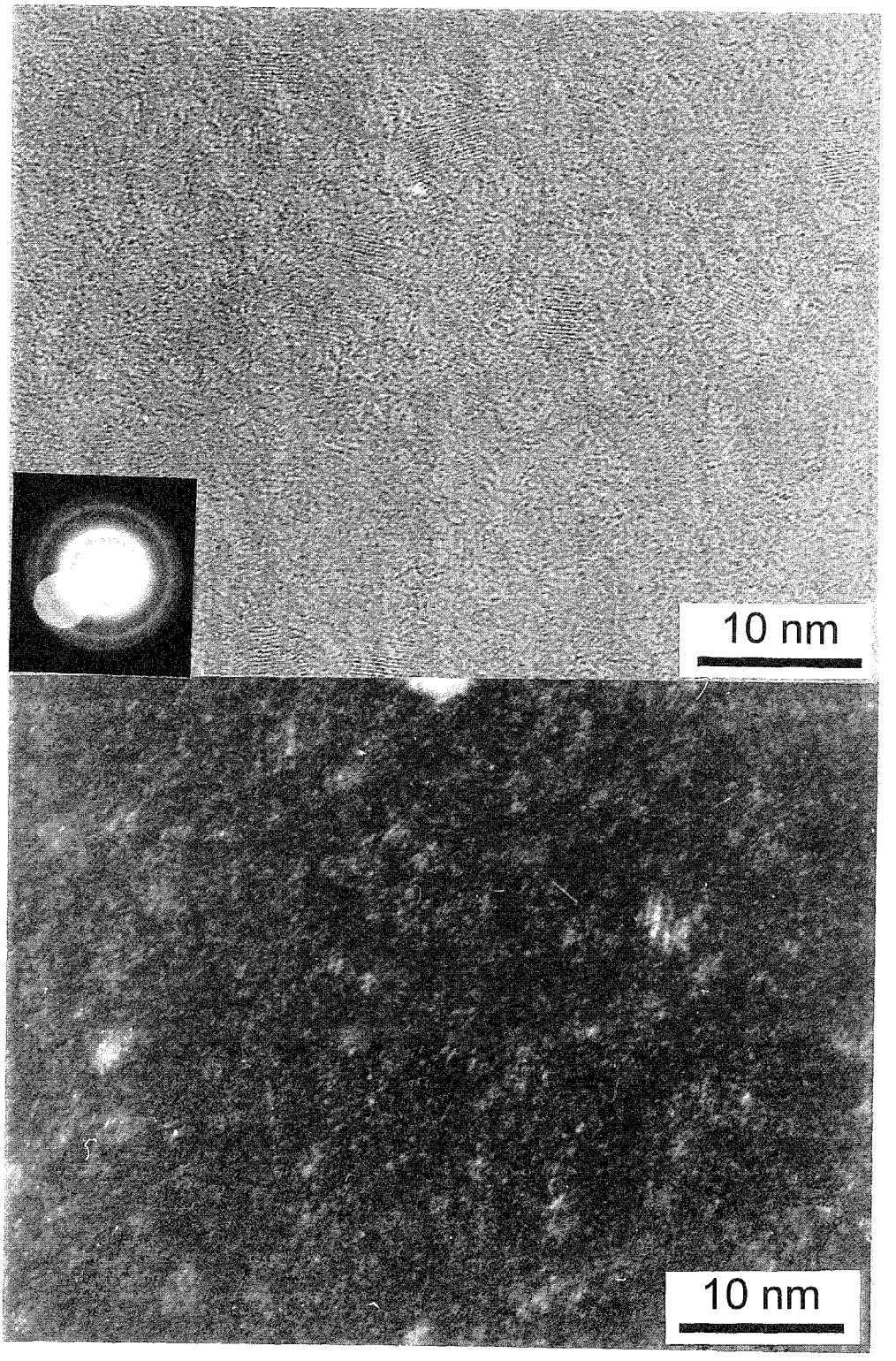

Fig. 3-1 HRTEM images of PCS-derived matrix. (A) bright field image, (B) dark field image.

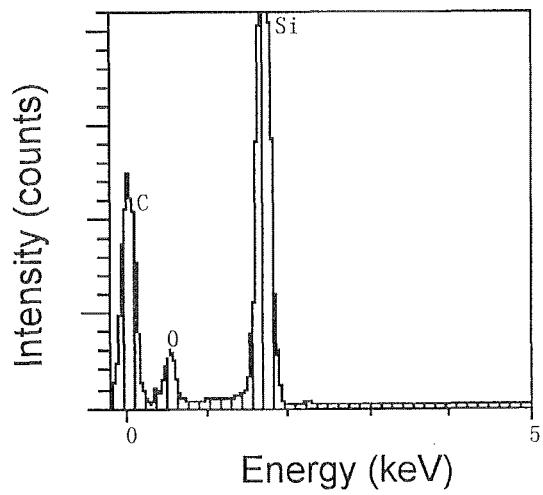

Fig. 3-2. EDX spectrum of matrix, indicating presence of oxygen in matrix.

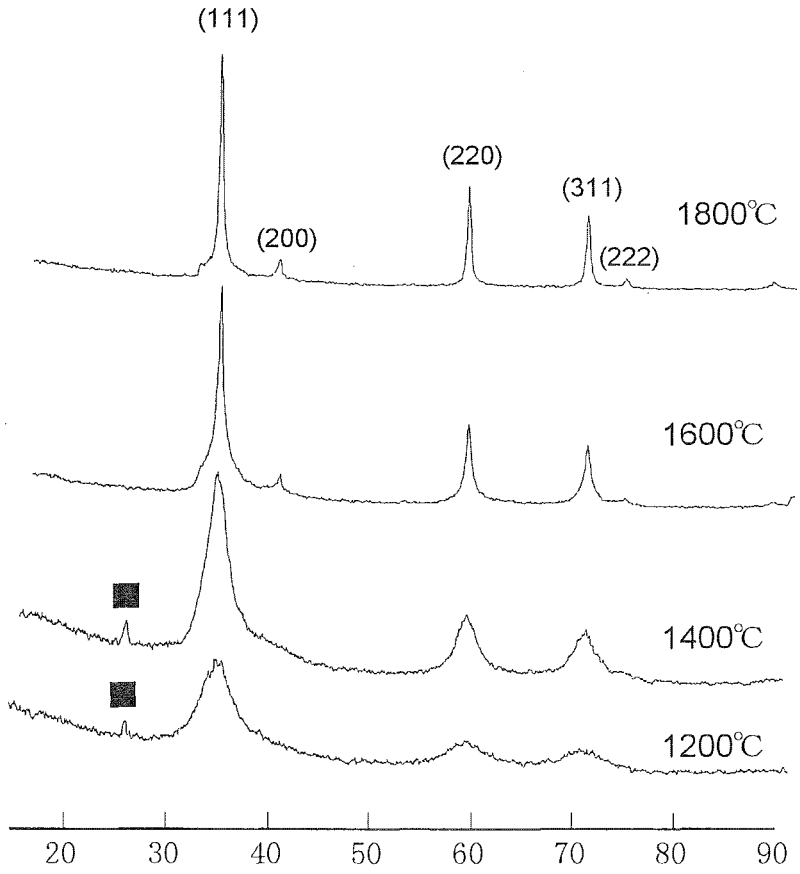

Fig. 3-3 XRD profiles of PCS-derived SiC heat-treated at different temperatures.

from broad rings to relatively sharp rings, suggesting that the crystallinity of matrix was not uniform. In the composite samples that were prepared by multiple impregnation and pyrolysis of PCS, the previously-impregnated matrix had longer heat treatment time at 1200°C, therefore, they had better crystallinity. Figure 3-2 shows the EDX spectrum of matrix, and it indicates existence of oxygen in the matrix. It was thought that the oxygen in the matrix originated from impurity oxygen in PCS and trace oxygen in atmosphere.

Figure 3-3 shows the XRD profiles of PCS-derived SiC powder samples that were firstly prepared at 1200°C and then heat-treated at 1400°C, 1600°C and 1800°C, respectively. The PCS-derived material at 1200°C was nearly amorphous state of β-SiC, as stated in Chapter 2. The three broad peaks of β-SiC, (111), (220) and (311), were detected. The small peak at 26.5° was believed to be a peak of SiO_2 (α-quartz). The three peaks became slightly narrow and sharp at 1400°C. With the increase of HTT, the peaks of β-SiC became markedly sharp. Both (200) and (222) peaks started to appear, and the peak at 26.5° disappeared at 1600°C.

Figure 3-4 shows the change of the crystallite size of β-SiC, L_{111}, with HTT. It was observed that the crystallite size of β-SiC increased slightly up to 1400°C, but increased rapidly above 1400°C with HTT. The value of L_{111} was about 3 nm after heat-treatment at 1400°C, about 12 nm after heat-treatment at 1600°C, and about 19.5 nm after heat-treatment at 1800°C. The powder heat-treated at 1400°C exhibited black color, while those heat-treated at 1600°C and 1800°C exhibited green-yellow color, which was the typical color of β-SiC. The samples heat-treated at 1600°C and at 1800°C showed a significant weight loss, and the green-yellow powder was found on the wall of the graphite boat. It was considered that the following reactions took place at 1600°C and at 1800°C:

$$2SiO_2 + 4C \rightarrow SiC + SiO(g) + 3CO(g) \qquad (3\text{-}1)$$

or

$$SiC_xO_y \rightarrow SiC + SiO(g) + CO(g) \qquad (3\text{-}2)$$

At 1400°C, the reaction was so slow that there was almost no weight loss, and the crystalline growth of SiC was suppressed by the presence of oxide and free carbon.

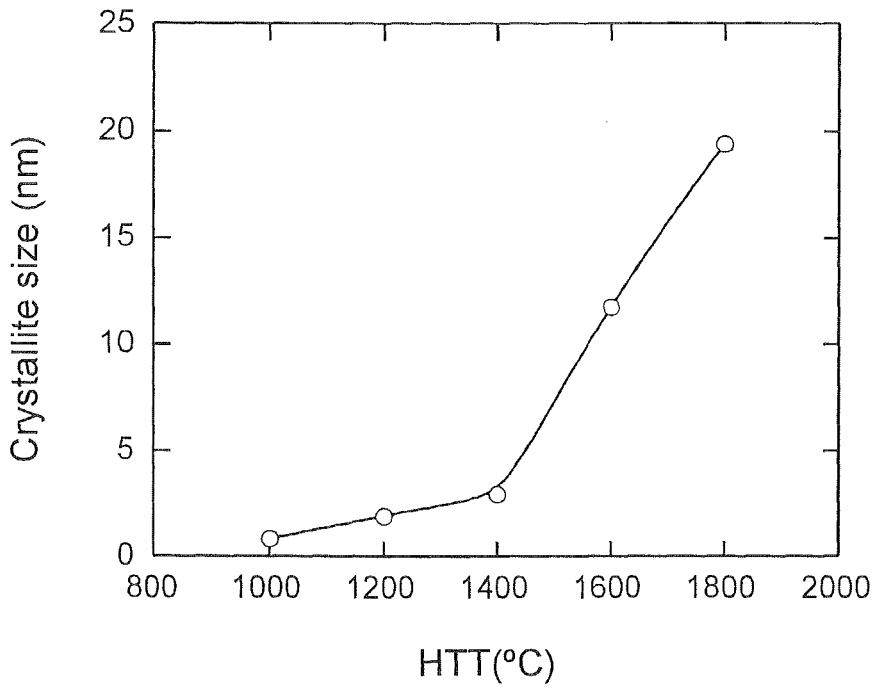

Fig. 3-4 The change of crystallite size (L_{111}) of PCS-derived SiC with HTT.

Table 3-1 The properties of HSCF/SiC and HCF/SiC with HTT.

	HSCF/SiC			HMCF/SiC		
HTT (°C)	Relative Weight (%)	Flexural strength (MPa)	Elastic modulus (GPa)	Relative Weight (%)	Flexural strength (MPa)	Elastic modulus (GPa)
1200	100	194	95	100	360	110
1400	99	196	87	99.6	384	111
1600	89	216	84	80.9	248	84.9
1800	88	192	148	79.1	257	72.2

Above 1600°C, oxide and free carbon reacted, so the crystalline growth was very fast. The gaseous SiO also reacted with the graphite boat and formed SiC.

$$SiO + C \rightarrow SiC + CO(g) \qquad (3\text{-}3)$$

3.3.2 Microstructure of HSCF/SiC and HMCF/SiC with HTT

The weight change of HSCF/SiC and HMCF/SiC with HTT is shown in Table 3-1. A minor change in weight was detected at 1400°C, and a significant change was observed at 1600°C and 1800°C. The weight loss was about 10% for HSCF/SiC and 20% for HMCF/SiC above 1600°C. The less weight loss for HSCF/SiC was due to a higher fiber volume fraction and less amount of the matrix.

The color of the matrix in both HSCF/SiC and HMCF/SiC changed to yellow-green at 1600°C and 1800°C as described in the previous section. The microstructures of HSCF/SiC heat-treated at different temperatures are illustrated in Fig. 3-5. It was

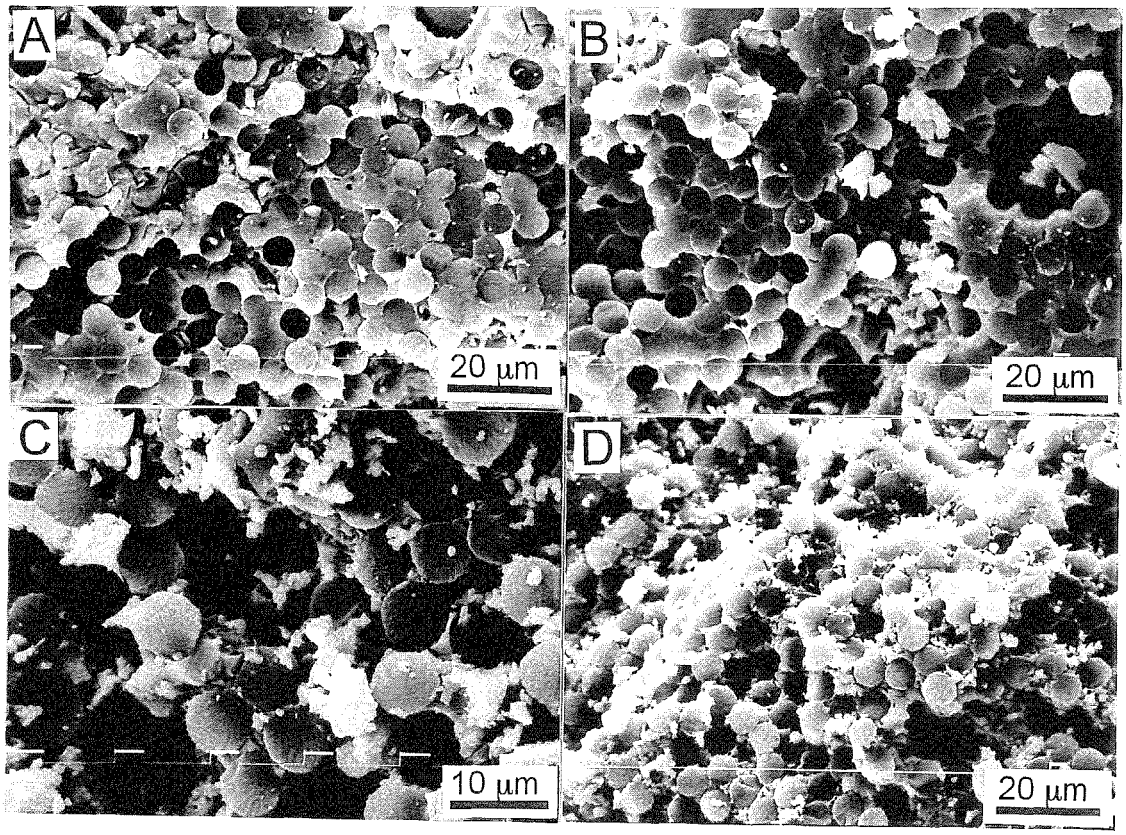

Fig. 3-5 Fracture surfaces of as-prepared HSCF/SiC (A) and those heat-treated at 1400°C (B), at 1600°C (C) and at 1800°C (D) after bending test.

observed that no change in microstructure occurred at 1400°C. However, for the samples heat-treated at 1600°C and at 1800°C, many pores formed in the matrix, and the matrix changed to agglomeration of particles. It was also observed that fibers reacted with matrix at 1600°C and at 1800°C as shown in Fig. 3-6. The reaction between fibers and matrix was thought to proceed according to the formula (3-3). SiO formed from decomposition of the matrix reacted with carbon fibers and formed SiC on the surface of the carbon fibers according to the reaction (3-3). Two types of particles were observed in the matrix heat-treated at 1600°C and at 1800°C. One type of the particles inherited the shape of the original particles before the decomposition and the other type of the particles was small with smooth surface. Many micro-pores were observed in the former particles. The micropores were thought to be formed by the reaction (3-1) or (3-2) which produced gaseous SiO and CO. Formation of whiskers were observed in HSCF/SiC heat-treated at 1600°C and at 1800°C, as shown in Fig.3-7.

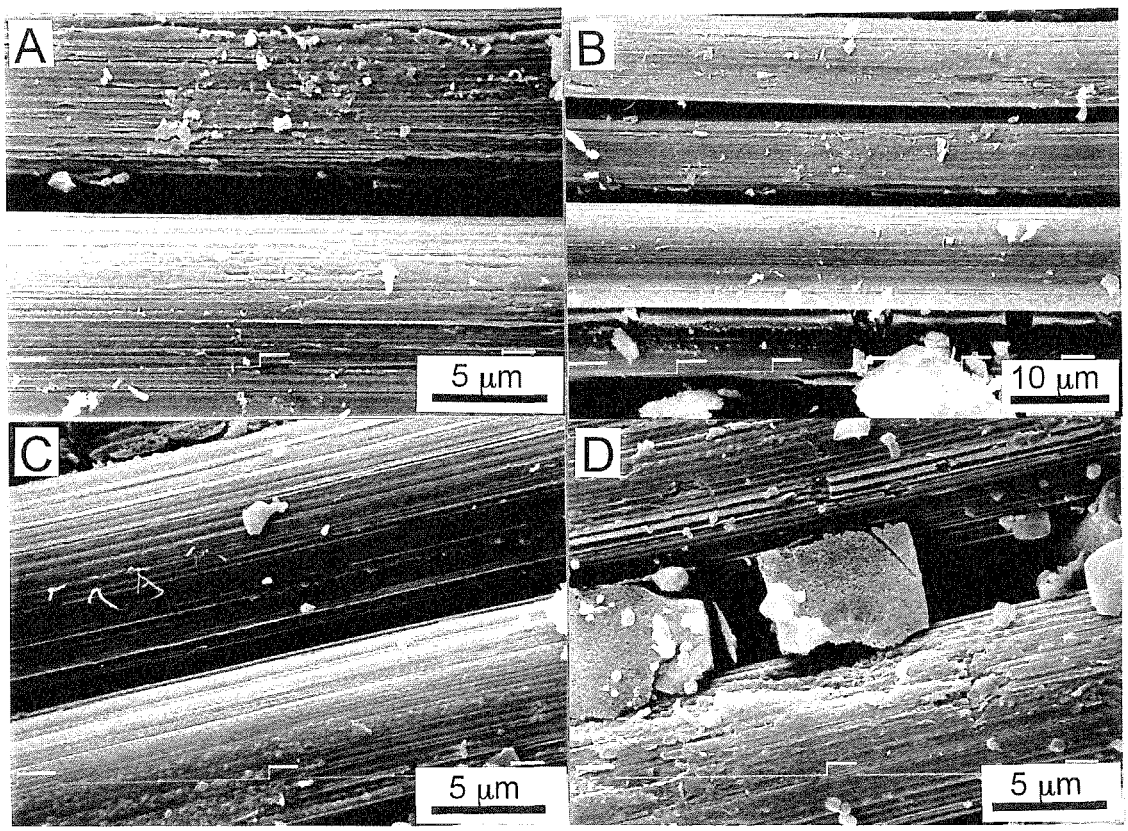

Fig. 3-6 Fiber surfaces in HMCF/SiC after heat-treatment at 1600°C (A, B) and at 1800°C (C, D)

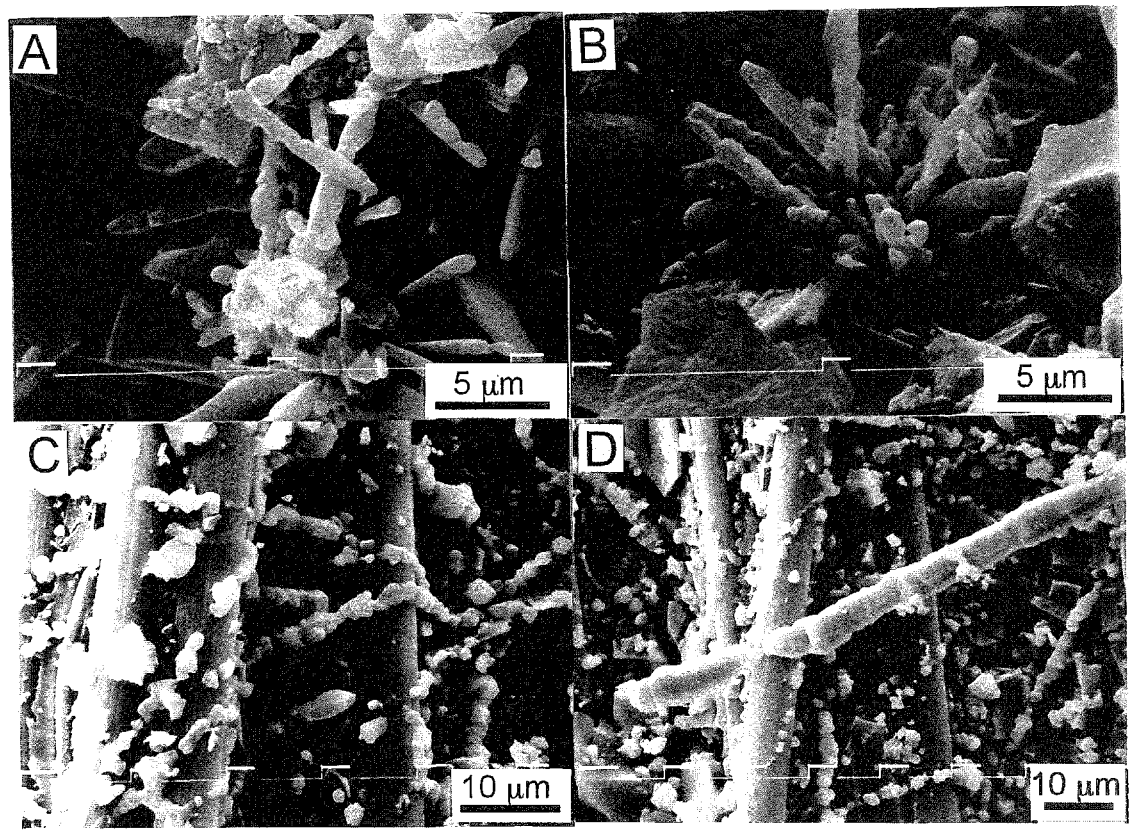

Fig. 3-7 Whiskers formed in HSCF/SiC heat-treated at 1600°C (A, B) and at 1800°C (C, D).

The whiskers had an average length of about 5 μm and a diameter of about 1 μm in HSCF/SiC heat-treated at 1600°C. The whiskers had an average diameter of about 2 μm, the length of whiskers was less than 100 μm in HSCF/SiC heat-treated at 1800°C. The XRD profiles of HSCF/SiC and HMCF/SiC heat-treated at different temperatures are shown in Fig. 3-8 and Fig.3-9. As no other peaks were detected except peaks of carbon and SiC. The whiskers were confirmed to be β-SiC. The formation SiC-whiskers was thought to proceed by reaction (3-2). The grains with smooth surface were also likely to be formed by this reaction as SiC whiskers formed.

Fig. 3-8 and Fig. 3-9 also shows that the crystallinities of both carbon fiber and SiC were improved with increasing temperature. The as-received carbon fibers were fabricated below 1500°C, therefore, their crystallinity was improved by the present heat treatment conditions. The details on heat treatment of carbon fibers will be investigated in the next Chapter.

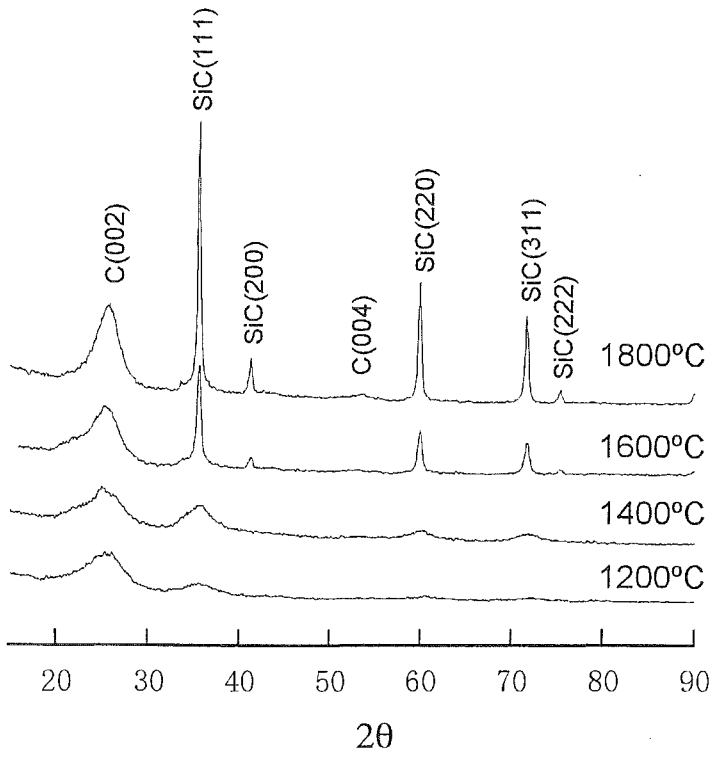

Fig. 3-8 XRD profiles of the as-prepared HSCF/SiC and those heat -treated at 1400, 1600, 1800°C.

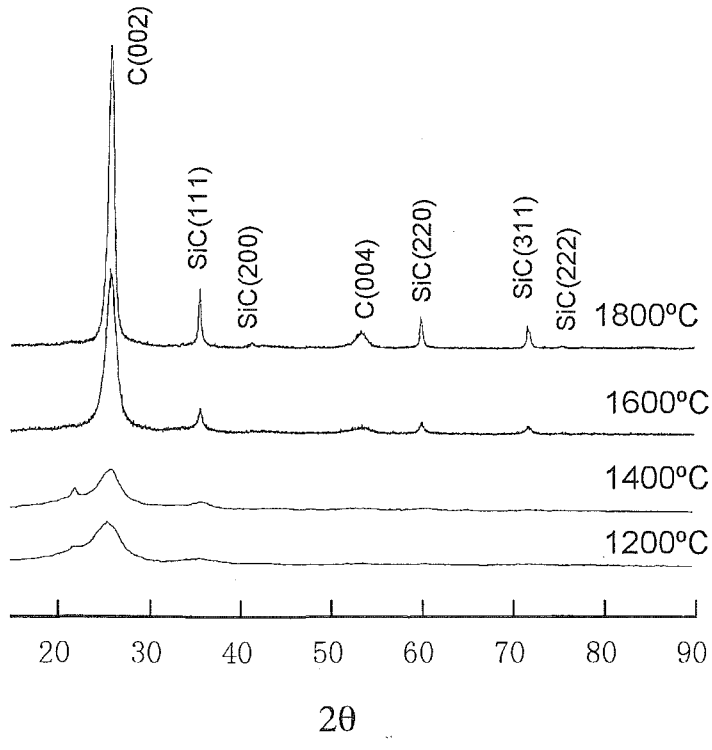

Fig. 3-9 XRD profiles of the as-prepared HMCF/SiC and those heat treated at 1400, 1600, 1800°C.

3.3.3 Flexural properties of CF/SiC with HTT

The four-point bending strength and modulus of both HSCF/SiC and HMCF/SiC are shown in Table 3.1. HSCF/SiC and HMCF/SiC heat-treated at 1400°C showed similar strength and modulus with those as-prepared at 1200°C. This was reasonable because there was almost no change in weight and microstructure from 1200°C to 1400°C.

HSCF/SiC heat-treated at 1600°C showed slightly higher strength than the as-prepared one, and HSCF/SiC heat-treated at 1800°C showed a similar strength with the as-prepared one. Their fracture surfaces after bending test are shown in Fig. 3-7. HSCF/SiC heat-treated at 1600°C and 1800°C showed somewhat fiber pullout, whereas HSCF/SiC as-prepared and heat-treated at 1400°C showed no fiber pullout. The heat-treatment at 1600°C and 1800°C gave rise to following changes in HSCF/SiC as follows.

- After heat-treatment, the elastic modulus of the carbon fibers increased because of improvement of crystallinity and the strength of carbon fiber decreased due to reactions with SiO
- A great amount of pores in matrix formed because of significant weight loss (Fig. 3-5c.d)
- Interface characteristics between fiber and matrix changed due to the changes of microstructures of the fibers and matrix.

Therefore, the flexural strength of HSCF/SiC heat-treated at 1600°C and 1800°C was the net effect of all these factors. The apparent stress-strain curves of HSCF/SiC composites are shown in Fig. 3-10. HSCF/SiC heat-treated at 1600°C underwent interlaminate fracture because of weak interface or weak matrix. HSCF/SiC heat-treated at 1800°C shows much higher modulus. It may be due to the increase of the elastic modulus of HSCF after heat-treatment at 1800°C.

HMCF/SiC heat-treated at 1600°C and 1800°C showed a significant decrease in flexural strength and modulus. Fig. 3-11 shows the apparent stress-strain curves of HMCF/SiC. The heat-treatment would bring the three effects as stated above. However, the large weight loss of 20% made the matrix can not transfer the load properly. Therefore, they showed low modulus and interlaminate fracture. Fig. 3-12 shows the

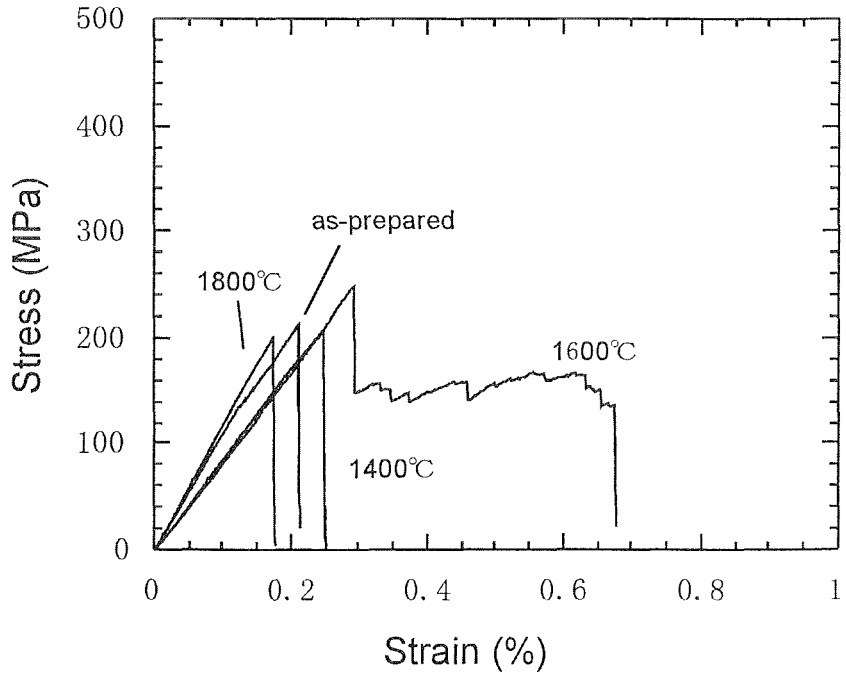

Fig. 3-10 The apparent stress-strain curves of HSCF/SiC heat-treated at different temperatures.

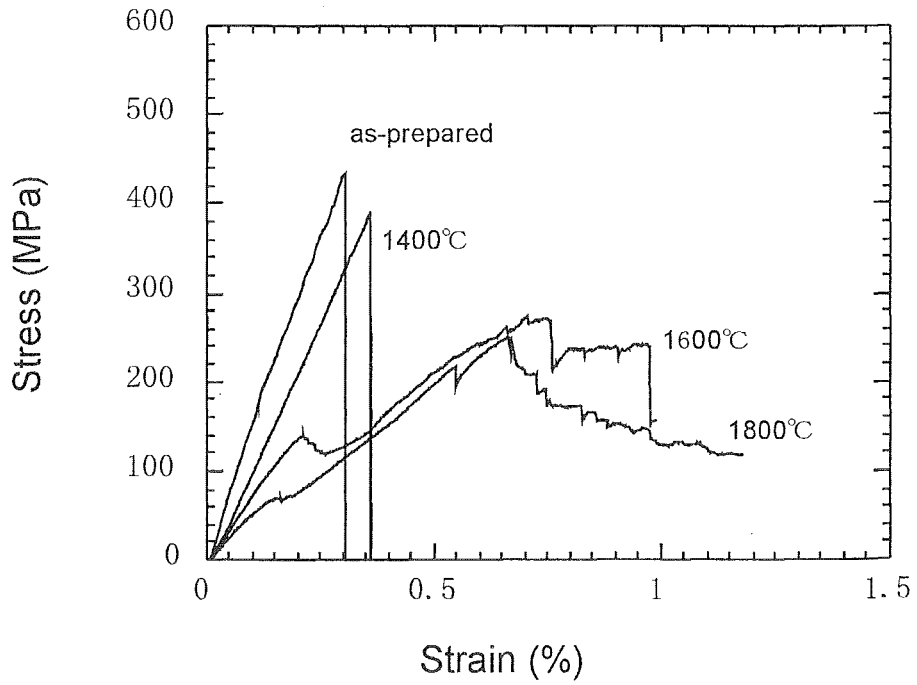

Fig. 3-11 The apparent stress-strain curves of HMCF/SiC heat-treated at different temperatures.

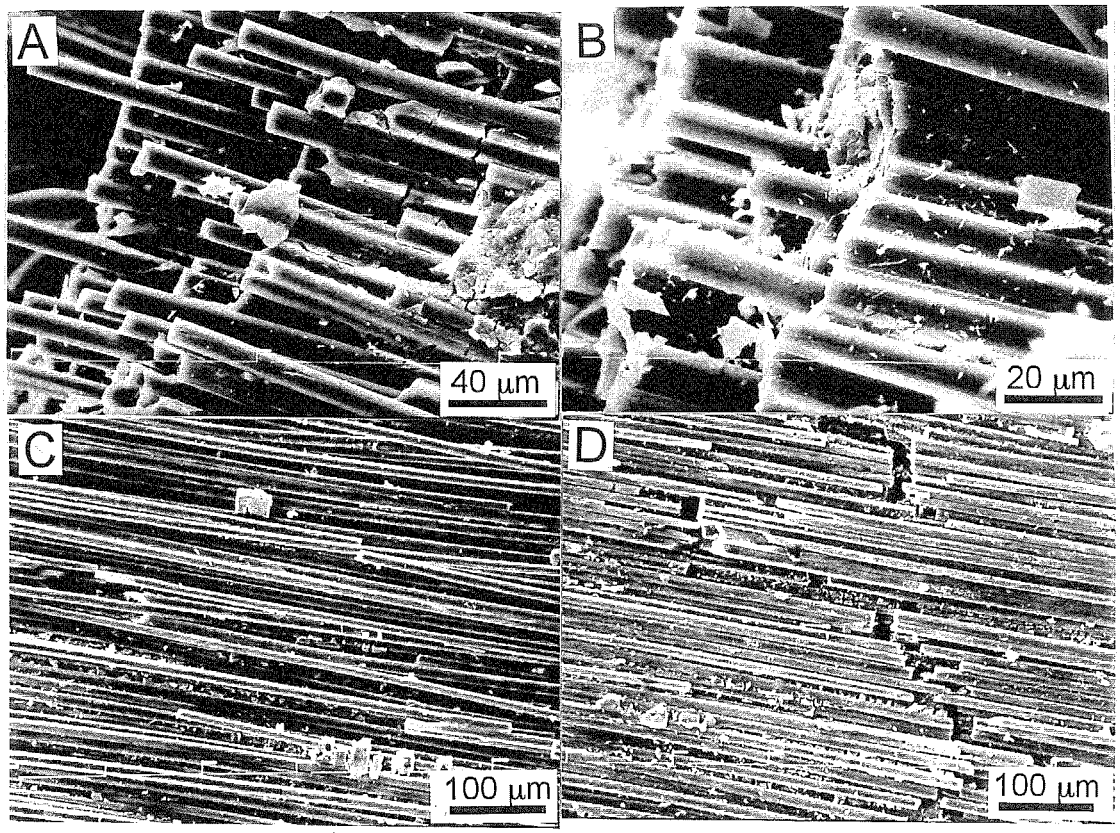

Fig. 3-12 Fracture surfaces of as-prepared HMCF/SiC (A) and those heat-treated at 1400°C (B), 1600°C (C) and 1800°C (D) after bending test.

fracture surface of HMCF/SiC. The as-prepared and HMCF/SiC heat-treated at 1400°C failed in a brittle mode with most fibers fractured in a same plane. HMCF/SiC heat-treated at 1600°C and 1800°C showed a gradual failure, not in a brittle mode.

3.4 Conclusion

Thermal stability of CF/SiC composites is important for their application. With heat-treatment at 1400°C, the crystallite size of the PCS-derived SiC matrix increased from 1.9 nm to 3 nm, although the weight loss was hardly observed. With heat-treatment at 1600°C and 1800°C, the crystallite size of the matrix markedly increased to 12 nm and 19.5 nm, respectively, accompanied by significant weight loss, due to the reactions in the matrix.

Despite the weight loss, HSCF/SiC showed no significant change in the mechanical properties. But HMCF/SiC showed somewhat degradation in the mechanical properties. The formation of SiC whiskers was also observed in HSCF/SiC at 1600°C and 1800°C.

Reference

1. T. Tanaka, N. Tamari, I. Kondoh and M. Iwasa, J. Ceram. Soc. of Japan, **103,** 1 (1995).
2. W. J. Sherwood, C. K. Whitmarsh, and J. M. Jacobs, Ceram. Eng. & Sci. Proc. **17** (3), 174(1996).
3. D. P. Stinton, T. M. Besmann, and R. A. Lowden, Ceram. Bullitin, **67**, 350 (1988).
4. K. Nakano, A. Kamiya, H. Ogawa, and Y. Nishino, J. Ceram. Soc. of Japan, **100**, 472 (1992).
5. Y. Hasegawa, and K. Okamura, J. Mater. Sci., **18**, 3633 (1983).
6. Y. Hasegawa, and K. Okamura, J. Mater. Sci., **21**, 321 (1986).
7. T. Shimoo, T. Hayatsu, M. Narisawa, M. Takeda, H. Ichikawa, T. Seguchi and K. Okamura, J. Ceram. Soc. of Japan, **101**, 809 (1993).

Chapter 4 Modification of the Interface between Fiber and Matrix by Heat Treatment of the Carbon Fibers

4.1 Introduction

The importance of interface between fiber and matrix in fiber/ceramic composites has been described theoretically [1,2] and demonstrated experimentally [3,4]. The interfacial characteristics in a fiber/ceramic composite depend upon the microstructures of the fibers and matrix as well as the processing conditions of the composite. In Chapter 2, it was shown that the interface characteristics between carbon fiber and SiC depended on the different types of carbon fibers. It suggests that it is possible to tailor the interface of fiber/ceramic composites by controlling the microstructure of the fibers.

Carbon fibers possess various structures, which are dependent on their precursors and processing conditions. In Chapter 2, it was described that different types of carbon fibers tended to give rise to different interfacial behavior in CF/SiC composites prepared by impregnation and pyrolysis of polycarbosilane (PCS). The graphitized carbon fibers had a weak interfacial bonding with the PCS-derived SiC matrix, while the carbon fibers heat-treated below 1500°C had a strong interfacial bonding with the SiC matrix. However, these carbon fibers were made from different precursors by different makers, and their detailed processing conditions were unclear. Thus, it was difficult to gain systematic insights into the influence of heat treatment temperatures (HTT) of carbon fibers on the properties of the composites. In this Chapter, pitch-based HMCF and PAN-based HSCF, which were previously found to have a strong interfacial bonding with the SiC matrix, were heat-treated at different temperatures to investigate the effect of HTT on the mechanical properties of the CF/SiC composites.

4.2 Experimental procedure

4.2.1 Heat treatment of carbon fibers and preparation of CF/SiC composites

Continuous pitch-based HMCF and PAN-based HSCF were cut to a length of about 50 mm, and then they were heat-treated at 1400°C in nitrogen in a tubular furnace and at 1500°C, 1600°C, 1800°C and 2000°C in argon in a graphite-resistance furnace for 1

hour, respectively. The heat-treated HMCF were denoted as HMCF14, HMCF15, HMCF16, HMCF18 and HMCF20, respectively. The heat-treated HSCF were denoted as HSCF14, HSCF16, HSCF18 and HSCF20, respectively. After heat treatment, each bundle of the respective carbon fibers was impregnated with a 50% polycarbosilane (PCS)-toluene solution under vacuum, and then they were dried and pyrolysed at 1200°C in nitrogen for 1 hour. The impregnation-pyrolysis process was repeated 9 times to obtain dense composite samples. The details of impregnation-pyrolysis process of PCS were described in Chapter 2.

4.2.2 Characterization

The tensile strength of the carbon fibers was measured by the monofilament method with a gauge length of 25 mm and a crosshead speed of 0.5 mm/min in a universal testing machine [5]. 30 monofilament specimens were measured for each kind of heat-treated carbon fiber. The strength distribution of the carbon fibers was evaluated using the Weibull statistics. The crystallinity of the carbon fibers after heat treatment was investigated by calculating (002) spacing, d_{002}, and crystallite size, $L_c(002)$, from X-ray diffraction (XRD) profiles according to the Gakushin method.

The CF/SiC samples were incorporated in resin. They were polished with SiC sand paper and diamond slurry. The polished samples were then observed by SEM.

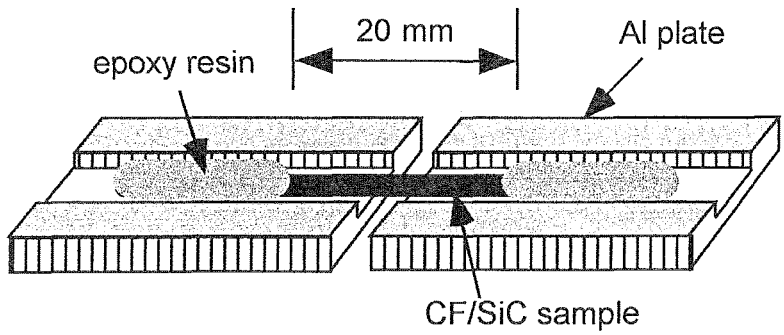

Fig. 4.1 A schematic of CF/SiC specimen for tensile test.

The mechanical properties of the CF/SiC composites were measured using the specimen shown in Fig. 4-1, in which CF/SiC composite sample was adhered to aluminum plates by epoxy resin with a gauge length of 20 mm. The tensile tests were performed by the universal testing machine with a crosshead speed of 0.5 mm/min. The load-displacement curves were recorded to examine the fracture behavior of the CF/SiC composites. Since the sizes of the samples vary, the strength values may lack normalization. While the number of fibers in the one-bundle composites was always the same, the ultimate tensile loads (UTL), defined as the highest tensile load in the load-displacement curves, of the composites rather than tensile stregnth were used to evaluate the mechanical properties of the composites. The fracture surfaces of the CF/SiC composites after tensile test were observed by scanning electron microscope (SEM), and the fiber pullout length of the CF/SiC composites after tensile test was measured from optical and SEM micrographs. The interface sliding stresses between the fiber and matrix were estimated according to the following equation [4,6].

$$h = (R\sigma_0 L_0^{1/m}/\tau)^{m/m+1} f(m) \qquad (4\text{-}1)$$

where h is the average fiber pullout length, τ is interface sliding stress, R is radius of the fiber, L_0 and σ_0 are scale parameters in Weibull expression, m is Weibull modulus and $f(m)$ is a function of m. The Weibull expression is as follows.

$$P_f(L,\sigma) = 1 - \exp(-\frac{L}{L_0}(\sigma/\sigma_0)^m) \qquad (4\text{-}2)$$

where $P_f(L, \sigma)$ is the probability of failure when the stress is σ and gauge length is L.

4.3. Results

4.3.1 Effect of heat treatment of carbon fibers on the properties of HMCF/SiC

4.3.1.1 Effect of heat treatment on structure and properties of carbon fibers

Figure 4.2 shows (002) peaks of the as-received carbon fibers and those heat-treated at 1400°C, 1500°C, 1600°C, 1800°C and 2000°C, respectively, and (111) peak of silicon as an internal standard. As (002) peak shifted to higher diffraction angle and became narrower with increasing HTT, it indicated improvement of crystallinity of the carbon fibers by heat treatment. Figure 4-3 shows the changes of d_{002} and $L_c(002)$ of the

carbon fibers with HTT. d_{002} of the carbon fibers decreased from 0.3476 nm of the as-received carbon fiber to 0.3422 nm of the carbon fiber heat-treated 2000°C, and $L_c(002)$ increased rapidly from 2.2 nm to 16 nm. Figure 4-4 shows the HRTEM image of the as-received HMCF. It was known that crystallites in HMCF had a good preferred orientation along the axis direction. Because of this, the crystallites could be easily improved by heat treatment at high temperatures.

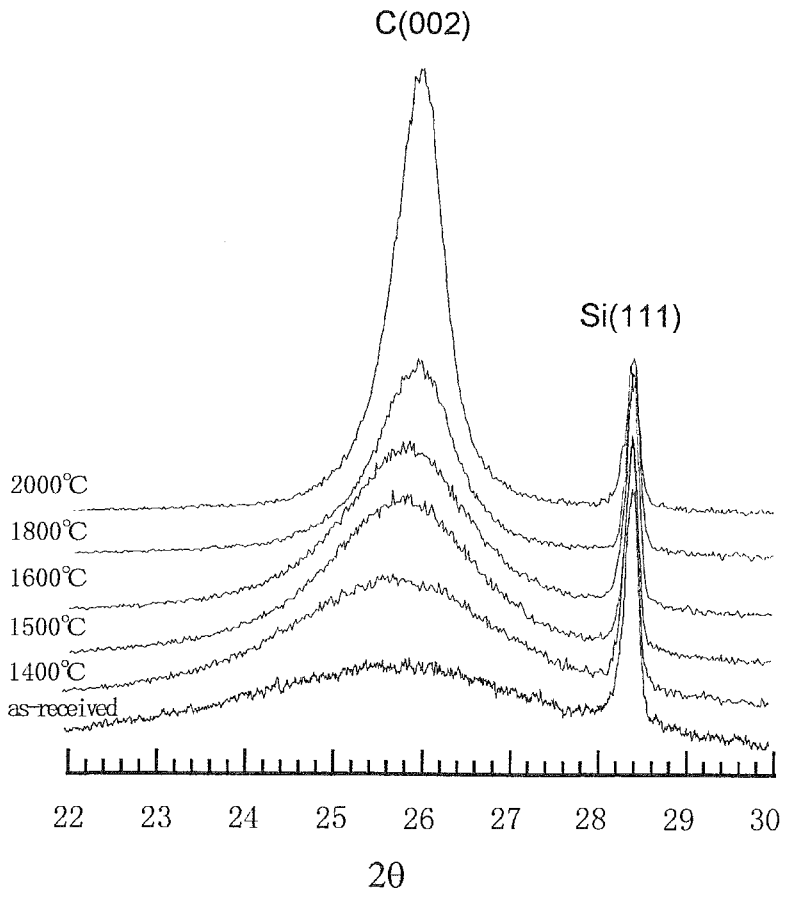

Fig. 4-2. (002) peaks of the HMCF heat treated at different temperatures for 1 hour.

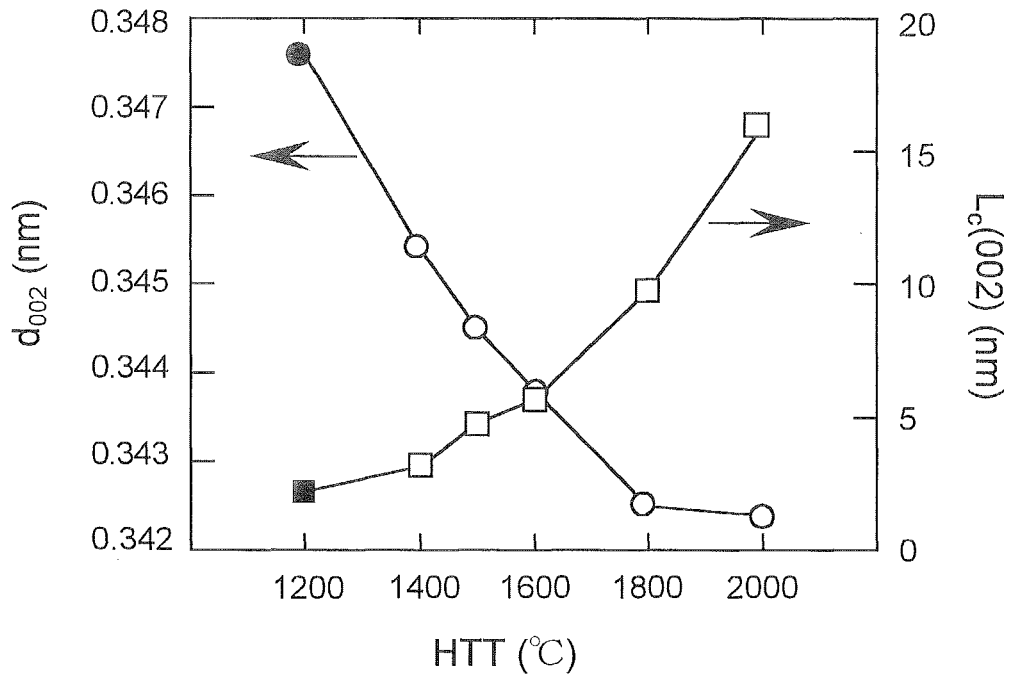

Fig. 4.3 Changes of d_{002} and L_c(002) of the carbon fibers with HTT. The black markers represent those of the as-received carbon fibers.

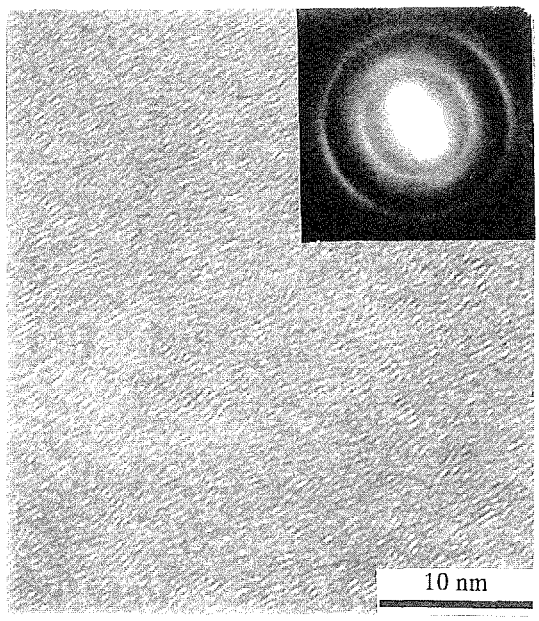

Fig. 4-4 (002) lattice fringe and electron diffraction pattern of HMCF.

Figure 4-5 shows the change of elastic modulus of the carbon fibers with HTT. The elastic modulus of HMCF increased slightly with HTT to 1600°C, then increased significantly above 1600°C. In general, elastic modulus of carbon fibers depends strongly on the crystallinity and crystallite preferred orientation of the carbon fibers. By examining Fig. 4-3, it was found that the crystallinity (d_{002} and $L_c(002)$) of HMCF showed a rapid change from 1600°C to 1800°C. This indicated that the increasing trend of elastic modulus of HMCF was consistent with that of the crystallinity. The good preferred orientation of crystallites in HMCF shown in Fig. 4-4 also suggested that elastic modulus of HMCF could be significantly improved by heat-treatment.

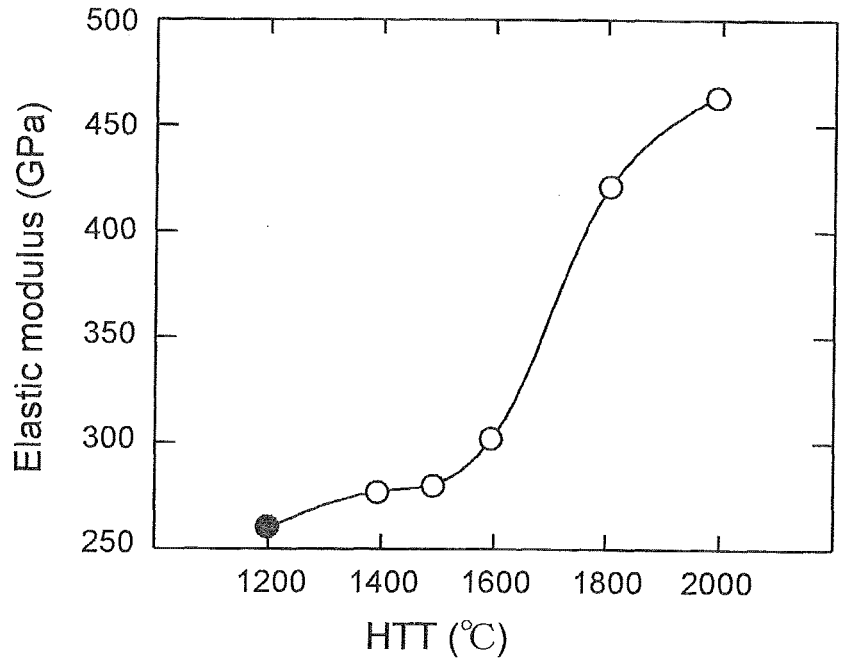

Fig. 4-5. Change of elastic modulus of HMCF with HTT.

Figure 4-6 shows changes of the tensile strength and Weibull modulus of HMCF with HTT. The average strength of HMCF increased slightly with HTT and the Weibull modulus decreased from around 5 to below 4 after heat treatment at all HTTs. The dependence of the strength of carbon fibers on the structure of the fibers was very complicated. The heat-treatment caused the evolvement of structure of the carbon fibers, including the improvement of degree of graphitization, growth of crystallites, preferred orientation of crystallites, change of the size and shape of pores and their distribution, etc. For example, the increase of elastic modulus has a positive contribution to the strength of fiber. The growth of crystallites makes the size of cracks large, thus has a negative effect on the strength of fiber. This indicated that the strength of carbon fibers can not be explained by only one structural parameter, as being described by Bright et al [7].

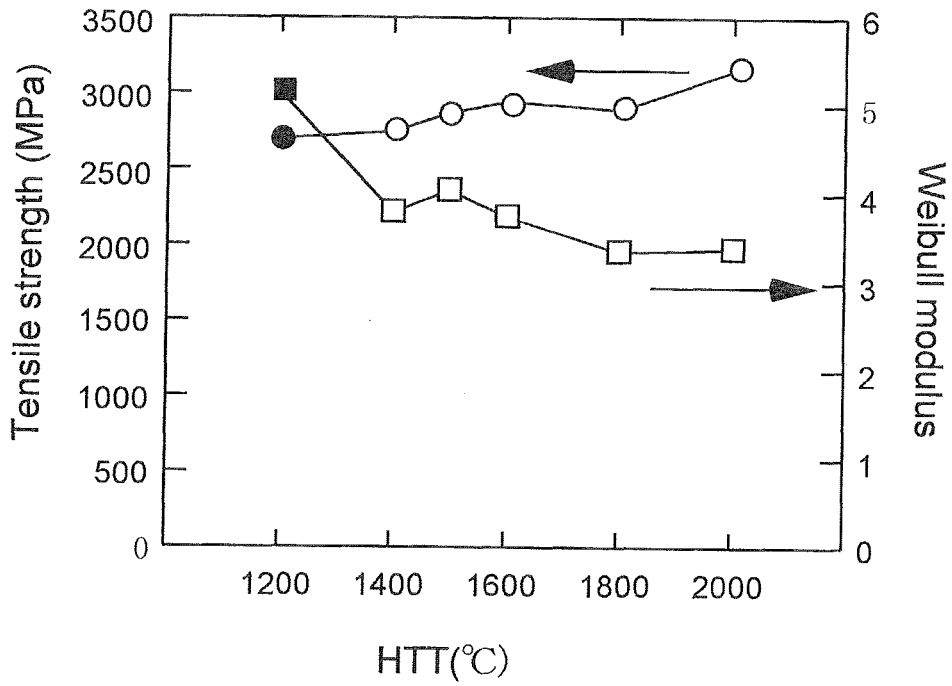

Fig.4-6. Change of tensile strength and weibull modulus of HMCF with HTT.

4.3.1.2 Effect of heat treatment of carbon fibers on properties of HMCF/SiC composites

Figure 4-7 shows the SEM micrographs of polished transverse sections of HMCF14/SiC, HMCF15/SiC and HMCF16/SiC. Some micropores formed by the decomposition of PCS existed in the samples. HMCF14/SiC showed relatively a higher fiber volume fraction of about 57%. HMCF15/SiC and HMCF16/SiC exhibited a lower fiber volume fraction of about 51-53%. HMCF18/SiC and HMCF20/SiC exhibited similar microstructures to those of HMCF15/SiC and HMCF16/SiC. The fiber volume fractions in the composites were about 51-57%. The porosity values of the composites after 9 times of impregnation of PCS were about 12-14%. It was observed that fibers were not well dispersed in HMCF15/SiC and in HMCF16/SiC. Many fibers were closely contacted, while the spacing between fibers is very large in some places.

Figure 4-8 shows change of UTL of the HMCF/SiC composites with HTT of the carbon fibers. UTL of HMCF/SiC exhibited a significant increase at the temperature range from 1400°C to 1500°C, while the strength of HMCF showed almost no change at this temperature range as shown in Fig. 4-6. HMCF14/SiC had low UTL of about 60~70 N. On the contrary, the UTL of the HMCF15/SiC were about 200 N, which was 3 times higher than that of the HMCF14/SiC. The UTL of HMCF/SiC did not change significantly with HTT above 1500°C.

The load-displacement curves of these HMCF/SiC samples are shown in Fig.4-9. HMCF14/SiC failed in a brittle mode, while the HMCF/SiC composites whose carbon fibers were heat-treated above 1500°C exhibited a non-linear fracture mode after initial elastic deformation. After the carbon fibers failed at the peak loads, extensive fiber pullout occured and the composites could still sustain some loads by the sliding friction stress between the fibers and the matrix. The tails of their load-displacement curves indicated the HMCF15/SiC had the longest and the HMCF16/SiC had the second longest fiber pullout, while the HMCF18/SiC and HMCF20/SiC showed the shortest fiber pullout. It was also found that the slope of initial linear deformation in the load-displacement curve increased with increasing HTT. This was consistent with the results of the elastic modulus of the carbon fibers as shown in Fig. 4-5.

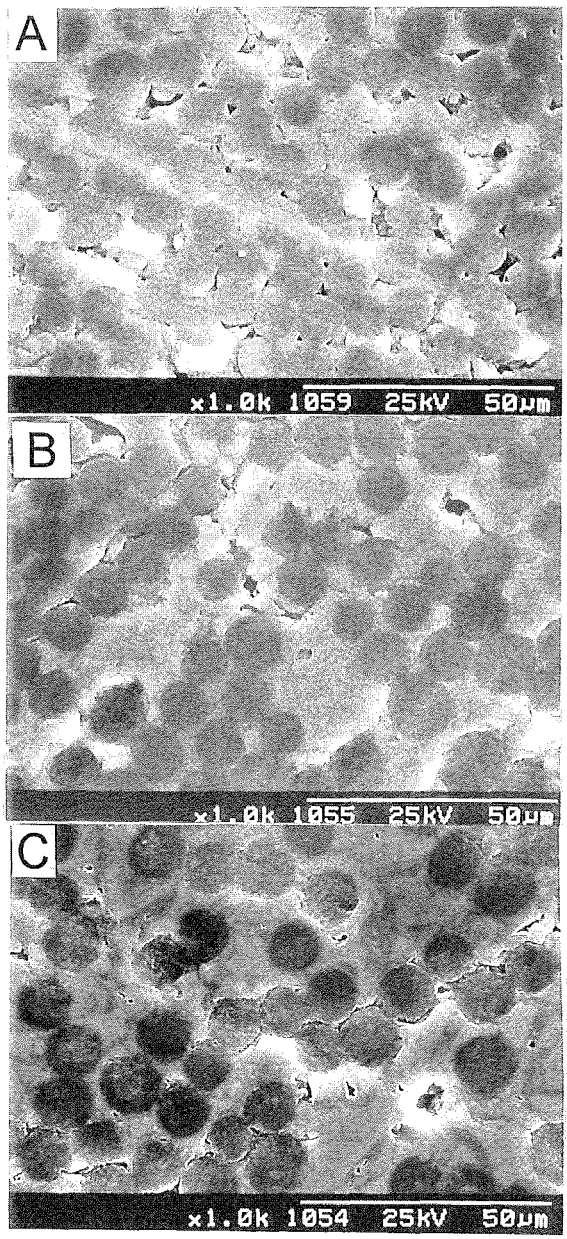

Fig. 4-7 SEM micrographs of polished transverse sections of HMCF14/SiC (A), HMCF15/SiC (B) and HMCF16/SiC (C).

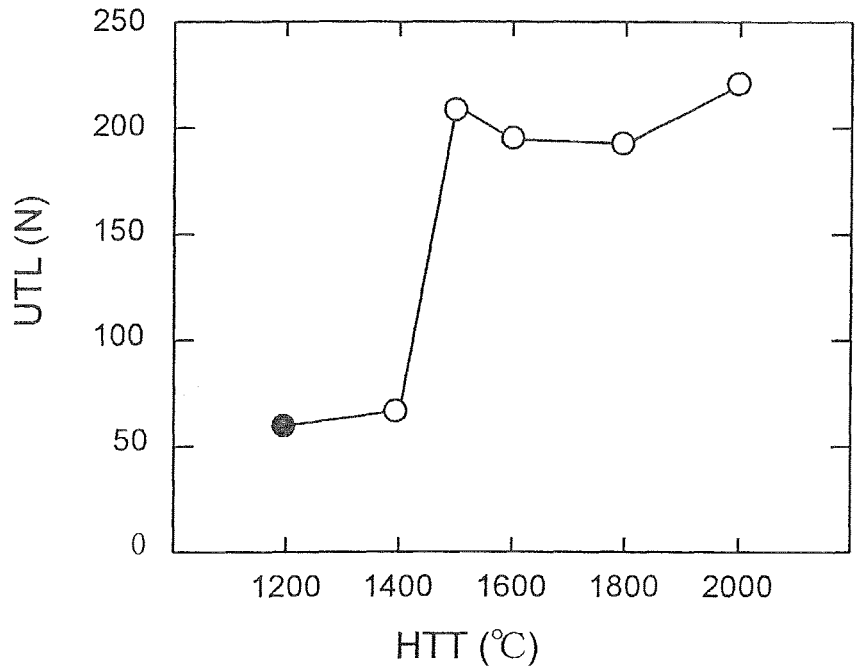

Fig. 4-8 Change of ultimate tensile load of HMCF/SiC with HTT of HMCF.

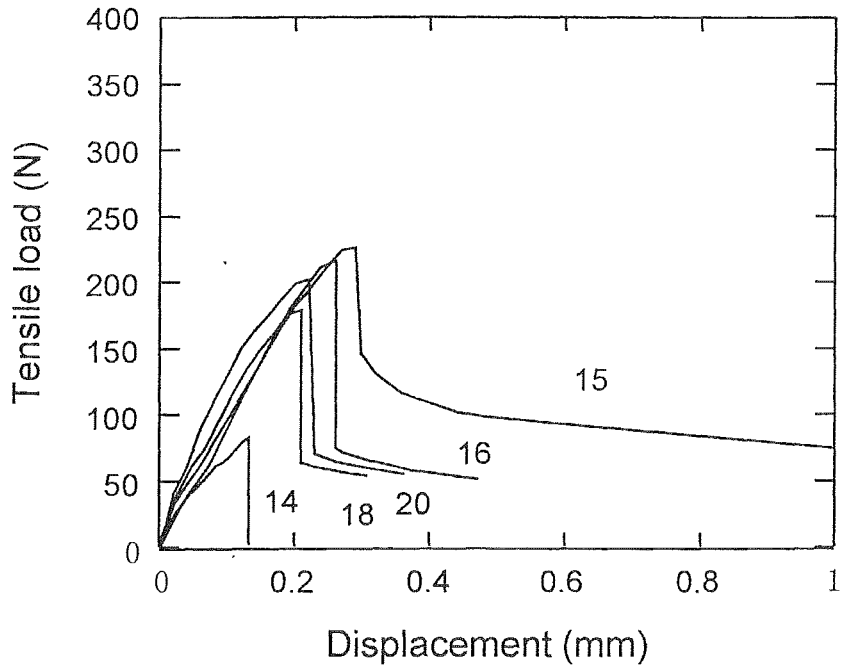

Fig. 4-9 The load-displacement curves of HMCF14/SiC, HMCF15/SiC, HMCF16/SiC, HMCF18/SiC and HMCF20/SiC.

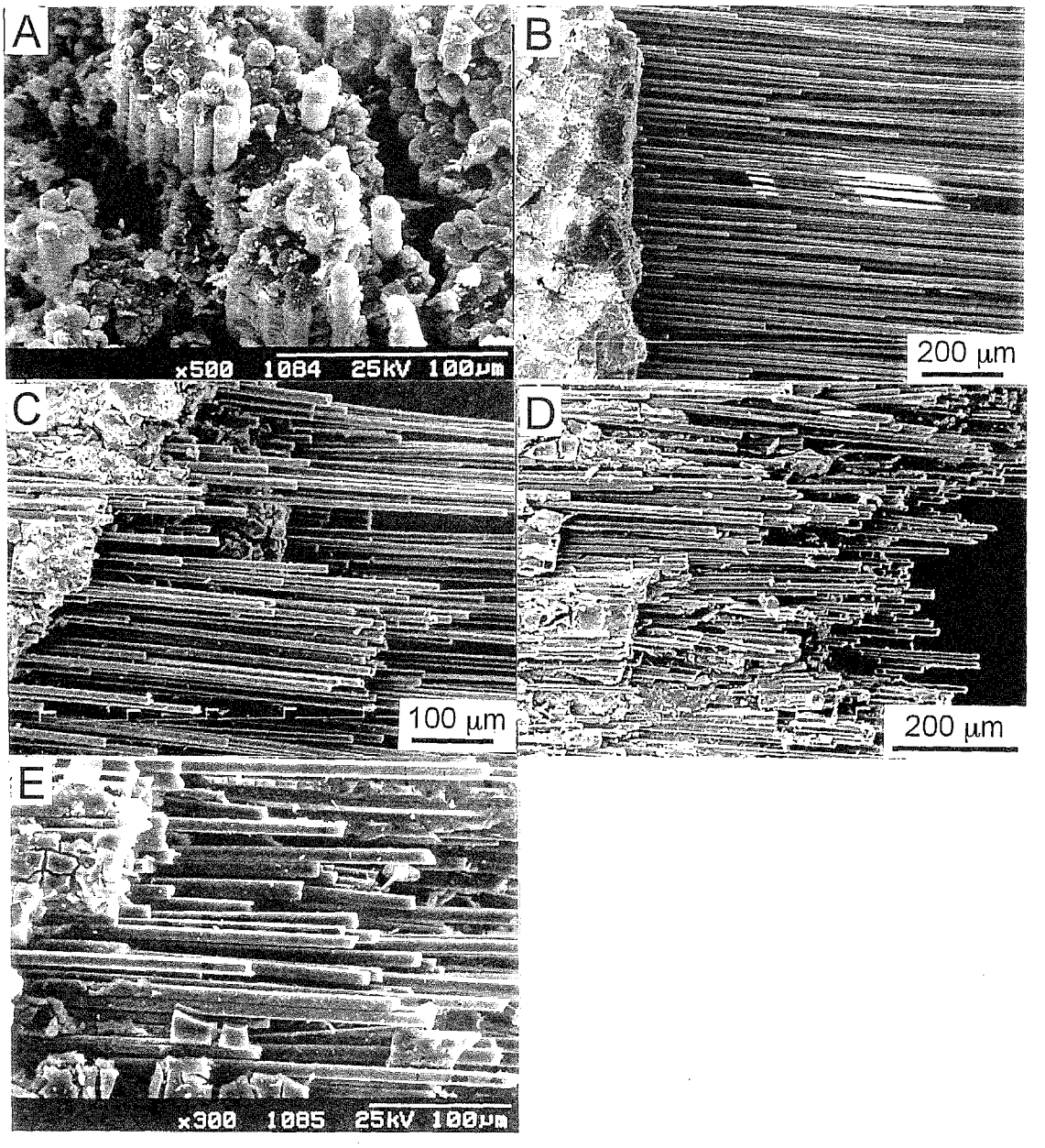

Fig. 4-10 SEM micrographs of the fracture surfaces of HMCF14/SiC (A), HMCF15/SiC (B), HMCF16/SiC (C), HMCF18/SiC (D) and HMCF20/SiC (E) composite samples after tensile tests.

Figure 4-10 shows the fracture morphology of the HMCF/SiC composites after tensile tests. HMCF14/SiC exhibited almost no fiber pullout and most of the fibers fractured at the same plane (Fig.10(a)). This brittle fracture behavior of HMCF14/SiC implied that the interface bonding between HMCF14 and the matrix was very strong. The propagation of matrix cracks could not be deviated since interfacial failure hardly happens, thus led to the fracture of the fibers because of the strong interfacial bonding. On the other hand, the HMCF/SiC composites whose carbon fibers were heat-treated above 1500°C exhibited extensive fiber pullout. In particular, HMCF15/SiC exhibited very long fiber pullout. The extensive fiber pullout suggested that the interface bonding strength in these composites was so weak that the matrix cracks could be blunted due to debonding of the interface.

After the debonding of the interface, the interface sliding stress becomes an important factor for controlling the properties of the composites. The interface sliding stresses were estimated from fiber pullout length according to the equation 4-2. As the *in situ* strength of the carbon fiber in the CF/SiC composites could not be measured directly, following experiments were carried out. The carbon fibers were incorporated in PCS powders, and heat-treated at 1200°C in N_2 for 1 hour. It was found that the strength of the carbon fibers showed no apparent change after the treatment. As no mechanical pressure was applied during the processing of the composites, the possible damage to the carbon fibers was chemical reactions between the fibers and matrix. Therefore, the Weibull parameters of carbon fibers were used. Accordingly, the interface sliding stresses of these composites were estimated as given in Table 4-1. The results showed that the interface sliding stress of the CF/SiC composites increases with the increase of HTT of the carbon fibers.

Table 4-1. Fiber pullout length and interface sliding stress of HMCF/SiC composite. (R=4.9 μm, L_0=25 mm)

samples	HTT of CF(°C)	h (μm)	τ (MPa)
HMCF15/SiC	1500	643.0	4.4
HMCF16/SiC	1600	128.0	39.6
HMCF18/SiC	1800	94.0	72.9
HMCF20/SiC	2000	74.3	106.6

4.3.2 Effects of heat treatment of carbon fibers on the properties of HSCF/SiC

4.3.2.1 Effects of heat treatment on the properties of HSCF

Figure 4-11 shows XRD (002) peaks of the as-received carbon fibers and those heat-treated at 1400°C, 1500°C, 1600°C, 1800°C and 2000°C, respectively, and (111) peak of silicon as an internal standard. The (002) peak shifted to higher diffraction angle and became narrower with increasing HTT, indicating the improvement of the crystallinity of the carbon fibers by heat treatment. Changes of the crystalline parameters, d_{002} and $L_c(002)$ with HTT are shown in Figure 4-12. d_{002} decreased gradually from 0.3479 nm of the as-received carbon fiber to 0.3433 nm of the carbon fiber heat-treated at 2000°C, and at the same time, $L_c(002)$ increased from 1.5 nm to 3.8 nm. However, it was obvious that improvement of the crystallinity was limited, since PAN-based carbon fibers were non-graphitizing carbon.

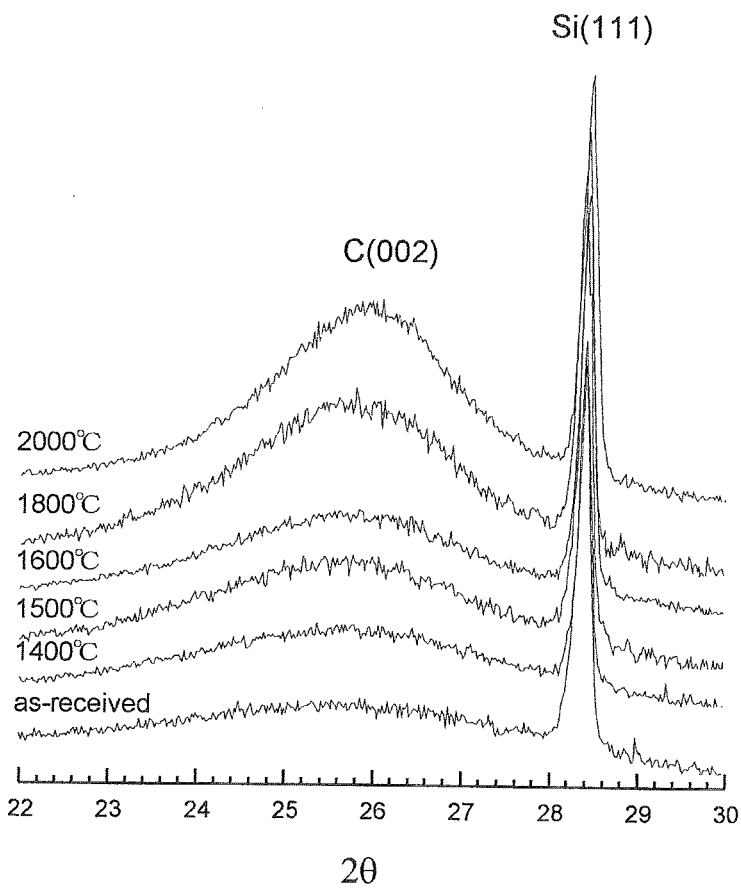

Fig. 4-11 The (002) peaks of the as-received HSCFand those after heat treated at 1400℃, 1500℃, 1600℃, 1800℃ and 2000℃.

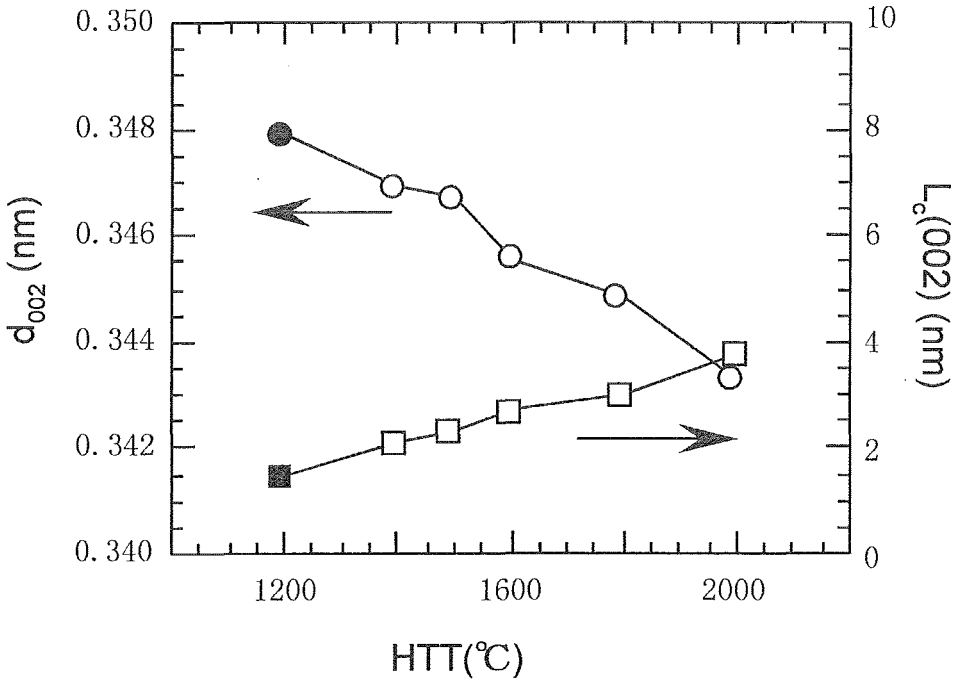

Fig. 4-12 Changes of d_{002} and $L_c(002)$ of HSCF with HTT. The black markers represent the as-received HSCF.

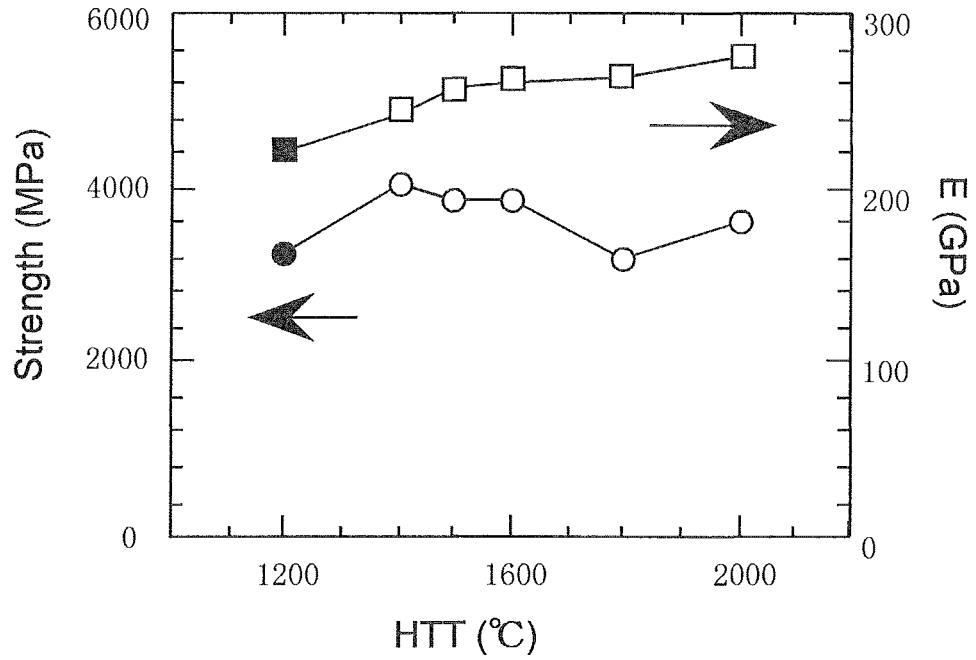

Fig. 4-13 Changes of tensile strength and elastic modulus of HSCF with HTT. The black markers represent the as-received HSCF.

Figure 4-13 shows changes of tensile strength and elastic modulus of the carbon fibers with HTT. The carbon fibers heat-treated at the temperatures between 1400°C and 1600°C showed the highest strength, and the strength of the carbon fibers decreased at the HTTs above 1600°C. The tendency was similar to the results of other researchers [8]. It was also observed that the elastic modulus of the carbon fibers increased slightly with increasing HTT from 225 GPa of the as-received carbon fibers to about 270 GPa of the fibers heat-treated at 2000°C. The elastic modulus of carbon fibers depend strongly on the crystallinity and crystallite preferred orientation of the carbon fibers. The increasing trend of the elastic modulus of the carbon fibers with HTT was consistent with those of d_{002} and $L_c(002)$. Since the PAN-based carbon fibers were non-graphitizing carbon, its crystallinity was only slightly improved by the heat treatment, consequently the modulus of the carbon fibers exhibited slight increase with increasing HTT.

4.3.2.2 Effect of heat treatment on the properties of HSCF/SiC composites

Figure 4-14 shows SEM micrographs of the polished transverse sections of HSCF14/SiC, HSCF15/SiC, HSCF16/SiC, HSCF18/SiC and HSCF20/SiC. HSCF14/SiC showed higher fiber volume fraction (about 65%) and existence of large pores between the fibers, which was similar microstructure with those HSCF12/SiC composites. While HSCF15/SiC, HSCF16/SiC and HSCF20/SiC showed lower fiber volume fraction (46-50%) and existence of small pores. The boundaries of particles of matrix, which were obviously formed during multiple impregnation-pyrolysis process, are clearly observed in HSCF15/SiC, HSCF16/SiC and HSCF20/SiC. Large particles formed in initial impregnation/pyrolysis processes when large pores still existed in the samples, and small particles formed at following impregnation/pyrolysis process when pores in the samples became much smaller. HSCF18/SiC showed similar fiber volume fraction and microstructure of HSCF15/SiC, HSCF16/SiC and HSCF20/SiC.

It was believed that the difference of the microstructures between HSCF14/SiC and the other composites was related with microstructures of the carbon fibers and the impregnation process of PCS. Since HSCF14 was heat-treated at lower temperature, it

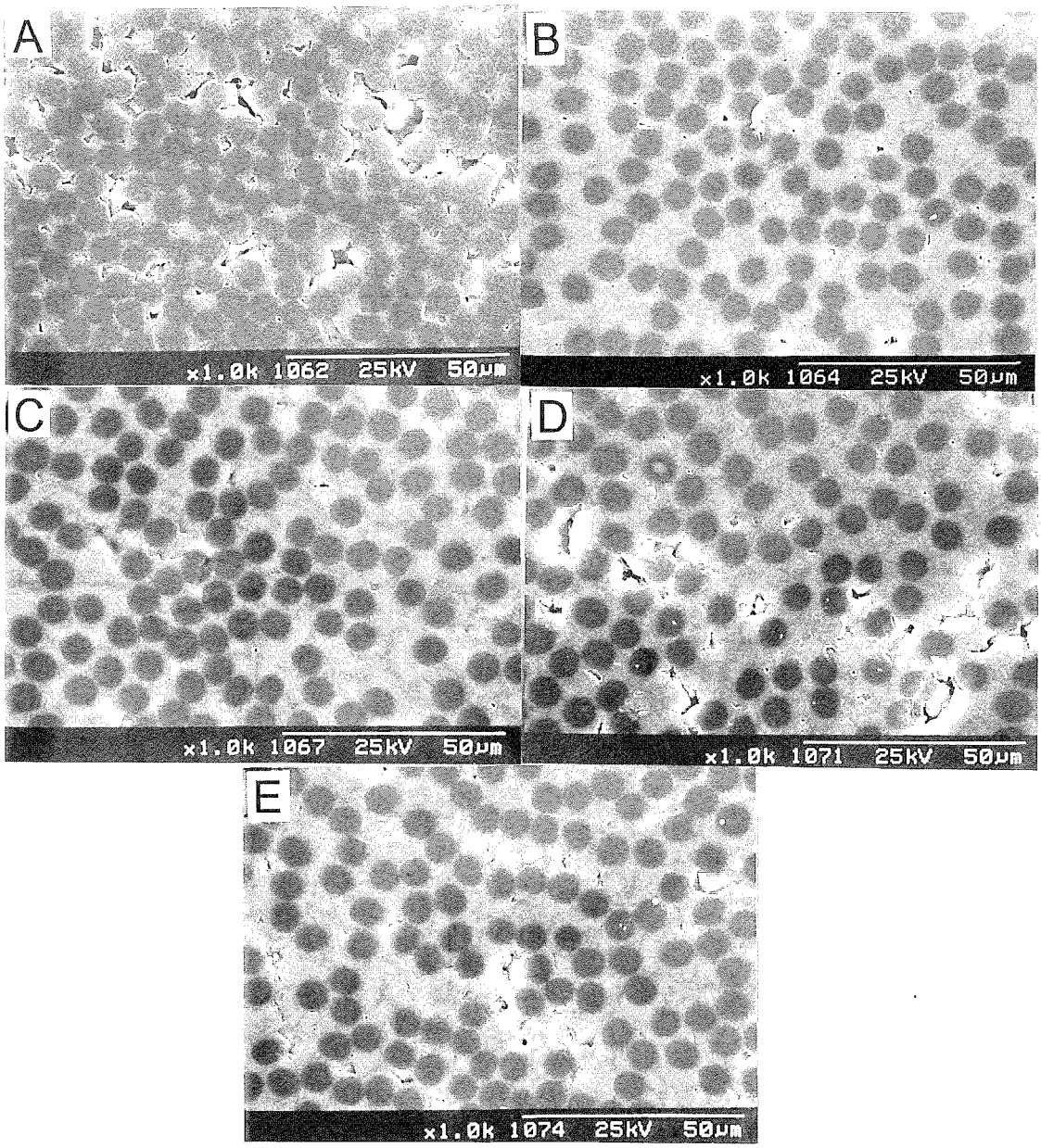

Fig. 4-14 SEM micrographs of polished transverse sections of HSCF14/SiC (A), HSCF15/SiC (B), HSCF16/SiC (C), HSCF18/SiC (D) and HSCF20/SiC (E).

exhibited strong bonding with PCS and its pyrolytic product. Consequently, the shrinkage of PCS occurred during drying and pyrolysis process made the spacing between carbon fibers smaller, leading to high fiber volume fraction. On the other hand, for the fibers heat-treated 1500°C or above, they exhibited relatively weak bonding with PCS and its pyrolytic product; hence, the shrinkage of PCS during drying and pyrolysis stages did not lead to significant decrease in the fiber spacing, because the matrix possibly separated from the fibers, and this resulted in lower fiber volume fraction. The possible separation of PCS-derived matrix from fibers permitted more effective subsequent impregnation of PCS.

Figure 4-15 shows the change of the ultimate tensile loads of the HSCF/SiC composites with HTT of the carbon fibers. By comparing Fig.4-13 and Fig.4-15, it appeared that the tensile loads had no direct relation with the strength of the reinforcing carbon fibers, and that strong fibers did not necessarily result in strong HSCF/SiC composites, because the strength of the fibers in fiber/ceramic composite was seldom fully exploited. The ultimate strength of the composites depended largely on how well the strength of the carbon fibers was exploited, in which the interface characteristics play an important role. From Fig.4-13, the as-received-HSCF/SiC and HSCF14/SiC whose carbon fibers were heat-treated below 1400°C exhibited low UTL of about 80 N, while HSCF15/SiC with carbon fiber heat-treated at 1500°C exhibited UTL of 230 N, although the strength of HSCF15 is similar to that of HSCF14. HSCF16/SiC and HSCF18/SiC exhibited highest UTL of about 370 N, but HSCF20/SiC exhibited UTL of about 260 N, lower than those of HSCF16/SiC and HSCF18/SiC.

Fig.4-16 shows the load-displacement curves of HSCF/SiC composites. HSCF14/SiC failed in a brittle mode after initial linear deformation; while HSCF15/SiC and HSCF20/SiC showed non-linear deformation and failed at moderate displacement after initial linear deformation. HSCF16/SiC and HSCF18/SiC showed non-linear deformation, failed at large displacement and exhibited high ultimate tensile loads. The difference of the fracture behavior between these composites was thought to be related with the interface strength between fiber and matrix. When the loads of all the composite samples reached peak values, they decreased to zero immediately, with no

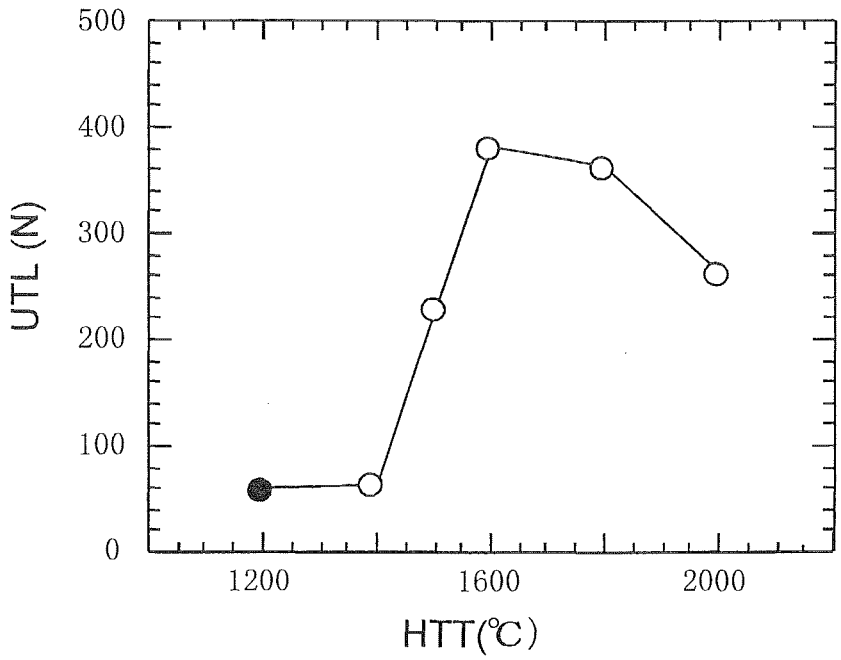

Fig. 4-15 Change of ultimate tensile loads of HSCF/SiC with HTT of the carbon fibers.

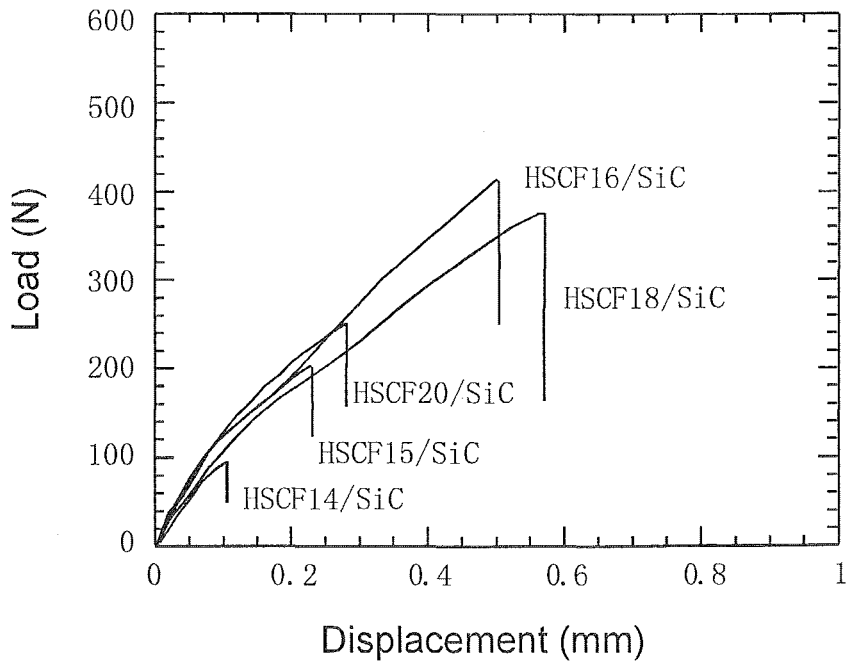

Fig. 4-16 Load-displacement curves of the HSCF/SiC. whose carbon fiber was heat-treated at different temperature.

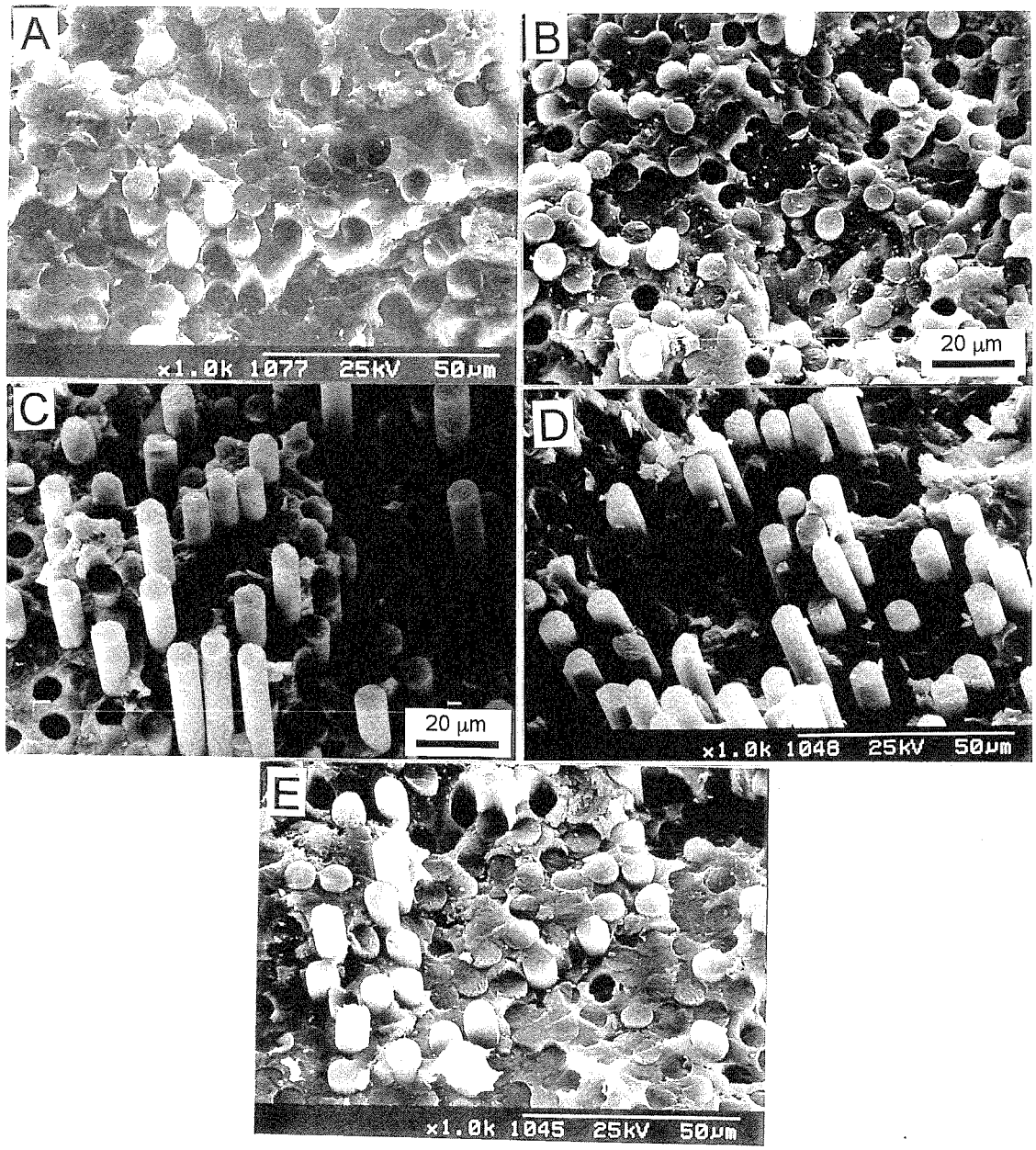

Fig. 4-17 SEM micrographs of fracture surfaces of HSCF14/SiC (A), HSCF15/SiC (B), HSCF16/SiC (C), HSCF18/SiC (D) and HSCF20/SiC (E).

gradual decrease in load being observed. Their fracture surfaces after tensile tests, as shown in Fig.4-15. HSCF14/SiC exhibited flat fracture surface, and the fibers and matrix failed at the same plane (Fig.4-15A). Observation of the fracture surfaces of the carbon fibers in higher magnification revealed that most of the fibers exhibited uniform fracture surfaces as shown in Fig.4-18a. It suggested that the failure of the carbon fibers in HSCF14/SiC were not caused by their own intrinsic flaws, but caused by rapid extension of matrix cracks. HSCF15/SiC and HSCF20/SiC exhibited short fiber pullout (less than 5 μm), and HSCF16/SiC and HSCF18/SiC exhibited extensive fiber pullout (about 20-30 μm) in their fracture surfaces, and the observation of the carbon fibers revealed that most of the carbon fibers exhibited typical "hackle form" surface (Fig.4.18b and Fig.4.18c), indicating the failure of the fibers in these composites were caused by their own intrinsic flaws, not by matrix cracks.

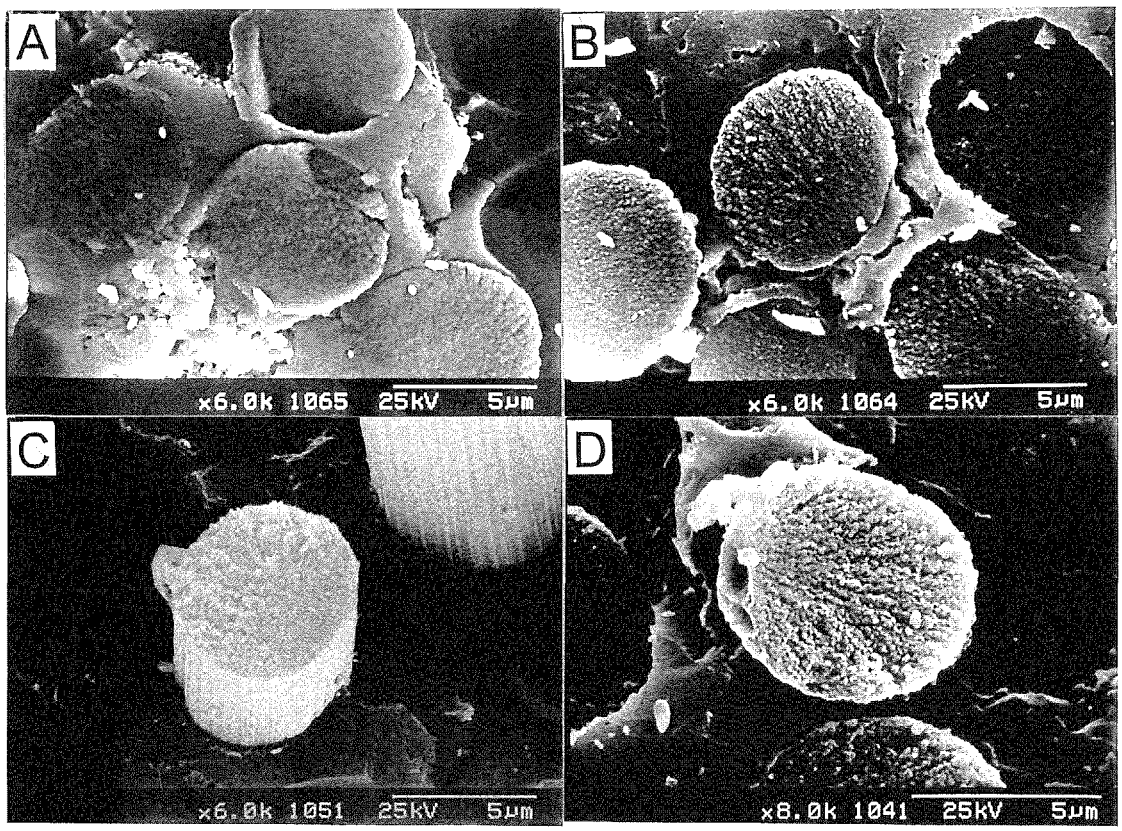

Fig. 4-18 The mophology of cross sections of the carbon fibers after tensile test of HSCF14/SiC (A), HSCF15/SiC (B), HSCF16/SiC (C), HSCF18/SiC (D) and HSCF20/SiC (E).

4.4 Discussion

4.4.1 Factors affecting interface bonding

The pitch-based HMCF is graphitizable, while the PAN-based HSCF is non-graphitizable. Therefore, the crystallinity of HMCF was significantly improved with increasing HTT, while that of HSCF was slightly improved. Consequently, elastic modulus of the HMCF increased remarkably with increasing HTT, whereas HSCF showed a slight increase in elastic modulus. They also showed different increasing trend of tensile strength with HTT.

The strength of fiber is seldom fully exploited in fiber/ceramic composites. The strength of CF/SiC is dependent on how well the strength of carbon fibers is exploited. The evolution of structure of the carbon fibers with HTT is more important to the mechanical properties of the CF/SiC composites. The interface bonding between the fibers and the matrix is dependent upon the structure of the fibers and the matrix as well as processing conditions. As the same matrix and processing conditions were applied for preparing the CF/SiC composites in this experiment, it was reasonable to consider that the interface was dependent upon only the structure of the carbon fibers with different HTT.

The PCS-derived product at 1200°C was nearly amorphous state, containing free carbon and silica, as stated in Chapter 2. This PCS-derived matrix tended to bond strongly with those carbon fibers heat-treated below 1500°C, but it showed weak interface bonding with the graphitized carbon fibers. Carbon fibers heat-treated below 1500°C had more functional groups on their surfaces and they were more active. The graphitized carbon fibers have lower activity and fewer functional groups on the surfaces, resulting in weak bonding with PCS-derived SiC matrix. For HSCF and HMCF heat-treated between 1400°C to 2000°C, the structural evolution of the carbon fibers should give a critical point. Interface debonding occurred above this point, and brittle failure occurred below this point. From the results in Section 4.3, the critical point was found to at 1500°C for HMCF, and at 1600°C for HSCF.

By comparing the cystallinity of HMCF heat-treated at 1500°C with that of HSCF heat-treated at 1600°C, the d_{002} and $L_c(002)$ of HMCF15 are 0.3444 nm and 48 nm

respectively; whereas the d_{002} and $L_c(002)$of HSCF16 are 0.3455 nm and 28 nm respectively. It was known that the crystallinity of HMCF15 was better than that of HSCF16. In fact, the d_{002} and $L_c(002)$of HSCF16 are almost same as those of HMCF14 which was heat-treated at 1400°C. These facts suggested that the crystallinity of carbon fibers, which was characterized by d_{002} and $L_c(002)$, was not an absolute criterion to distinguish if interface debonding would occur for CF/SiC with different carbon fibers. This is because the d_{002} and $L_c(002)$ only give an average information on the entire fibers. Many researchers pointed out that the structure of skin of carbon fibers were different from the structure of inner part of carbon fibers. The results in Chapter 2 also demonstrated it. For the same fibers, the crystallinity still provides useful information to explain the interface bonding.

4.4.2 Interface sliding stresses

After interface debonding occurs, the interface sliding stress between fiber and matrix plays an important role in the properties of composites. The interface sliding stress is expressed as following [9,10]:

$\tau=\tau_0+\mu\sigma_{rr}$

where μ is the Coulomb friction coefficient, σ_{rr} is the compression normal to the interface and τ_0 is a term associated with fibre roughness.

The interface sliding stress between the fibers and matrix is related to the roughness of the fibers and residual compressive stresses normal to the interface. The residual compressive stress is caused by the shrinkage of pyrolysed PCS and the thermal expansion misfit between the fibers and the matrix. Because all the carbon fibers have similar thermal expansion, and the composites were processed under completely same conditions, it is reasonable to assume all the CF/SiC composites have a similar compressive stress and only the roughness of the fibers needs to be considered. Based on this assumption, the increase of interfacial sliding stress implies that the roughness of the carbon fibres increases with increasing HTT. With the increase of HTT, the crystallites in the carbon fibers became larger and stiffer. On the fiber surface, some places shrank and some places expanded, so that the surface of the carbon fibers might

become rougher with the increase of HTT.

4.5 Conclusions

From the above results and discussion, the following conclusions were obtained:

(1) The tensile strength of pitch-based HMCF increased slightly with increasing heat treatment temperature. The elastic modulus of the carbon fibers increased slightly below 1600°C and significantly above 1600°C, which was consistent with the trend of the crystallinity of the carbon fibers with HTT.

(2) The HMCF/SiC composites with carbon fibers heat-treated below 1400°C gave a low strength and brittle fracture behavior. On the other hand, the HMCF/SiC composites with carbon fibers heat-treated above 1500°C possessed 3 times higher strength and non-brittle fracture behavior with extensive fiber pullout. This was attributed to the weakening of the interface bonding by the heat treatment of the carbon fibers.

(3) In the HTT range of 1500°C to 2000°C, the fiber pullout length of the HMCF/SiC composites decreased and the interface sliding stress between the fibers and the matrix increased with HTT, which was considered to be due to enhanced surface roughness of the carbon fibers with increasing HTT.

(4) The PAN-based HSCF exhibited highest strength when heat-treated at 1400°C, 1500°C and 1600°C, and the strength decreased when the fiber was heat-treated at higher temperatures. The elastic modulus of the carbon fibers increased slightly with HTT, and the tendency was consistent with that of the crystallinity of the carbon fibers with HTT.

(5) The HSCF/SiC composites whose carbon fibers were heat-treated below 1400°C showed low strength and completely brittle fracture behavior. With the increase of HTT to 1800°C, the HSCF/SiC composites showed increased ultimate tensile load and long fiber pullout length, because of decreased interface bonding. For the carbon fibers heat-treated at 2000°C, the HSCF/SiC composite showed lower ultimate tensile load and shorter fiber pullout than HSCF16/SiC and HSCF18/SiC. It might be due to the increase of the interface sliding stress caused by the surface

roughening of the carbon fibers.

(6) The above results indicated that the mechanical properties of the composites could be controlled by heat treatment of the reinforcing carbon fibers. HMCF/SiC exhibited longer fiber pullout, thus had a higher toughness than HSCF/SiC.

References

1. A. G. Evans and F. W. Zok, J. Mater. Sci., **29**, 3857 (1994).
2. W. A. Curtin, J. Am. Ceram. Soc., **74**, 2837 (1991).
3. Cao, H. C., Bischoff, E., Sbizero, O., Ruhle, M., Evans, A. G., Marshall, D. B., and Brennan, J. J., J. Am. Ceram. Soc., **73**,1691 (1990).
4. Thouless, M. D., Sbaizero, O., Sigl, L. S. and Evans, A. G., J. Am. Ceram. Soc., **72**, 525 (1989).
5. Otani S., Okuda, K. and Matsuda, S., In "Tanso Seni", Kindai Hensyu Sya, Japan, 1986, p.676.
6. M. Sutcu, J. Mater. Sci., **23**, 928 (1988).
7. A. A. Bright and L. S. Singer, Carbon, **17**, 59 (1979).
8. W. N. Reynolds, Chemistry and Physics of Carbon, Vol. 11 (Edited by P. A. Thrower) pp. 2-65, Marcel Dekker, Inc.
9. P. D. Jero, R. J. Kerans, and T. A. Parthasarathy, J. Am. Ceram. Soc., **74**, 2793 (1991).
10. R. J. Kerans, and T. A. Parthasarathy, J. Am. Ceram. Soc., **74**, 1585 (1991).

Chapter 5 Modification of the Interface between fiber and matrix by Boron Addition and Oxidation Resistance of CF/SiC-B Composites

5.1 Introduction

In the previous chapters, it has been found that the highly-graphitized carbon fiber/SiC prepared from impregnation and pyrolysis of polycarbosilane exhibited high strength with non-brittle fracture mode, while the poorly-graphitized carbon fiber/SiC showed low strength with brittle fracture mode. The results suggested that the interface of CF/SiC could be controlled by tailoring the structure of fibers. Particularly, surface of the fiber gave an important role to fiber/matrix interface and the interface controlled the mechanical properties of the composites. To control the fiber/matrix interface, many studies have focused on coatings of fiber by pyrolytic carbon or BN [3,4]. As another method to control the interface, it was considered to modify the fiber/matrix interface by introducing some additives to matrix. In this chapter effect of boron addition on the mechanical properties of the composites will be clarified.

On the other hand, CF/SiC composites have a serious drawback that carbon fibers are rapidly oxidized at elevated temperatures in an oxidizing environment. To protect the composites from oxidation, diffusion-barrier coatings of various materials such as SiC, TiC, BN, Si_3N_4, TiB_2, $MoSi_2$, or their multi-layer coating have been developed [5,6], and they gained success to some extent. Among coating materials, boron and their compounds were found to be good oxidation resistant materials to prevent oxidation of carbon materials, especially when they were combined with other refractory materials. However, if cracks occurred because of the mismatch of thermal expansion between the coatings and the composites, or if the coatings are damaged, the coatings will be difficult to prevent the oxidation of the carbon fibers. Kobayashi *et al* demonstrated that borosilicate glass could be formed on the surface of SiC/B_4C/C ternary composites when they were oxidized, and it protected the carbon component from oxidation [7]. These composites tended to exhibit self-healing effect, because oxidation of B_4C and SiC resulted in borosilicate which filled the cracks or pores. Greil *et al* also reported that boron could be used as active filler in ceramic matrix composites [8,9]. In

boron/preceramic-polymer system, reactions of boron with N_2 or polymer at high temperature resulted in expansion of volume, and the porosity of the composite caused by decomposition of the polymer decreased. This active-filler technique was considered as a method to diminish the processing time of fiber/ceramic composites. Therefore, it could be expected that boron addition to CF/SiC would influence not only the mechanical properties but also the oxidation-resistance of the composites.

In this chapter, the effects of boron addition were studied on the mechanical properties and oxidation resistance of CF/SiC prepared by impregnation of polycarbosilane.

5.2 Experimental Procedure

The boron powder used in the experiments had an average size of 0.1 μm. Three types of continuous carbon fibers, HSCF, HMCF and CF70, were used as the reinforcements. Polycarbosilane (PCS) was used as the precursor for the SiC matrix. The carbon fibers were passed through a boron-PCS-toluene slurry with a mass ratio of 10:5:100 in ultrasonic bath and they were wound on a metal frame by using the filament winding technique. The fiber form unidirectionally wound was placed in a metal die and pressed. After drying at 80°C, the prepregs were pyrolysed in N_2 at 1200°C for 1 hour. To densify the composites, the prepregs were repeatedly impregnated with 50wt% PCS toluene solution in vacuum and subsequently pyrolysed in N_2 at 1200°C for 1 hour for 9 to 12 times. The composites obtained with boron addition were named as HSCF/SiC-B, HMCF/SiC-B and CF70/SiC-B, respectively.

The mechanical properties of the composites were evaluated using four-point bending test with a cross head speed of 0.5 mm/min and support span of 30 mm and loading span of 10 mm in a universal testing machine. The load-displacement curves were recorded simultaneously by using a load-cell and laser extensometer. The sizes of specimens for flexural strength tests were about 3.5 mm in width and 1 mm in thickness.

Fracture surfaces of the specimens after four-point bending test were examined by SEM. To understand the reaction of boron with N_2, boron powders were heat-treated at 1200°C in N_2 for 3 hour and analyzed by x-ray diffraction (XRD). HMCF/SiC-B

samples were polished and thinned by ion-milling, and then were observed by transmission electron microscope (TEM).

The composite samples were cut to the size of $5 \times 5 \times 1$ mm^3 for oxidation tests. The oxidation tests were conducted in a TGA furnace with a heating rate of 5°C/min and an air flow rate of 30 cc/min. Some of the cut samples were coated with B-SiC by dipping the samples in the above mixed slurry of polycarbosilane, boron and toluene, and subsequently pyrolysed at 1200°C for two times. These samples with the coating were named as CF/SiC-B-coating, and they were also evaluated by oxidation test in the TGA furnace. The samples before and after oxidation were also observed by SEM. The samples after oxidation were incorporated in resin and polished. Then they were observed by SEM.

5.3 Results and Discussion

5.3.1 Microstructure of CF/SiC with boron addition

Fig. 5-1 shows SEM micrographs of carbon fiber after dipping in the slurry of boron-PCS-toluene and drying. It was observed that boron-PCS were distributed on the surfaces of the carbon fibers as well as in the spaces between the fibers. Although B-PCS did not form a complete coating, they were relatively uniformly distributed on the fibers. Because boron had an average size of about 0.1 μm and was well dispersed in the slurry, it was thought that B and PCS were uniformly mixed in the B-PCS layer on the carbon fibers. By assuming that the ratio of B to PCS is the same as that in slurry, the amount of boron addition in ultimate CF/SiC composites was calculated from weight change of carbon fibers after slurry infiltration, as shown in Table 5-1.

Table 5-1 The effects of B addition on the properties of CF/SiC

Composites	V_f	Amount of boron relative to CF	Porosity (%)	Flexural strength (MPa)	Fracture mode
HSCF/SiC-B	50%	10%	13.5	269	brittle
HMCF/SiC-B	49%	12%	12.2	690	non-brittle
CF70/SiC-B	35%	7%	10.2	757	non-brittle

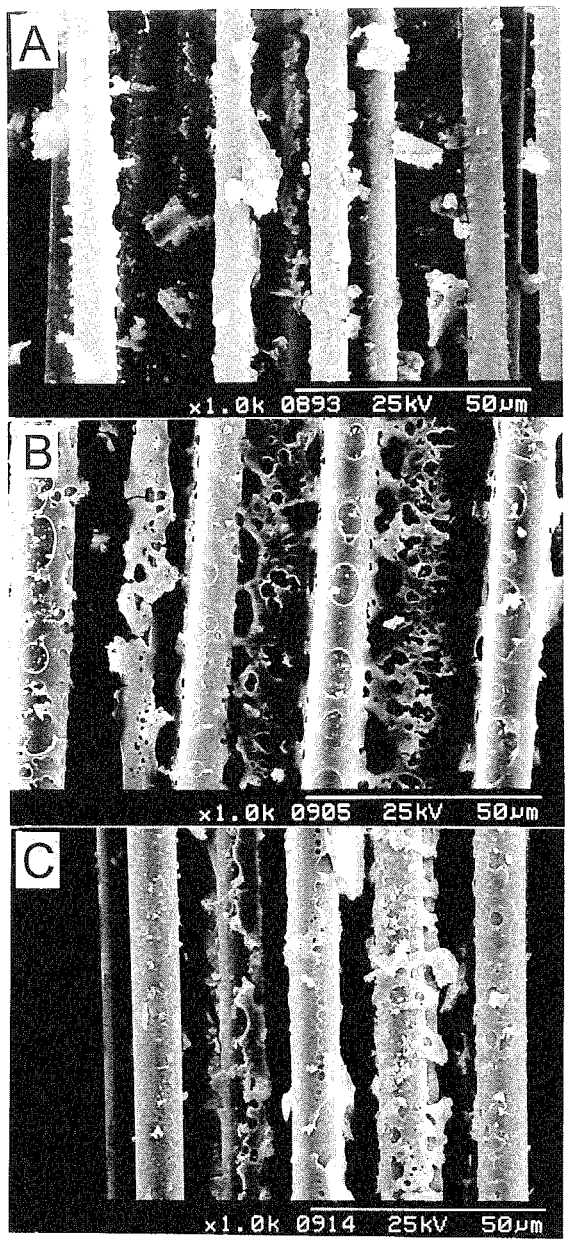

Fig. 5-1 The morphology of the carbon fibers after B/PCS slurry infiltration (A) HSCF, (B) HMCF, and (C) CF70.

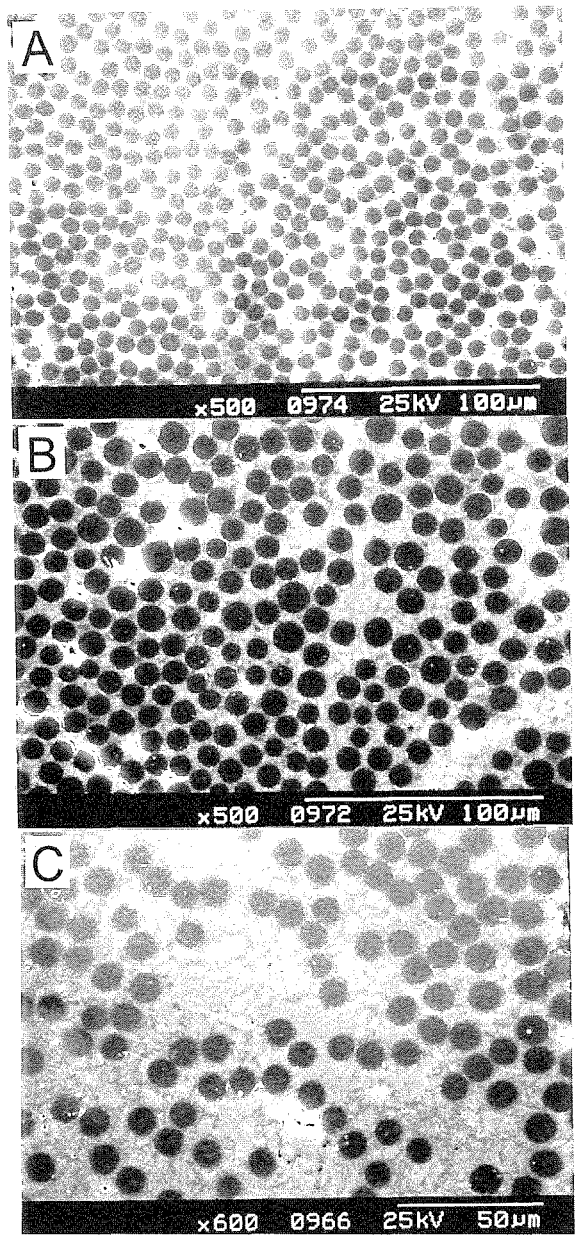

Fig. 5-2 SEM micrographs of polished transverse sections of HSCF/SiC-B (A), HMCF/SiC-B (B) and CF70/SiC-B (C).

HSCF/SiC-B, HMCF/SiC-B and CF70/SiC-B were polished and observed with an optical microscope. As shown in Fig. 5-2, the carbon fibers were uniformly distributed in the matrix. By comparing the data of Table 5-1 with the results in Chapter 2, it was found that the boron addition lowered the fiber volume fractions of HSCF/SiC-B and HMCF/SiC-B. The decrease of fiber volume fraction was thought to be due to enlargement of spacing between fibers by boron powder addition. The CF70/SiC had a low fiber volume fraction, so boron addition gave a minor effect on the fiber volume fraction of CF70/SiC-B.

5.3.2 Flexural properties of CF/SiC with boron addition

By comparing the data of Table 5-1 with the results in Chapter 2, it was noted that boron addition increased the flexural strength of HSCF/SiC from 220 MPa to 269 MPa. Considering the lower fiber volume fraction in HSCF/SiC-B, the effects of boron addition would be more marked. However, their fracture modes were both brittle. So the effect of boron addition on HSCF/SiC was thought to be slight.

On the other hand, addition of boron had a remarkable effect on the flexural strength of HMCF/SiC. The strength of HMCF/SiC-B was 690 MPa which was about 2.5 times higher than the strength of the composite without boron addition. Moreover, the fracture mode of HMCF/SiC-B showed non-brittle behavior, while HMCF/SiC without boron showed brittle behavior. It was considered that the conversion of fracture mode by boron addition for HMCF/SiC was due to weakening of fiber/matrix interface to a critical level that interface debonding occurred.

It was also found that boron addition decreased the flexural strength of CF70/SiC. CF70 was a highly-graphitized carbon fiber found to bond weakly with SiC matrix in composite, therefore, CF70/SiC had a high strength and non-brittle fracture mode. The boron addition to CF70/SiC decreased the interfacial strength of CF/SiC, as a result, the shear strength of CF70/SiC was also reduced, hence, CF70/SiC with boron addition showed lower flexural strength.

Fig. 5-3 shows the load-displacement curves of CF/SiC-Bs during bending tests. As mentioned above, HSCF/SiC and HSCF/SiC-B showed brittle fracture mode that the

specimens failed catastrophically. In these composites, the propagation of cracks into fiber could not be suppressed due to strong fiber/matrix interface. So boron addition had no significant effect on the interfacial strength of HSCF/SiC.

CF70/SiC and CF70/SiC-B showed non-linear load-displacement curves. After initial elastic deformation, load increased non-linearly with displacement. This suggested that matrix cracks were propagated to debond fiber/matrix interface, and only fibers had to support the further load. From the curves, it was suggested that shear failure occurred in CF70/SiC-B during loading, probably because boron addition lowered the interfacial strength and shear strength.

HMCF/SiC exhibited brittle fracture mode like HSCF/SiC. However, HMCF/SiC-B did not fail in a brittle mode. After initial elastic deformation, shear fracture occurred and the sample could still support load. The boron addition probably decreased the interfacial strength and therefore the interface debonding occurred when matrix cracks propagated.

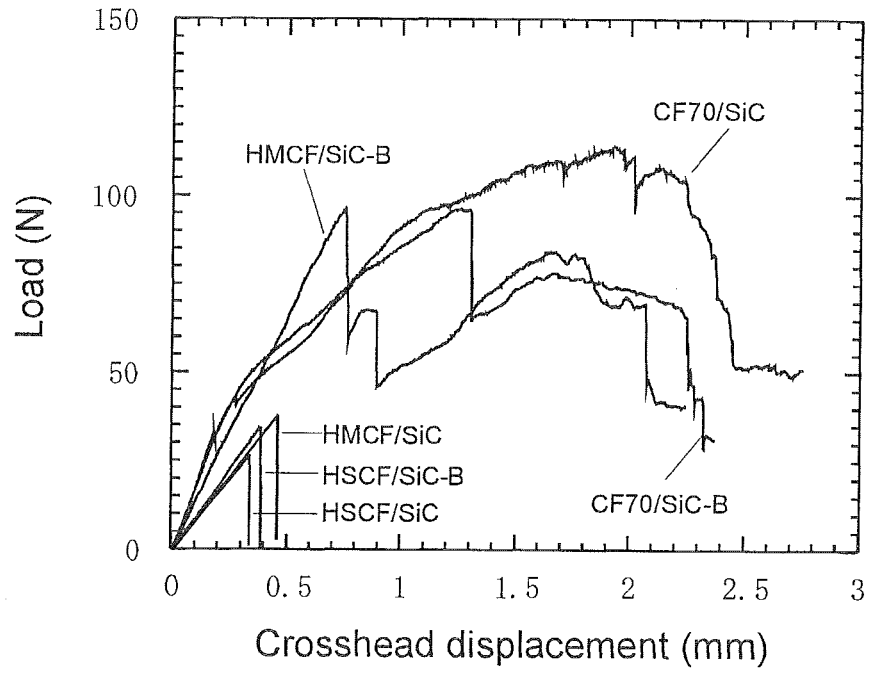

Fig. 5-3 The Load-displacement curves of CF/SiC with or without boron addition in four point bending test.

Fig. 5-4 shows the fracture surfaces of HSCF/SiC-B and HMCF/SiC-B. By comparing Fig. 5-4 with Fig. 2-10 in Chapter 2, it was found that HSCF/SiC and HSCF/SiC-B exhibited almost no fiber pullout. This suggested that the interface of HSCF/SiC was very strong and could not resist the propagation of matrix cracks into the fibers. HMCF/SiC exhibited rather flat fracture surface with few and short fiber pullout. On the other hand, HMCF/SiC-B showed long fiber pullout. It also could be observed that there are many matrix cracks near the fracture surface of HMCF/SiC-B. The propagation of matrix cracks did not damage the fibers, and it strongly verified that debonding of interface occurred. Both CF70/SiC and CF70/SiC-B exhibited extensive fiber pullout, indicating the weak interface of CF70/SiC.

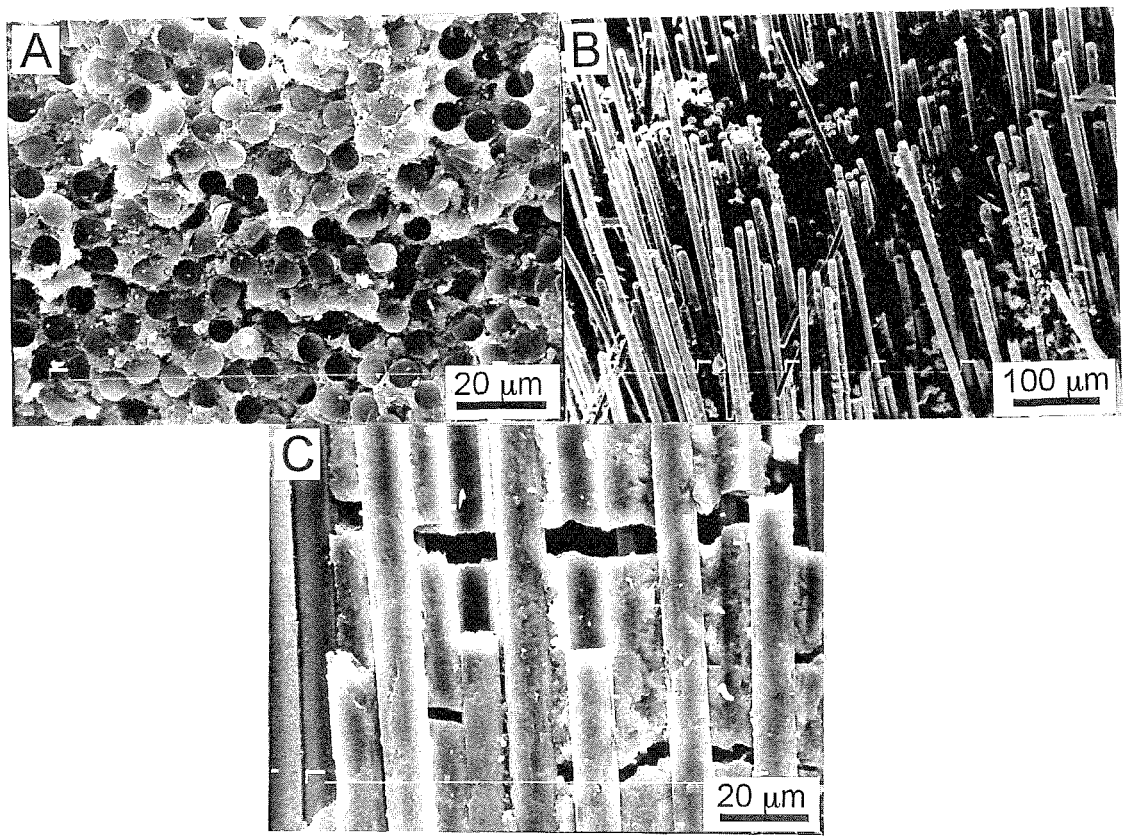

Fig. 5-4 Fracture surfaces of HSCF/SiC-B (A), HMCF/SiC-B (B, C).

The mechanical properties of fiber/ceramic composites are dependent upon the properties of fiber and matrix as well as the bonding strength of interface between fiber and matrix. The role of interface is not only to transfer the load from matrix to fiber, but also to influence the extension of matrix cracks in the composites. If the fiber/matrix interface is strong, the matrix cracks can extend into the fiber, as a result, the fiber fails at the moment matrix cracks start propagating. The composites exhibited low strength, because the properties of fibers were not sufficiently exploited. On the other hand, if the fiber/matrix interface is sufficiently weak, propagation of matrix cracks can be suppressed by the debonding of interface and fibers remain intact. The loading transfer between fiber and matrix in the debonding zone is achieved through the friction shear stress of interface.

In the previous chapters, it was found that highly-graphitized CF70 had weak bonding with matrix SiC, while HSCF and HMCF tended to bond strongly with matrix SiC. The difference in their bonding strength was demonstrated to be caused by difference of the microstructures of the carbon fibers.

As described above, HSCF/SiC and CF70/SiC with boron addition exhibited a slight change in flexural strength, and their fracture mode was not changed. However, HMCF/SiC with boron addition showed a remarkable change compared with HMCF/SiC without boron addition. From the above discussion, it was thought that boron addition weakened the interface strength of HMCF/SiC to a critical level so that the matrix cracks could be resisted by the debonding of the interface. For CF70/SiC with weak interface, the further weakening of interface by boron addition did not change the fracture mode greatly. As for HSCF/SiC with a strong interface, boron addition weakened the interfacial strength to some extent, but not enough to cause the interface debonding in order to resist the matrix cracks.

The mechanism of lowering bonding strength by boron addition might be very complicated. From the morphology of B/PCS on carbon fibers in Fig. 5-1, a simple model of microstructure of CF/SiC-B was proposed to explain the mechanism as shown in Fig. 5-5. A B/SiC layer that contained a high concentration of boron was formed by initial impregnation-pyrolysis of boron-PCS-toluene slurry. Subsequent multiple

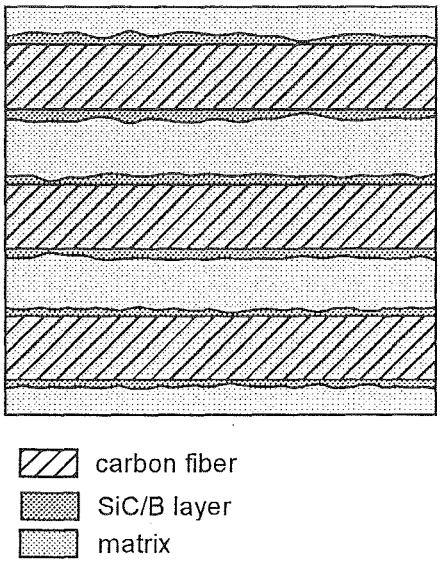

Fig.5-5 A proposed model of the microstructure of CF/SiC-B composites. The SiC/B layer contained high concentration of boron which was considered to lower the bonding strength of interface.

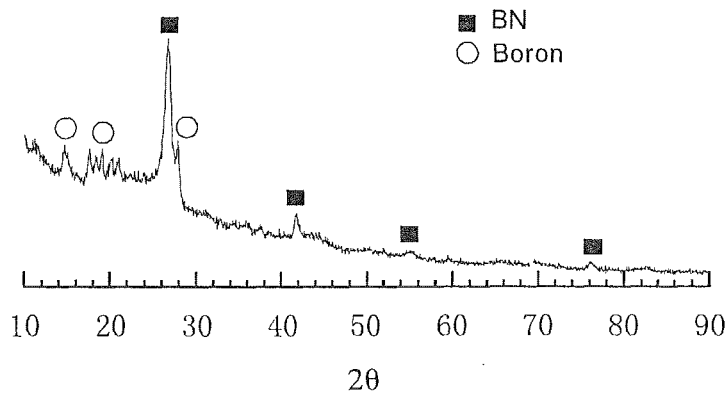

Fig. 5-6 XRD profile of boron heat-treated in N_2 at 1200°C.

impregnation with PCS resulted in SiC matrix. It was considered that the boron/SiC layer played an important role in the interface weakening mechanism.

Boron powder heat-treated at 1200°C in N_2 for 3 hours was examined by XRD. The XRD pattern is shown in Fig. 5-6. Peaks of boron and BN were detected, indicating that some of the boron powders reacted with N_2 and formed BN at 1200°C. Suttor et al also reported that BN formed in the B-polysiloxane-N_2 system [10], which was similar to this B-PCS-N_2 system.

It was reported by many researchers that BN coating weakened the interfacial bonding strength between fiber and matrix in CMCs. In this CF/B/SiC system, initial impregnation of carbon fiber with B-PCS slurry introduced a B-SiC layer on carbon fiber and then BN was formed on the surface of boron. It was considered that the layer played three roles to weaken the interface of CF/SiC. Firstly, the existence of BN decreased the contacting area between carbon fiber and SiC, therefore, it decreases the interfacial strength between fiber and matrix. Secondly, B/PCS layer had a weak bonding with matrix. TEM observation of HMCF/SiC-B indicated the possibility of the two mechanisms above mentioned as shown in Fig. 5-7. Thirdly, the layer had a low shear strength due to poor bonding between BN and SiC. This layer failed first during loading and resulted the debonding of the interface. In Fig. 5-4, it can be observed that

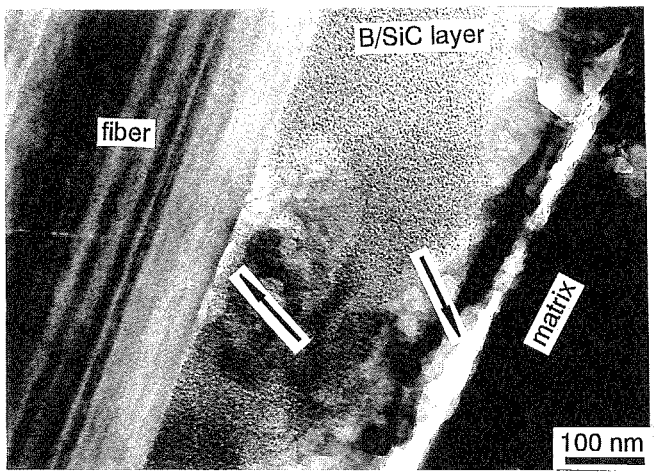

Fig. 5-7 TEM image of the interface of HMCF/SiC-B. The arrows indicate where the interface was weakened.

many particles were adhered on the surface of pull-out fibers. This phenomenon was an evidence to support the third way of debonding. However, compared with a complete BN coating, these effects were slight, because a large fraction of the carbon fiber was still in contact with SiC.

5.3.3 Oxidation behavior of boron-added CF/SiC

Fig. 5-8 shows the weight loss curves of HSCF, HSCF/SiC, HSCF/SiC-B, HSCF/SiC-B-coating, and Fig. 5-9 shows the weight loss curves of HMCF, HMCF/SiC, HMCF/SiC-B, HMCF/SiC-B-coating with increase of oxidation temperature. By comparison with those of the carbon fibers, the weight loss curves of HSCF/SiC and HMCF/SiC were shifted to higher temperature side, because SiC matrix decreased the area of the carbon fibers which could be accessed by oxygen. However, the carbon fibers in the composites were still oxidized by oxygen in two ways, one was oxidation of the carbon fibers from the cross sections along fiber axes, the other was oxidation of the carbon fibers by the diffusion of oxygen through pores in the matrix. With boron addition, the weight loss curves of HSCF/SiC-B and HMCF/SiC-B were further shifted to higher temperatures. Jones *et al* reported that boron solid-solved in carbon could improve oxidation resistance of the carbon [10]. However, solid-solved boron could not be formed here because of the low heat-treatment temperature. Mackee reported that boron oxide could block the active sites of carbon, therefore it improved the oxidation resistance of carbon [11]. The mechanism could be also applied to the present systems. But more importantly, the formation of B_2O_3 in matrix can easily seal the pores in the matrix and suppress the diffusion of oxygen. Moreover, the formed B_2O_3 and the fluidity of the glass at high temperature could fill partly the pores left by the oxidation of the fibers; hence the diffusion of oxygen to the depth of the samples was suppressed. The morphology of the samples after oxidation shown in Fig. 5-10 verified that the formation of glass phase sealed the pores in the matrix.

Although boron addition into the matrix had some effect on the oxidation resistance of the CF/SiC composites because of the formation of boron oxide during oxidation, it seems to be difficult for glassy boron oxide to completely cover the cross sections of the

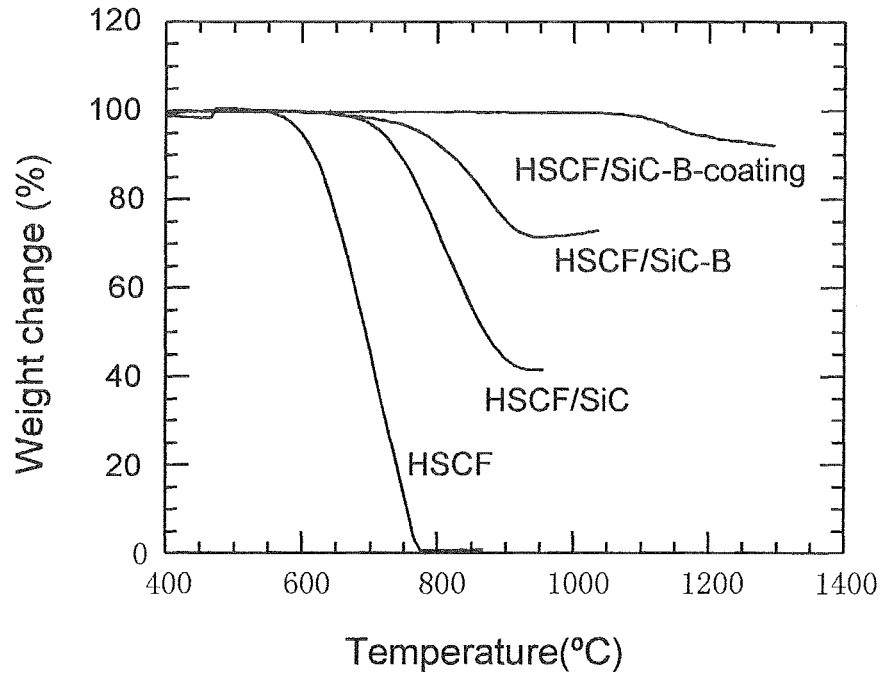

Fig. 5-8 Weight changes of HSCF, HSCF/SiC, HSCF/SiC-B, HSCF/SiC-B-coating in air with heating rate of 5°C/min.

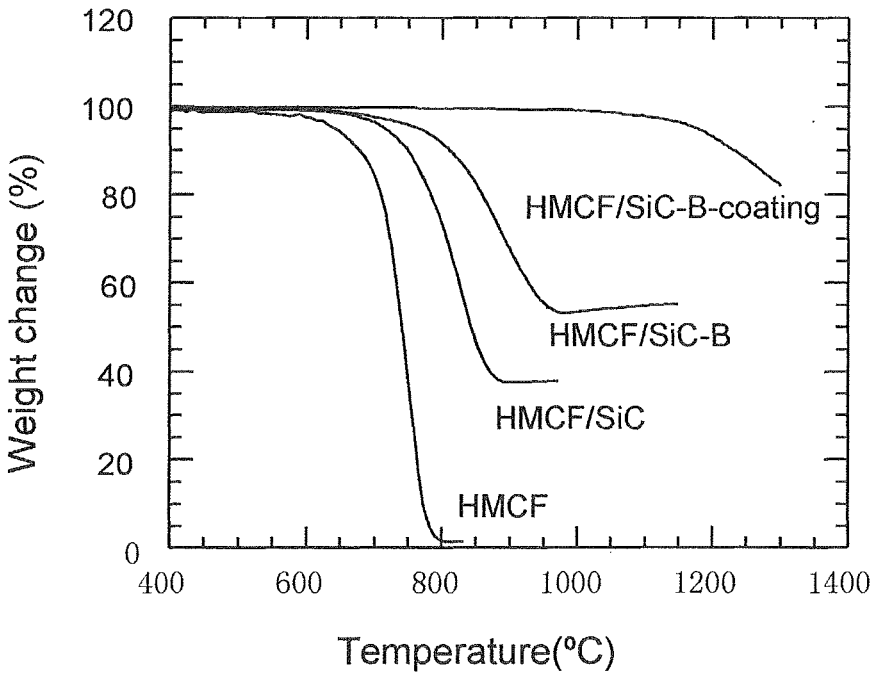

Fig. 5-9 Weight changes of HMCF, HMCF/SiC, HMCF/SiC-B, HMCF/SiC-B-coating in air with heating rate of 5°C/min.

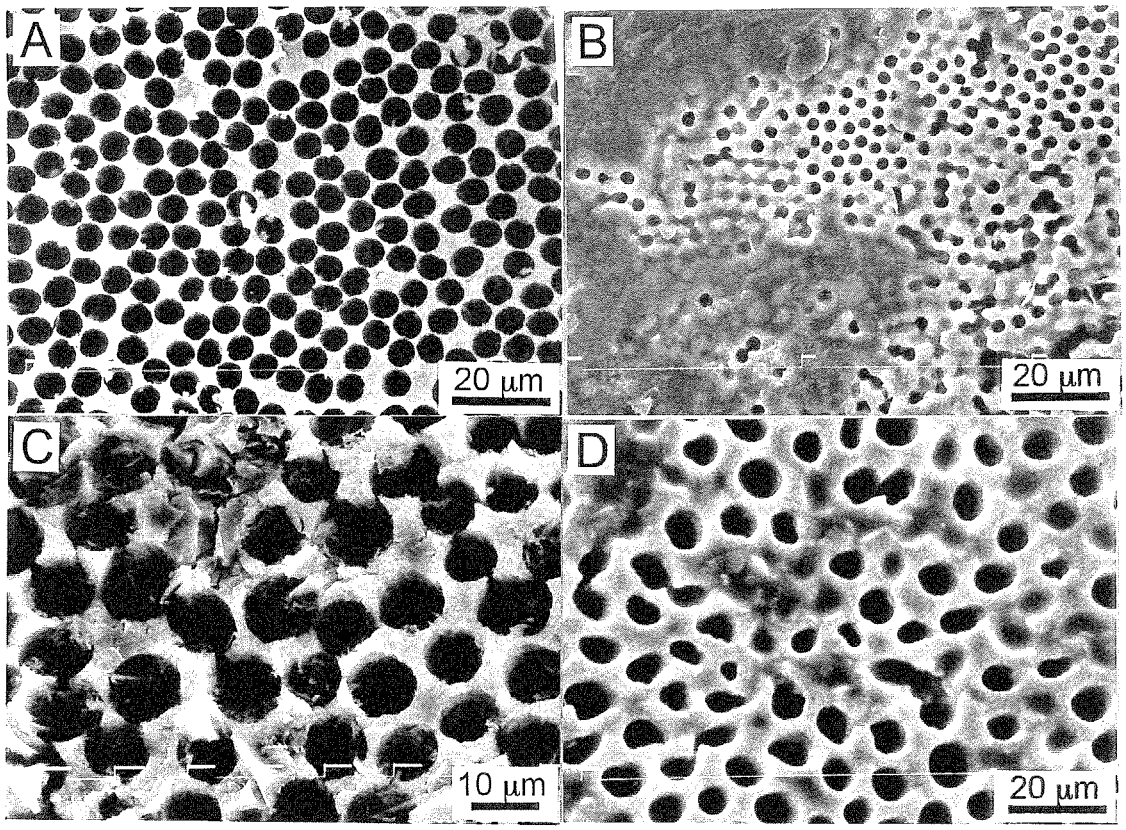

Fig. 5-10 The morphology of the transverse sections of HSCF/SiC (A), HSCF/SiC-B (B), HMCF/SiC (C) and HMCF/SiC-B (D) after oxidation.

samples. Hoshii reported similar results in CF/ borosiloxane-derived-ceramic composites [12]. By comparing the weight loss curves of HSCF/SiC-B and HMCF/SiC-B, it was found that the former has a lower oxidation rate than the latter. It can be conceived that, because the diameter of HSCF is only 7 μm and that of HMCF is 9.8 μm, the pores left by the oxidation of HSCF were small and therefore they are easier to be filled by the glass phase, as being exhibited by SEM observation.

As boron addition in matrix could not completely protect the fibers, we tested the oxidation behavior of HSCF/SiC-B-coating and HMCF/SiC-B-coating which had combination of boron addition and SiC/B coating. Weight loss curves of these samples exhibited much better oxidation resistance as shown in Fig. 5-8 and Fig. 5-9. They showed small weight loss only above 1000°C. Fig. 5-11 shows the morphology of B/SiC coating on the composites. Fig. 5-12 shows the polished sections of the samples

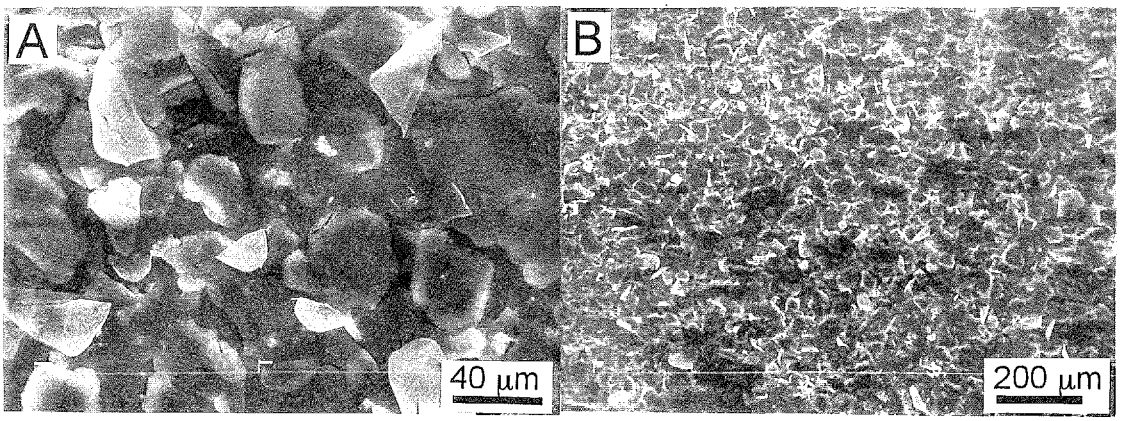

Fig. 5-11 The morphology of SiC-B coating on the composite.

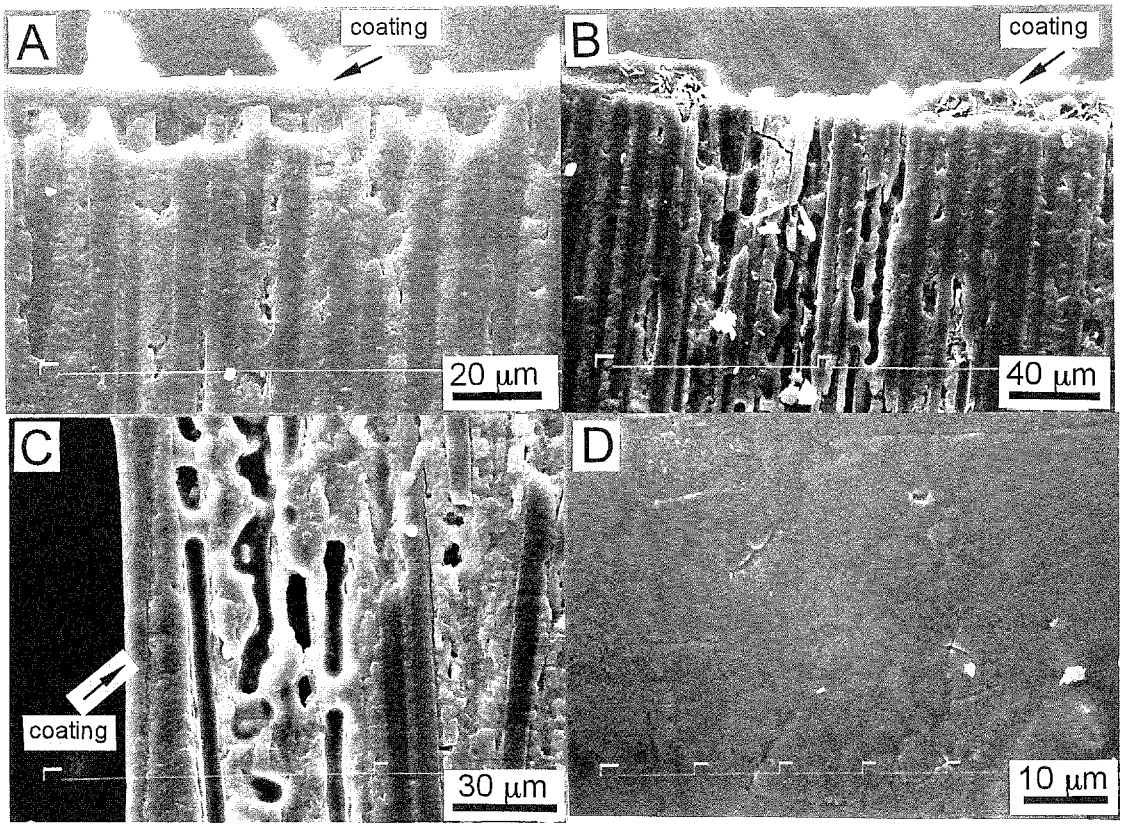

Fig. 5-12 The polished sections (A, B, C) and the surface (D) of HSCF/SiC-B-coating after oxidation.

after oxidation tests. It can be seen that a good coating with a thickness of about 10 μm was formed on the samples during oxidation (Fig. 5-12A), in contrast with the coating before oxidation, which had many cracks. The coating was bonded with the composite substrate very well. Even though HSCF were oxidized along the axis at some places where the coating was damaged (Fig. 5-12B), the diffusion of oxygen along the direction perpendicular to the fibers was resisted because of the existence of boron in matrix. It is also seen that the weight loss tendency became slow at about 1300°C. On the other hand, HMCF/SiC-B-coating exhibited an increasing tendency of the weight loss. Because the diameter of HMCF was large, it was more difficult to protect the fibers from oxidation beyond 1000°C at which the vaporization of B_2O_3 became rapid.

5.4 Conclusions

(1) Although boron addition to HSCF/SiC slightly increased the flexural strength, it did not have an obvious effect on the brittle fracture mode of HSCF/SiC.

(2) Boron addition to HMCF/SiC increased the flexural strength of HMCF/SiC by 2.5 times, and changed the brittle fracture mode to non-brittle mode.

(3) Boron addition to CF70/SiC decreased slightly the flexural strength of CF70/SiC without changing non-brittle fracture mode.

(4) The main effect of boron addition was to decrease the interfacial bonding strength. It was believed that the B/SiC interlayer played a main role in weakening interface bonding. The formation of BN from the reaction of B and N_2 was thought to cause the weakening of interface bonding.

(5) Boron addition to the carbon fiber/polycarbosilane-derived-SiC composites improved their oxidation resistance, especially for the carbon fibers with small diameter, because the formation of boron oxide sealed the pores in the composites. The additional B/SiC coating on the samples helped cover the cross sections of the carbon fibers in CF/SiC composites, thus resulted in much better oxidation-resistance.

References

1. A. G. Evans and F.W. Zok, J. Mater. Sci. **29,** 3857 (1994).
2. J.-K. Kim and Y.-W. Mai, in "Materials Science and Technology: vol.13 Structure and Properties of Composites" (VCH, Germany, 1993), p. 239.
3. G. N. Morscher, J. Am. Ceram. Soc., **80,** 2029 (1997).
4. E. Y. Sun, S. R. Nutt and J. J. Brennan, J. Am. Ceram. Soc., **79,** 1521 (1996).
5. M. E. Westwood, J. D. Webster, R. J. Day, F. H. Hayes and R. Taylor, J. Mater. Sci., **31,** 1389 (1996).
6. R. D. Wang, H. Sano, Y. Uchiyama and K. Kobayashi, J. Mater. Sci., **31,** 1389 (1996).
7. K. Kobayashi, K. Maeda, H. Sano and Y. Uchiyama, Tanso, **151,** 20 (1992).
8. D. Suttor, T. Erny and P. Greil, J. Am. Ceram. Soc., **80,** 1831 (1997).
9. P. Greil, J. Am. Ceram. Soc., **78,** 835 (1995).
10. L. E. Jones and P. A. Thrower, Carbon, **29,** 251 (1991).
11. D. W. Mckee, C. L. Spiro and E. S. Lamby, Carbon, **22,** 507 (1984).
12. S. Hoshii, A. Kojima, M. Shimoda, S. Otani, T. Satou, Y. Nakaido and Y. Hasegawa, Tanso, **161,** 23 (1994).

Chapter 6 Modification of the Interface between Fiber and Matrix by BN Addition

6.1 Introduction

As described in the previous chapters, the mechanical properties of CF/SiC composite depend strongly on the characteristics of the interface between fiber and matrix. A strong interface gives a high strength and toughness. A weak interface allows interface debonding prior to the failure of the fibers, thus deviates the propagation of matrix cracks. After interface debonding, interface sliding stresses between the fibers and matrix have a significant effect on the toughness of the composites [1,2].

The interface characteristics depend on the surface structure of the fibers, the structure of the matrix and the processing conditions of the composite. The effect of the structure of carbon fibers on the mechanical properties of CF/SiC has been investigated in Chapter 2 and 3. It was found that the mechanical properties of CF/SiC could be controlled by the structure of carbon fiber. In many cases, surface coatings of fibers, typically pyrolytic carbon or BN, are applied as interface layers to tailor the interface in fiber/ceramic composites [3,4]. However, coatings bring extra high cost for the composites fabricated by non-CVI techniques. Since BN coating has been found to weaken interface bonding in many fiber/ceramic systems, in the present study, BN powder was added in CF/SiC composites which were prepared by impregnation/pyrolysis process of polycarbosilane, to investigate the effect of BN addition on the mechanical properties of the CF/SiC composites.

6.2. Experimental procedure

6.2.1 Preparation of CF/SiC

Two types of carbon fibers, HSCF and HMCF, were used as reinforcing fibers. Their ultimate heat-treatment temperatures were lower than 1500℃; they were found to be bond strongly with polycarbosilane-derived SiC matrix as stated in previous chapters. BN powder (Showa Denco Co. Japan) with an average size of 0.8 μm was used.

The carbon fibers were passed through a slurry consisting of BN, polycarbosilane and

toluene in an ultrasonic bath, and wound on a wire frame. The frame was then placed and pressed in a metal die to form a prepreg. Several slurries with different compositions were used, with respective mass ratio of BN:PCS:toluene as following: 0:30:70, 5:5:100 (slurry1), 10:5:100 (slurry2) or 20:10:100 (slurry3). After being dried at 80°C, the prepreg was took out from the metal die and pyrolysed at 1200°C in nitrogen for 1 hour. The process of impregnation with 50wt% PCS-toluene solution and subsequent pyrolysis at 1200°C samples was repeated 9 times to obtain dense composite samples. The ultimate size of the composites was about $38\times80\times1mm^3$. The composites were designated as HMCF/SiC, HMCF/SiC-BN1, HMCF/SiC-BN2, HMCF/SiC-BN3, HSCF/SiC, HSCF/SiC-BN1, HSCF/SiC-BN2 and HSCF/SiC-BN3, respectively. HSCF and HMCF stand for the carbon fiber used. BN1, BN2 and BN3 mean that the corresponding composite was prepared from slurry1, slurry2, and slurry3. CF stands for both HMCF and HSCF.

6.2.2 Characterization

To measure the amount of BN additives, CF/PCS-BN after the slurry impregnation and drying was weighed to get the increased amount. By assuming BN powder was homogeneously distributed in the slurry under the ultrasonic vibration, the slurry that infiltrated into the fiber tows had the same compositions in the slurry. Thus, the amount of BN additive amount could be obtained.

The CF/SiC-BN composites were embedded in resin, polished with diamond slurry, and then observed on SEM to examine the fiber distribution and BN distribution in the matrix. The mechanical properties of the composites were evaluated using tensile test. Tensile testing is relatively difficult for fiber/ceramics composites, because of the difficulty to prepare the specimen and because of the sensitivity to stress concentration caused by grip. Therefore, bending test is frequently used to evaluate the mechanical properties of fiber/ceramic composites. The composite samples were cut to adequate size for four-point bending test and tensile test. The size of the specimens for bending tests was about $40x3.5x1mm^3$. The four-point bending test was conducted using a universal testing machine with a crosshead speed of 0.5 mm/min, a support span of 30

mm and a loading span of 10 mm. The size of specimens for tensile test was about 80x5x1mm^3. As shown in Fig. 6-1, aluminum plates was stuck using epoxy on the specimen with a grip length of 25 mm and a gauge length of 30 mm. A strain gauge was stuck on the surface of each specimen to measure the strain. The tensile test was conducted using the same universal testing machine with a crosshead speed of 0.5 mm/min. The load-displacement (or strain) curves were recorded for both bending and tensile tests to examine the fracture behavior of the composites. The fracture surfaces of the specimens after test were observed by SEM.

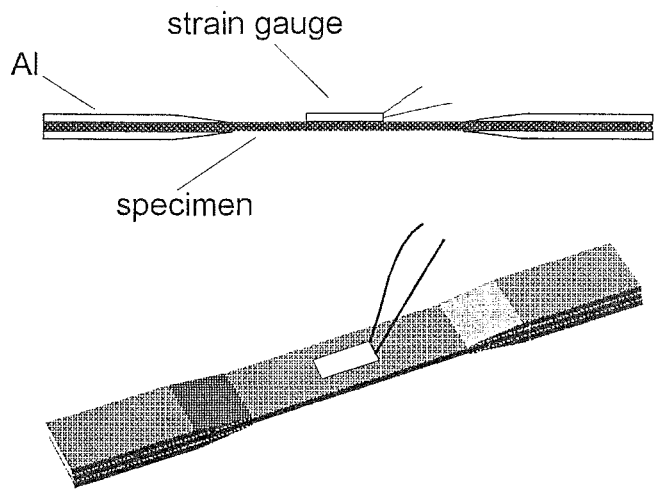

Fig. 6-1 A schemetic of specimen for tensile test.

6. 3. Results

6.3.1 HMCF/SiC-BN

6.3.1.1 Microstructure of HMCF/SiC-BN

The BN amount added in the matrix was expressed as the ratio to the fibers, as listed in Table 6-1. The amount of BN addition increased with the increased concentration of BN in the slurry. Figure 6-2 shows the morphologoy of HMCF/SiC-BN after initial

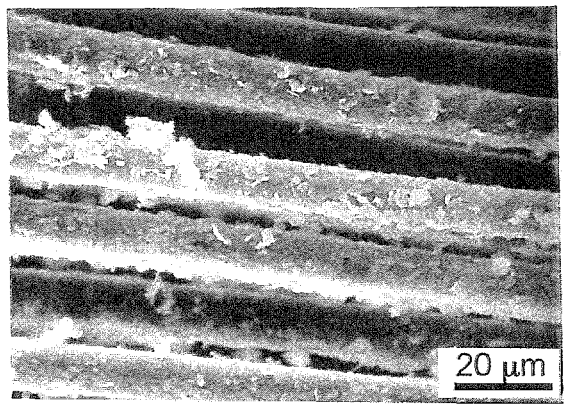

Fig. 6-2 The morphology of HMCF/SiC-BN after first time impregnation of the slurry (BN:PCS:toluene ratio of 20:10:100) and subsequent pyrolysis.

Table 6-1 Properties of the CF/SiC composites with and without BN addition.

samples	Composition of slurry (BN:PCS:toulene)	Amount of BN relative to CF (%)	Density (g/cm^3)	Porosity (%)	V_f (%)
HMCF/SiC	0 : 30 : 70	0	1.86	12.4	48.5
HMCF/SiC-BN1	5 : 5 : 100	6	1.78	11.0	50.8
HMCF/SiC-BN2	10 : 5 : 100	14	1.87	11.3	54.3
HMCF/SiC-BN3	20 : 10 : 100	26	1.77	10.4	51.2

slurry (20:10:100) infiltration and pyrolysis. It seems that BN powders were adhered to carbon fibers by PCS-derived-SiC like a binder. In comparison with carbon fibers infiltrated with B-PCS-toluene slurry in Chapter 5, the SiC-BN on the carbon fibers appears much rougher, since the average particle size of BN was 0.8 μm, in contrast to 0.1 μm of the boron powders. The PCS is decomposed to an amorphous state SiC at 1200°C, and no reaction occurred between BN and PCS, so the resultant is composed of BN and SiC. In the first cycle impregnation/pyrolysis process of carbon fibers with PCS without BN, large SiC particles are generally formed, as illustrated in Fig. 2-6 (Chapter 2). However, no large particles were observed in HMCF/SiC-BN. Since PCS particles were formed when the infiltrated composite was dried, the size of PCS particles depended on the space between the solid phases. The distribution of BN powders inhibited the formation of large PCS particles, hence large SiC particles. Table 6-1 also listed the open porosity of the ultimate composites, which was in the range of 10-13%. The SEM micrographs of the polished transverse sections of the composites are given in Fig. 6-3. The microstructure of the matrices with BN addition (Fig. 6-3b-d) is apparently different from the matrix without BN (Fig.6-3a). BN (white particles) is uniformly distributed in matrix. Some pits were observed in the matrix, which formed due to pealing of the matrix during polishing. It suggested that BN did not well bond with SiC.

6.3.1.2 Mechanical properties of HMCF/SiC-BN

Four-point bending strength and elastic modulus of HMCF/SiC-BN with different BN content are shown in Fig. 6-4. The flexural strength of HMCF/SiC-BN1 and HMCF/SiC-BN2 was about 270 MPa, which was higher than that of HMCF/SiC. HMCF/SiC-BN3 exhibited a flexural strength of about 580 MPa, which was much higher than those of all other composite samples. On the other hand, HMCF/SiC, HMCF/SiC-BN1 and HMCF/SiC-BN2 showed similar elastic modulus of about 80 GPa, whereas HMCF/SiC-BN3 showed an elastic modulus of about 110 GPa, higher than those of other samples. The stress-strain curves of the four composite samples in bending test are illustrated in Fig. 6-5. SEM micrographs of the specimens after bending

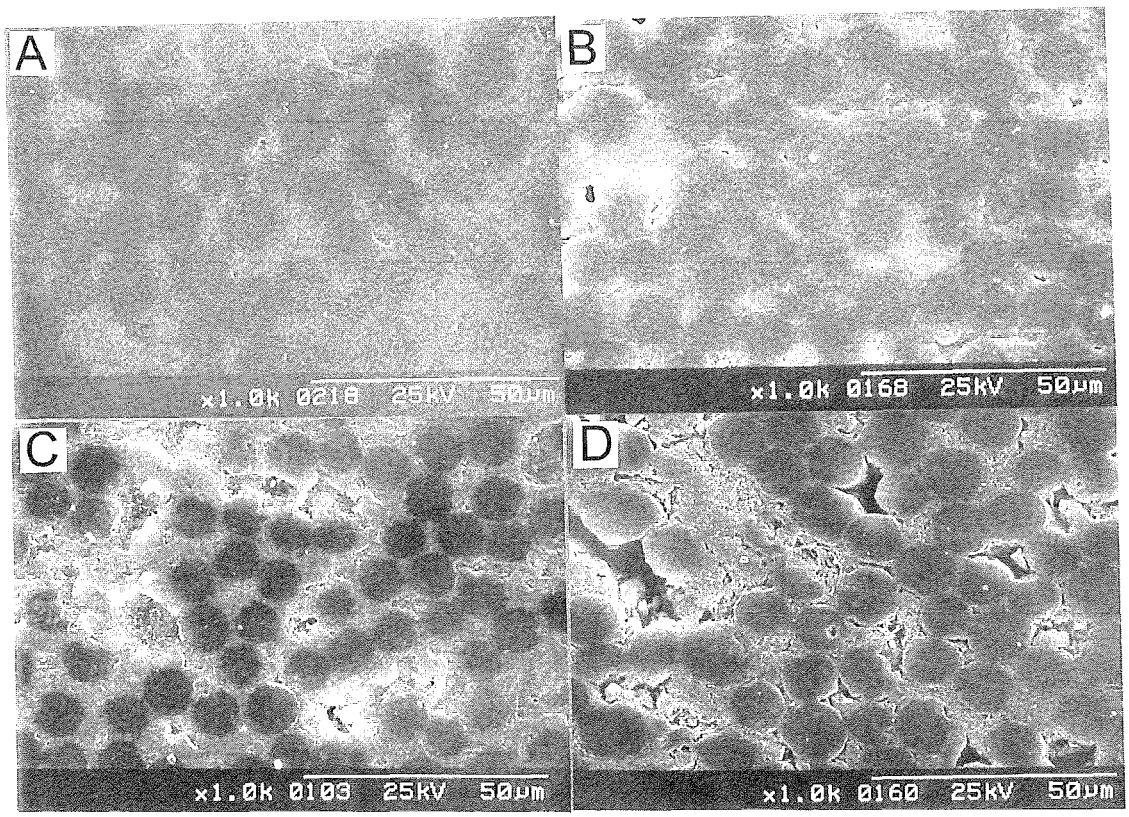

Fig. 6-3 SEM micrographs of polished transverse sections of HMCF/SiC (A), HMCF/SiC-BN1 (B), HMCF/SiC-BN2 (C) and HMCF/SiC-BN3 (D).

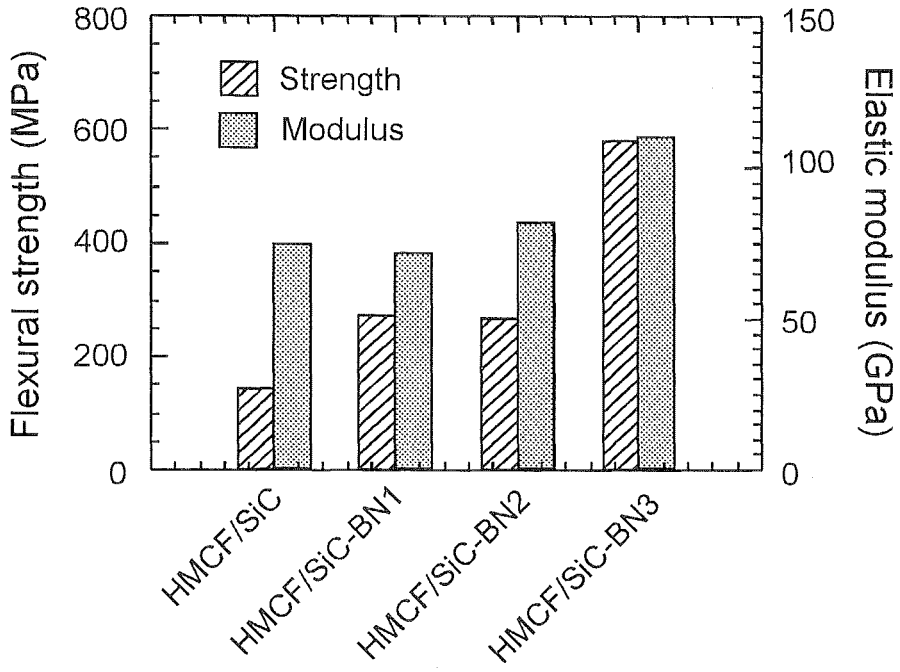

Fig. 6-4 Four-point bending strength and elastic modulus of CF/SiC composites with or without BN addition.

test were given in Fig. 6-6. The stress-strain curve and fracture morphology of HMCF/SiC revealed that it failed in a completely brittle way. HMCF/SiC-BN1 and HMCF/SiC-BN2 exhibited interlaminar failure in test. The relatively weak interlaminar shear strength is apparently attributed to the addition of BN powder in the matrix, since BN particles are weakly bonded with SiC. For HMCF/SiC-BN3, no apparent crack propagation normal to the sample was observed, because of extensive interlaminar shear failure. The large amount of BN powder in matrix weaken the matrix, so that the matrix in the vicinity of the interface fails prior to the fibers, thus, the HMCF/SiC-BN3 exhibited much higher strength.

Fig. 6-7 shows the tensile strength and corresponding elastic modulus of the composites. HMCF/SiC, HMCF/SiC-BN1 and HMCF/SiC-BN2 showed a similar tensile strength of about 100 MPa and a similar elastic modulus of about 100 GPa. Their strain-in-failure of these composites in tensile test was only about 0.1%, as shown in Fig. 6-8. On the other hand, HMCF/SiC-BN3 showed an average tensile strength of about 300 MPa, which was 3 times higher than that of all the other composites. The elastic modulus of HMCF/SiC-BN3 is about 130 GPa, a little higher than that of the other composites. The stress-strain curve of HMCF/SiC-BN3 in tensile test indicates that the specimen deformed linearly to the strain of 0.1%, then exhibited inelastic behavior due to matrix cracking, and failed ultimately at the strain between 0.4% to 0.5%. When the specimen failed at a peak value, the stress abruptly dropped to zero, without a typical pullout tail. It suggested the composite had a short fiber pullout.

The fracture surfaces of the composite specimen after tensile test are shown in Fig. 6-9. Almost all of the fibers in HMCF/SiC fractured in the same plane with matrix, indicating the strong interface between fiber and matrix. The fracture surfaces of HMCF/SiC-BN1 and HMCF/SiC-BN2 showed somewhat fiber pullout, but most of the fibers still fractured in the same plane, which was caused by the propagation of matrix cracks. This indicated that BN addition in the two composites weakened the interface to some extent, but not enough to allow the interface bonding occurring. The fracture surface of HMCF/SiC-BN showed a zigzag shape, so Fig. 6-9d only shows a part of the fracture surface. Although the fiber pullout of HMCF/SiC-BN3 was not long (Fig.6-9d),

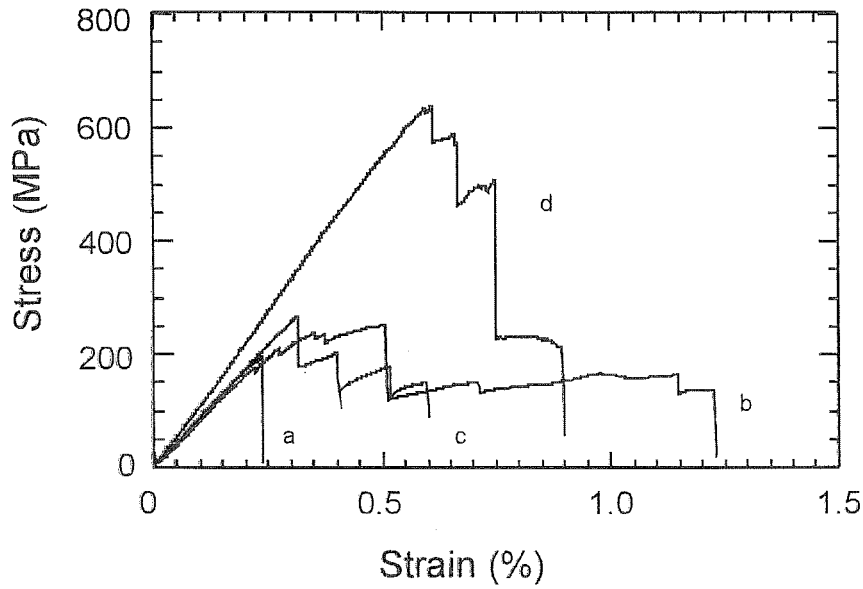

Fig. 6-5 The apparent stress-strain curves of CF/SiC, CF/SiC-BN1, CF/SiC-BN2 and CF/SiC-BN3 in four-point bending test.

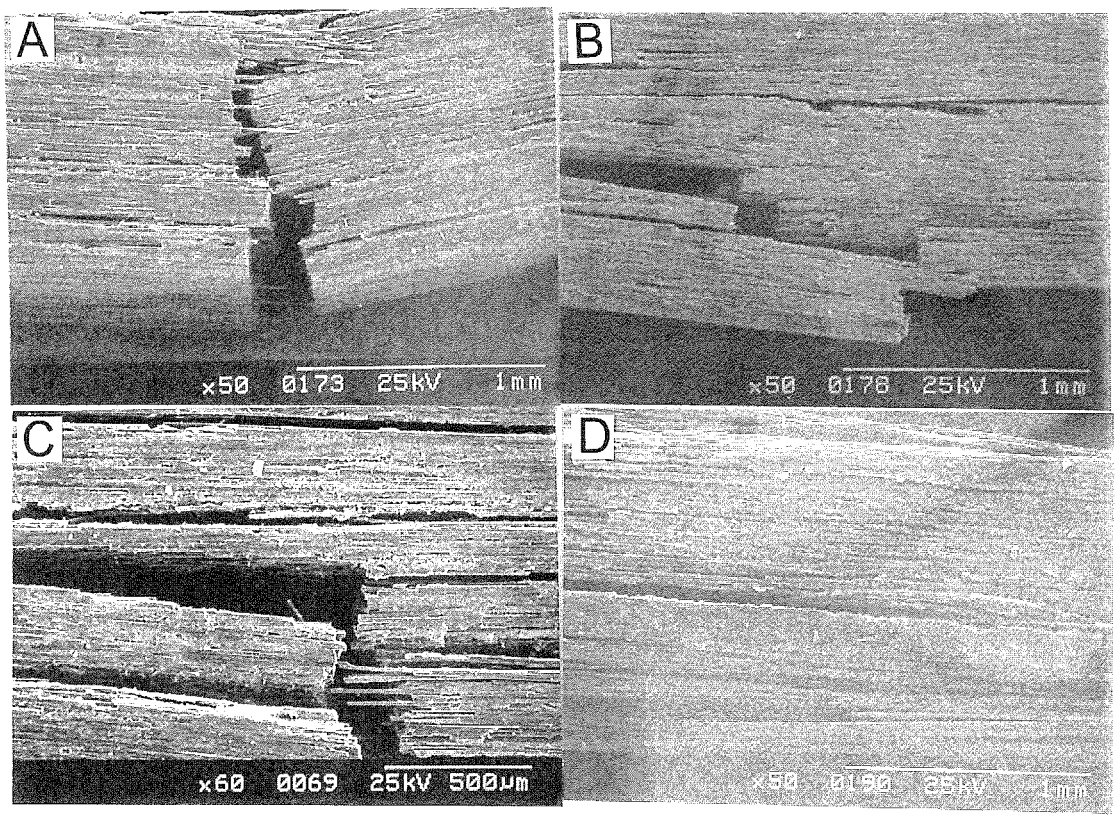

Fig. 6-6 The specimens after bending test. HMCF/SiC (A), HMCF/SiC-BN1 (B), HMCF/SiC-BN2 (C) and HMCF/SiC-BN3 (D).

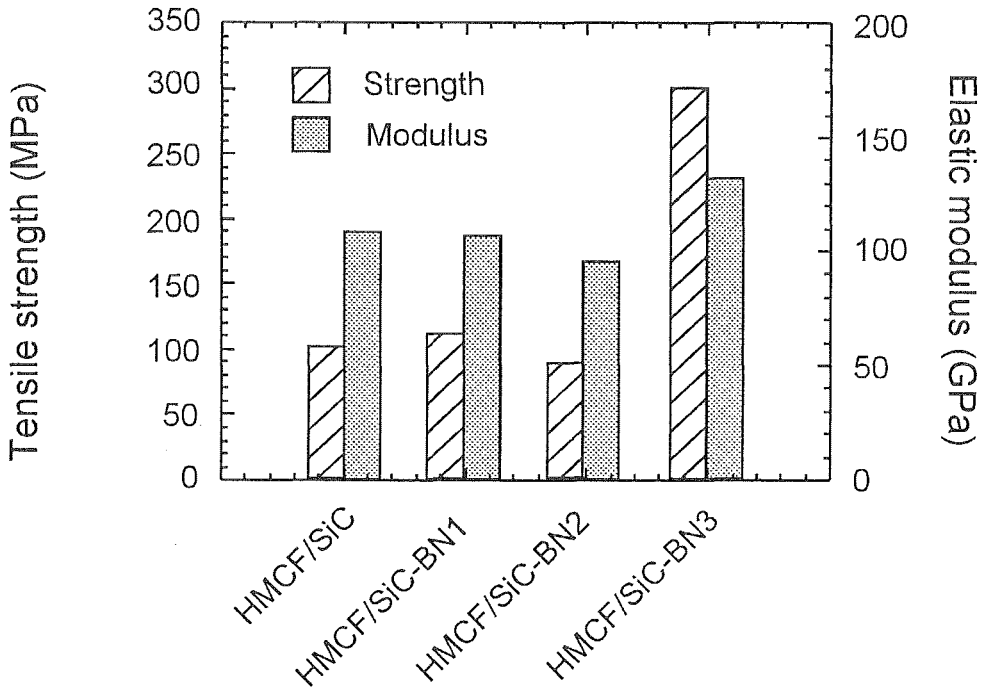

Fig. 6-7 Tensile strength and elastic modulus of HMCF/SiC composites with or without BN addition.

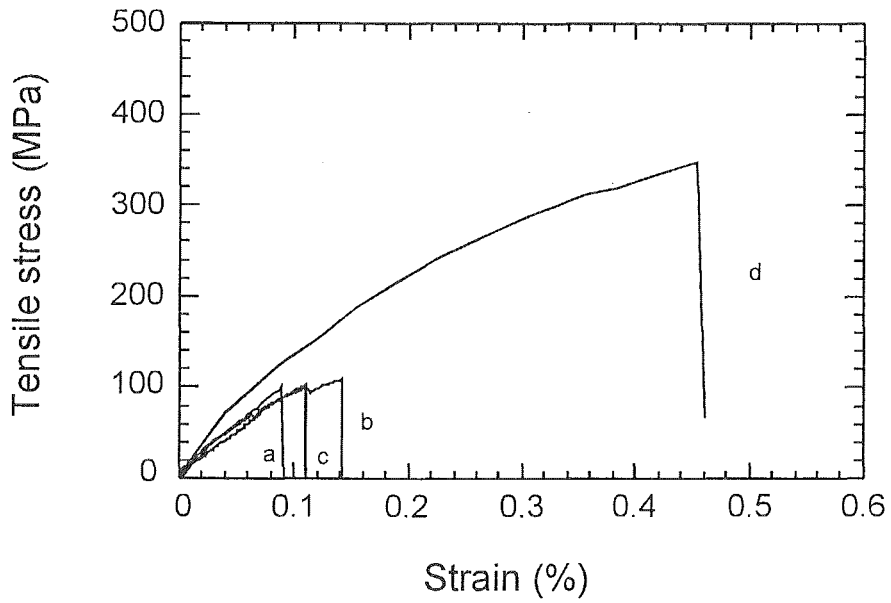

Fig. 6-8 The stress-strain curves of HMCF/SiC (a), HMCF/SiC-BN1 (b), HMCF/SiC-BN2 (c) and HMCF/SiC-BN3 (d) in tensile test.

as expected from the tail of the stress-strain curve, most of the fibers did not fracture in the same plane. By examining carefully the surfaces of the pullout fibers, it was known that many particles adhered to the fibers. This phenomenon strongly suggested that the interface debonding occured due to the fail of the matrix in the vicinity of the interface. However, the interface sliding stresses between fiber and matrix seem very strong because of the roughness of the interface.

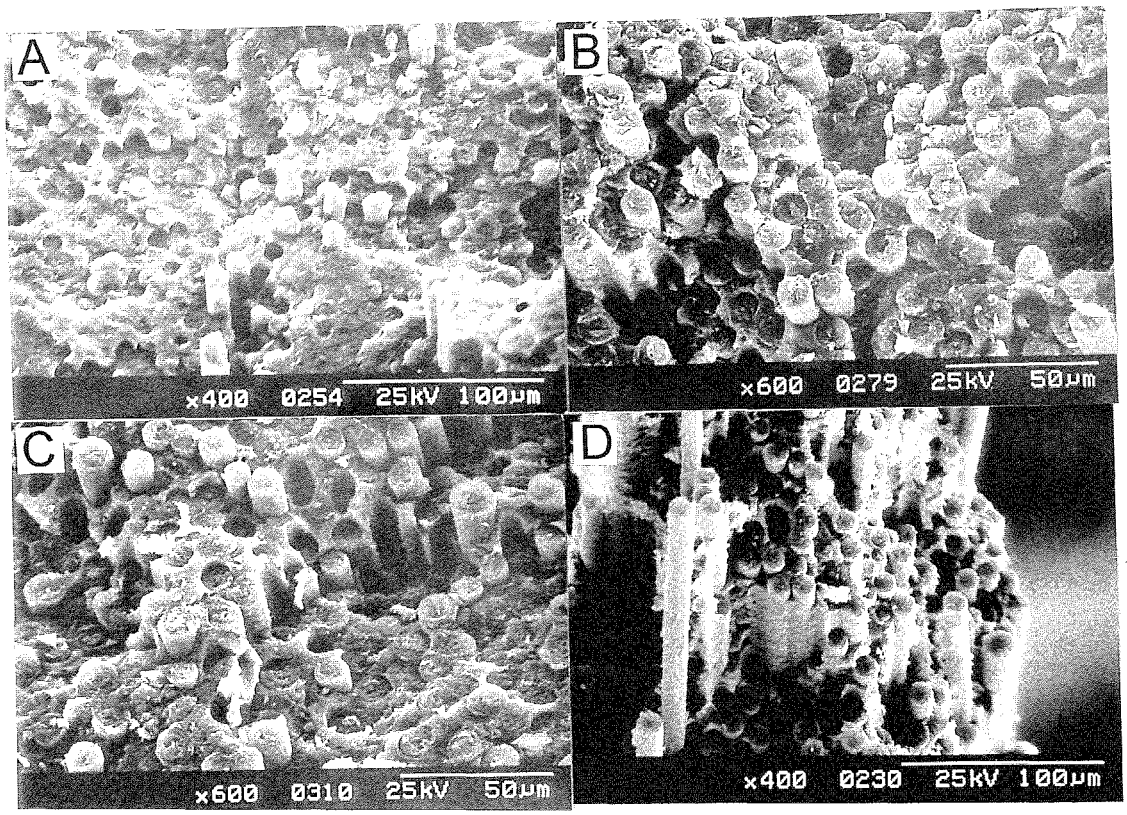

Fig. 6-9 The fracture surfaces of HMCF/SiC (A), HMCF/SiC-BN1 (B), HMCF/SiC-BN2 (C) and HMCF/SiC-BN3 (D) after tensile test.

6.3.2 HSCF/SiC-BN Composites

6.3.2.1 Microstructure of HSCF/SiC-BN

The HSCF/SiC-BN composites were prepared similarly as the HMCF/SiC-BN composites. Table 6-2 shows the amount of BN addition in composites, the density and porosity in the HSCF/SiC-BN composites. By compared with Table 6-1, it was known that the BN amount in HSCF/SiC-BN2 and HSCF/SiC-BN3 was higher than that in HMCF/SiC-BN2 and HMCF/SiC-BN3. The V_f of the composites decreased slightly due to BN addition. The density values of HSCF/SiC-BN were smaller than those of HMCF/SiC-BN, because the density of HSCF was smaller than that of HMCF. The porosity values of the composites were similar with those of HMCF/SiC-BN, except HSCF/SiC-BN1.

Fig. 6-10 shows the polished transverse sections of HSCF/SiC-BN composites. HSCF/SiC-BN2 and HSCF/SiC-BN3 exhibited a different microstructure with HSCF/SiC, since a remarkable amount of BN was incorporated in the composites. The white BN particles in matrix can be observed. As HMCF/SiC-BN, many pits were observed in HSCF/SiC-BN2 and HSCF/SiC-BN3, caused by pealing of the matrix during polishing. It indicated that the bonding between BN particle and PCS-derived SiC was not strong, as described in 6.3.1.1.

6.3.2.2 Mechanical properties of HSCF/SiC-BN composites

Fig. 6-11 shows four-point bending strength of HSCF/SiC-BN composites. The flexural strength of HSCF/SiC, HSCF/SiC-BN1 and HSCF/SiC-BN2 was about 200 MPa, whereas the flexural strength of HSCF/SiC-BN3 was 567 MPa. The strength of HSCF/SiC-BN showed almost no improvement until the slurry3 with high concentration of BN was used to prepare the composites. This trend is similar with that of HMCF/SiC-BN. The load-displacement curves of the HSCF/SiC-BN composites in bending test are shown in Fig. 6-12. The HSCF/SiC, HSCF/SiC-BN1 and HSCF/SiC-BN2 failed in a brittle mode, resulting in low fracture stresses, while HSCF/SiC-BN3 failed in a non-brittle mode with high fracture strength.

Fig. 6-13 shows the SEM micrographs of HSCF/SiC-BN after bending test. It was

Table 6-2 Properties of the HSCF/SiC composites with and without BN addition.

samples	Composition of slurry (BN:PCS:toulene)	Amount of BN relative to CF (%)	Density (g/cm^3)	Porosity (%)	V_f (%)
HSCF/SiC	0 : 30 : 70	0	1.68	10.7	63.3
HSCF/SiC-BN1	5 : 5 : 100	5	1.57	18.7	59.8
HSCF/SiC-BN2	10 : 5 : 100	19	1.63	12.8	57.9
HSCF/SiC-BN3	20 : 10 : 100	35	1.59	11.2	56.5

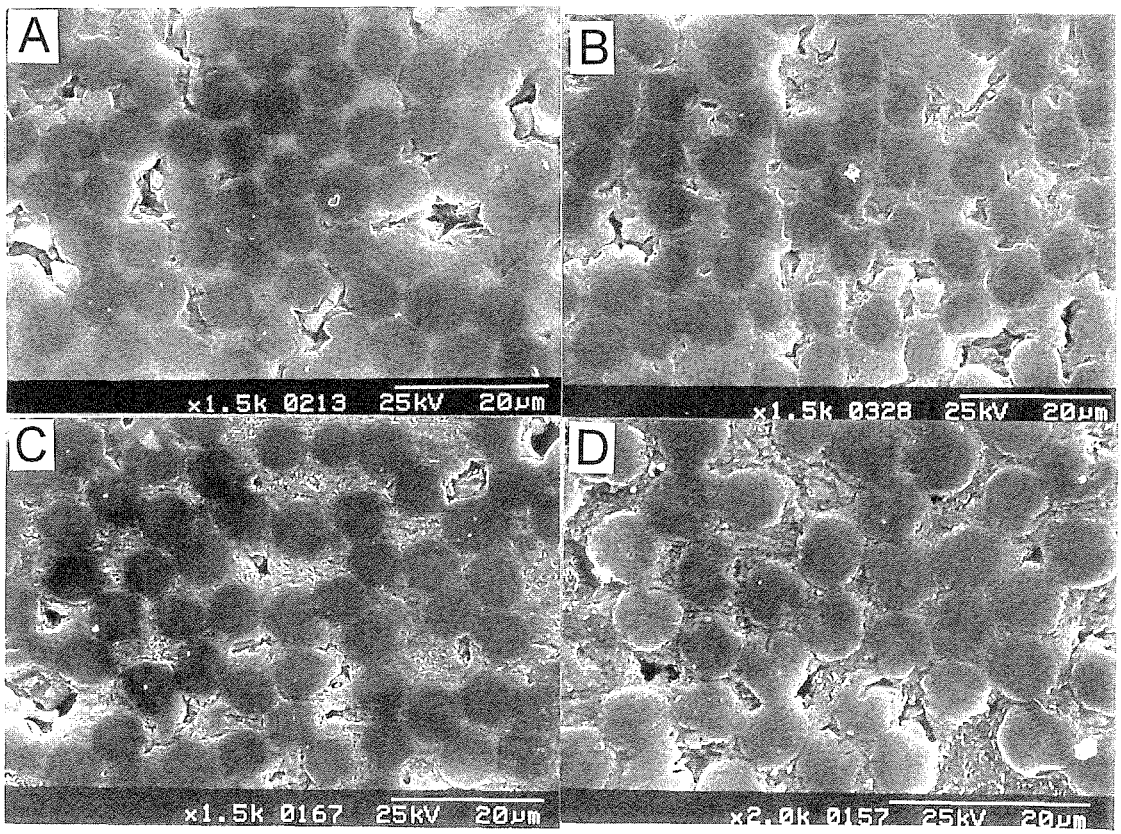

Fig. 6-10 SEM micrographs of polished transverse sections of HSCF/SiC (A), HSCF/SiC-BN1 (B), HSCF/SiC-BN2 (C) and HSCF/SiC-BN3 (D).

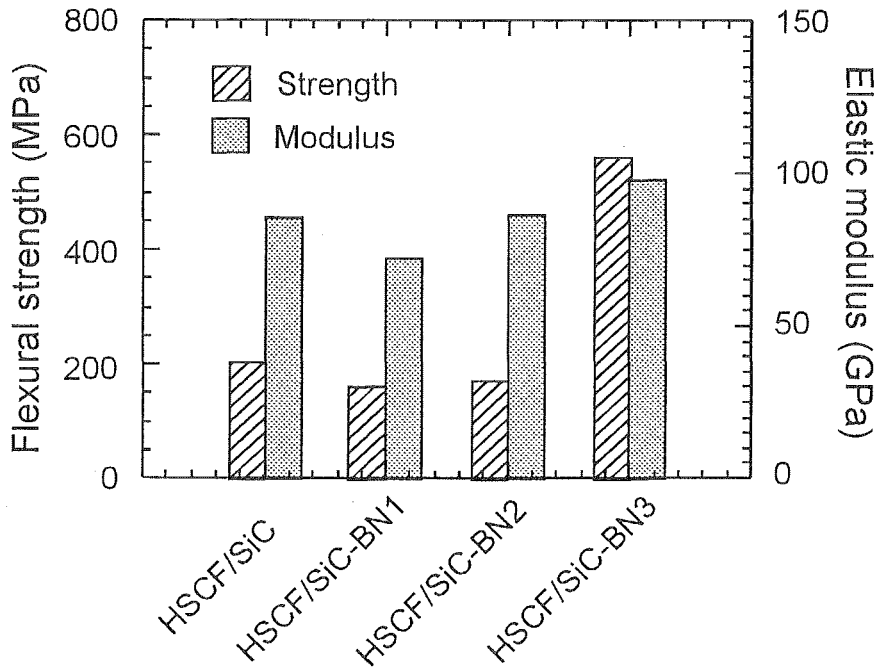

Fig. 6-11 Four-point bending strength and elastic modulus of HSCF/SiC composites with or without BN addition.

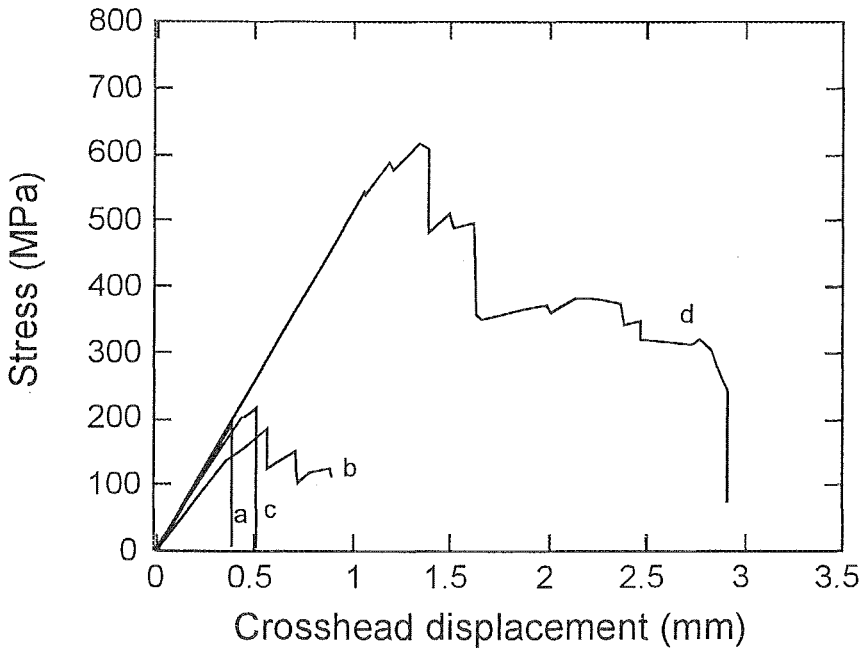

Fig. 6-12 The Stress-displacement curves of HSCF/SiC-BN composites. (a) HSCF/SiC, (b) HSCF/SiC-BN1, (c) HSCF/SiC-BN2, and (d) HSCF/SiC-BN3.

observed from Fig. 6-13A that a large crack propagated through HSCF/SiC sample. It is a typical brittle failure. In Fig. 6-13B, although delamination was observed in HSCF/SiC-BN1 sample, the strength or toughness of the composite was not improved, since the fracture in the laminae was still brittle. In Fig. 6-13C, the propagation of crack was deviated, due to weak interlayer shear strength in matrix. But the fracture in each layer was mainly brittle, so the sample showed brittle failure and the properties of carbon fibers were not well exploited. In Fig. 6-13D, it was observed that the HSCF/SiC-BN3 sample was delaminated to many layers, some layers failed with fiber pullout. Because of the weak interface in HSCF/SiC-BN3, the composite survived in matrix cracking, and sustained at higher stress. So the interlayer shear stress in the sample also increased with the testing load, resulting in extensive interlaminate failure. From the fracture mode of the four samples, it was thought that weakening of interface between fiber and matrix was more important than the weakening of interlayer shear strength. The weakening of interface prevent the fiber from being damaged by matrix cracking.

Fig. 6-14 shows the tensile strength and modulus of HSCF/SiC-BN composites. It was observed that the elastic modulus of these samples showed no great change. The tensile strength of HSCF/SiC-BN3 reached 260 MPa, which was the highest in the four composites. HSCF/SiC and HSCF/SiC-BN2 shows a tensile strength below 100 MPa. HSCF/SiC-BN1 exhibited a strength of 180MPa, which seemed abnormal. The porosity of HSCF/SiC-BN1 was 18%, much higher than that of other three composites. The high porosity decreased the stress concentration of the interface, whereas the samples with low porosity had higher stress concentration. Therefore, the composites with high porosity had high tensile strength.

Fig. 6-15 shows the stress-strain curves of HSCF/SiC-BN during tensile test. The HSCF/SiC, HSCF/SiC-BN1 and HSCF/SiC-BN2 all showed a brittle failure, while HSCF/SiC-BN3 showed initial elastic behavior, and then non-linear behavior.

Fig. 6-16 shows the fracture surfaces of HSCF/SiC-BN composites after tensile test. The former three composites in Fig. 6-16 A, B, C exhibited a planar fracture surface with no fiber pullout. On the other hand, HSCF/SiC-BN3 in Fig. 6-16D showed fiber

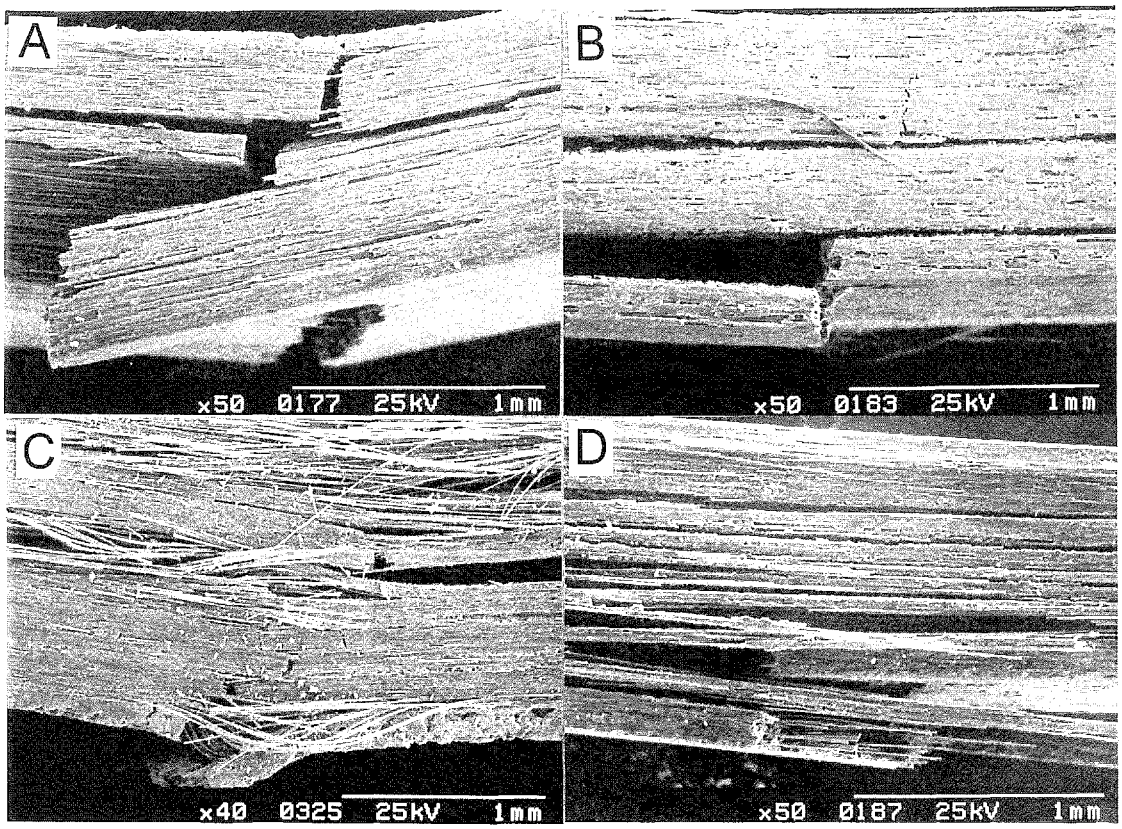

Fig. 6-13 SEM micrographs of HSCF/SiC (A), HSCF/SiC-BN1 (B), HSCF/SiC-BN2 (C) and HSCF/SiC-BN3 (D) after bending test.

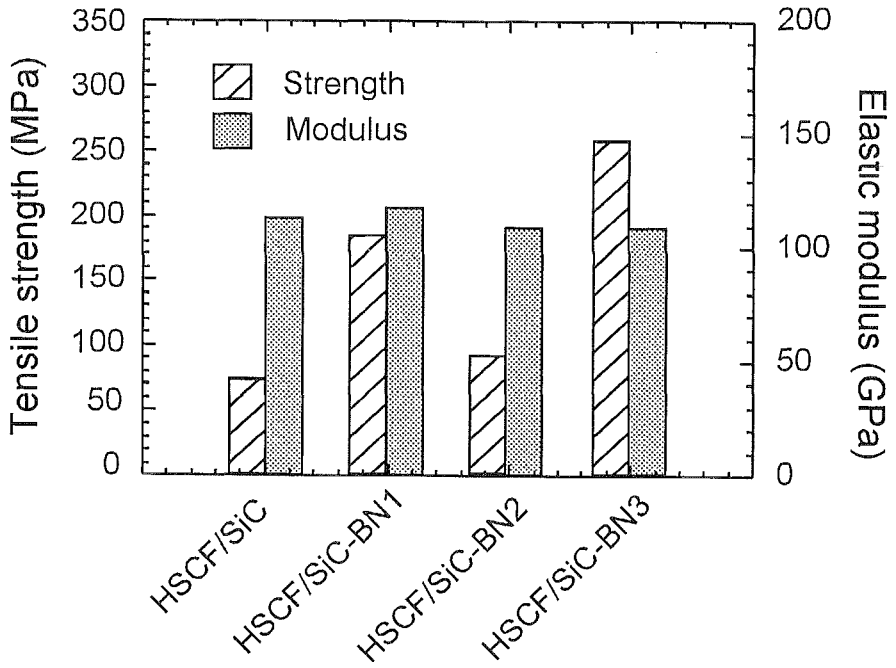

Fig. 6-14 Tensile strength and elastic modulus of HSCF/SiC composites with or without BN addition.

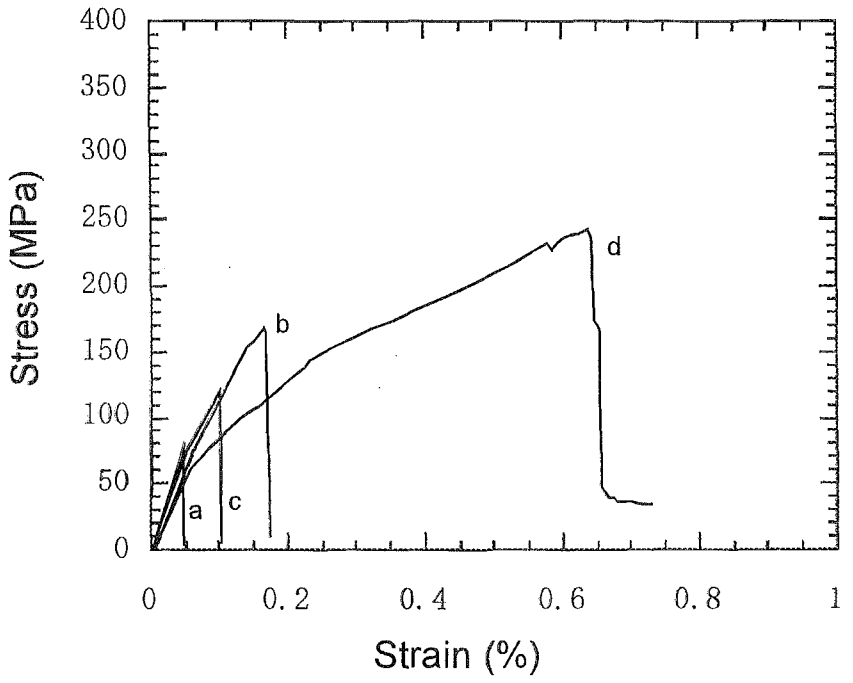

Fig. 6-15 The stress-strain curves of HSCF/SiC-BN composites in tensile test. (a) HSCF/SiC, (b) HSCF/SiC-BN1, (c) HSCF/SiC-BN2, and (d) HSCF/SiC-BN3.

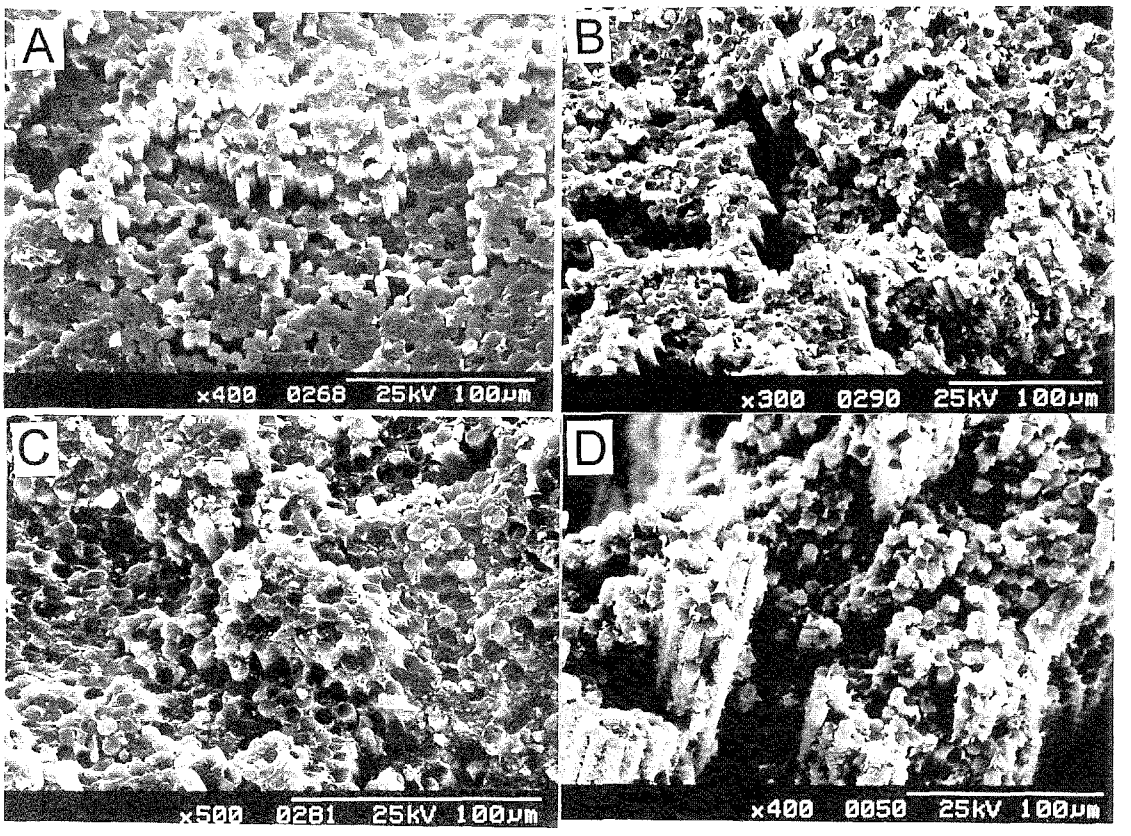

Fig. 6-16 SEM micrographs of the fracture surface of HSCF/SiC (A), HSCF/SiC-BN1 (B), HSCF/SiC-BN2 (C) and HSCF/SiC-BN3 (D) after tensile test.

pullout, but not very long. Careful observation of the surface of pulled-out carbon fibers revealed that many particles were adhered to the carbon fibers, so the surface of pulled-out fibers became very rough. It was thought that the roughness of the interface made the fiber pullout short.

6.4. Discussion

6.4.1. Interface between fiber and matrix

The interface characteristics between fiber and matrix in fiber/ceramic composites are related with the surface structure of fibers, the structure of matrix [5]. The as-received carbon fibers had been shown to have a very strong interface bonding with PCS-derived SiC matrix. In the present investigation, BN powder was distributed in the matrix, in order to tailor the interface between the fiber and matrix. From the above results, it is apparent that BN addition has a significant effect on the mechanical properties of CF/SiC composites only if an appreciable amount of BN powder was incorporated in the matrix. For CF/SiC-BN3 which was prepared from slurry3, the strength and fracture behavior exhibited a significant improvement.

He *et al* pointed out that the debonding energy of the interface should not exceed an upper bound, about one forth of the fiber fracture energy, to allow interface debonding occurring, rather than fiber failures [6]. Interface debonding gives rise to a significant change in the mechanical properties of fiber/ceramics composites. Therefore, with increasing amount of BN addition in the composites, the mechanical properties of CF/SiC-BN showed an abrupt change when the interface debonding occurred.

Fig. 6-17 shows the XRD profiles of BN, HSCF/SiC-BN and HMCF/SiC-BN. Except peaks of BN, C and SiC, no other peaks were detected by X-ray diffraction analyses. Researches on Nicalon SiC fiber reinforced ceramic systems with BN coating also verified there were no reactions between BN and SiC at this temperature [7]. Because BN has a structure like graphite, BN powder is bonded poorly with PCS-derived SiC matrix. Thus, the SiC/BN matrix should be weaker than PCS-derived SiC alone, since the interfaces between BN particles and SiC give rise to many microcracks. With increasing amount of BN in the SiC-BN matrix, SiC-BN will become weaker. When

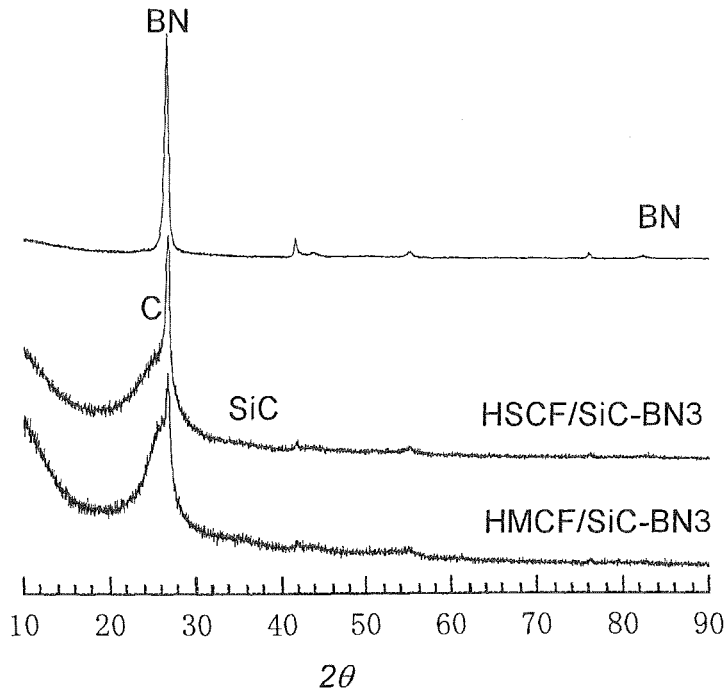

Fig. 6-17 The X-ray diffraction profiles of BN, HSCF/SiC-BN3and HMCF/SiC-BN3

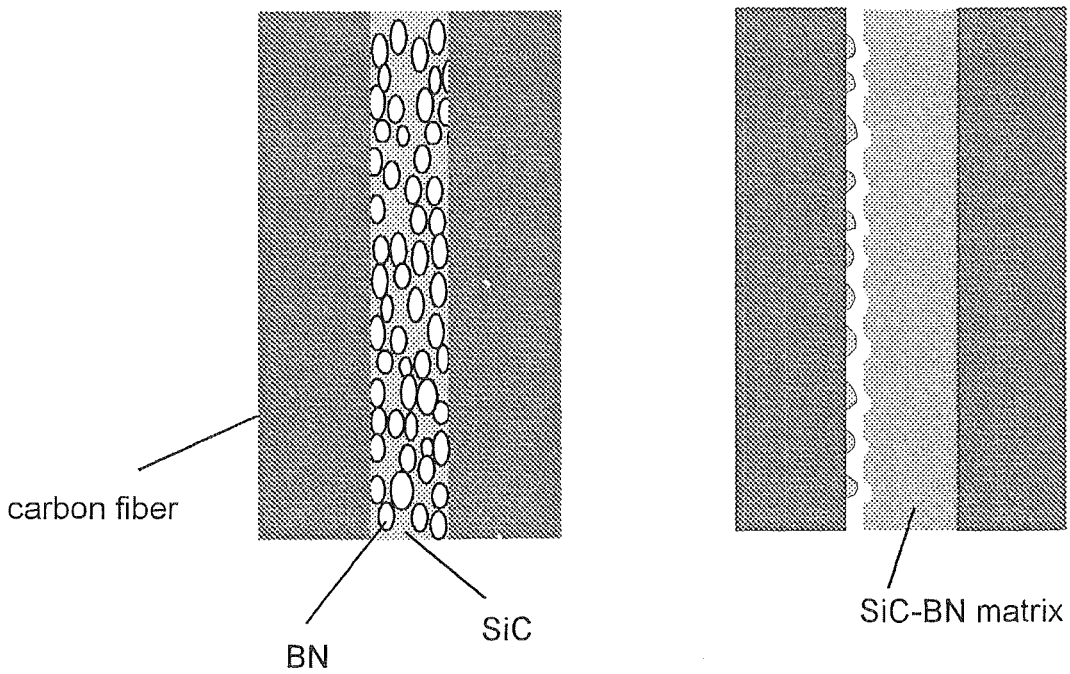

Fig. 6-18 The debonding model of the interface between carbon fiber and SiC-BN matrix. The rough interface caused high interface sliding stress and resulted in short fiber pullout.

matrix cracks propagate in CF/SiC-BN, the matrix near the interface may fail in a shear way, so that the stress concentration at the front of the matrix cracks is released. This process is illustrated in Fig. 6-18. A great amount of BN particles was distributed on the surface of carbon fiber (Fig. 6-18A). Although the bonding between SiC and carbon fiber was strong, the bonding between BN and carbon fiber or SiC was weak, so that debonding between BN and carbon fiber or SiC would take place. With increasing amount of BN amount, the interface between fiber and matrix should become easier to debond. In addition, the presence of BN in the matrix may lead to many microcracks which also contribute to the release of stress concentration of matrix cracks. After debond, the surfaces of pullout fibers in CF/SiC-BN3 were adhered by many matrix particles and thus very rough as illustrated in Fig. 6-18B, so the interface sliding stresses between fiber and matrix were very high. This is thought to be the main reason for the short fiber pullout of the CF/SiC-BN [7].

The weak interlaminar shear strength due to the BN addition seems a problem. If the interlaminar shear strength of the composites is improved, CF/SiC-BN3 should show higher strength. The improvement of interlaminar shear strength may be achieved by the pyrolysis under adequate pressure.

6.4.2. Flexural test and tensile test

In the current study, flexural test and tensile test were used to evaluate the mechanical properties of the composites. Since the stress distribution in the samples during flexural test was very complicated, the results obtained from flexural test were more difficult to elucidate. Tensile test could provide more direct information about the fracture behavior of the composites.

According to the results in 6.3, it was found that the flexural strength values of the composites were about 2 times higher than the tensile strength values. It was considered that the relative low tensile strength was caused by the following reasons:

Some samples were failed at the part which was gripped. Although the gripped parts were protected with aluminum plate, the gripping stress was still strong, the samples had same width and thickness throughout the samples, so that the gripped parts were

easy to be fractured.

The second reason is that the samples for tensile tests were small. When the samples during tensile test deviated from the axis direction, the stress would be decreased, since the transverse and shear strength of the unidirectional composites were very low.

Despite that, the relative tensile strength among these composites still provided the beneficial information about the effect of BN on the mechanical properties of CF/SiC composites and the interface characteristics. The tensile stress-strain curves also gave the fracture behavior of the composites which was not clearly known by flexural stress-strain curves obtained during bending tests.

6.5 Conclusion

BN powder were distributed in PCS-derived SiC matrix through the slurry impregnation technique to tailor the interface between the carbon fiber and the matrix. BN powder exhibited a significant effect on the mechanical properties of the composites when the BN was incorporated by using the slurry with highest concentration of BN, i.e. the slurry consisting of BN, PCS and toluene with the ratio of 20:10:100. The HMCF/SiC-BN3 exhibited an average bending strength of 580 MPa, tensile strength of 300 MPa and strain-to-failure of 0.4-0.5%. And the HSCF/SiC-BN3 possessed an average bending strength of 570 MPa, tensile strength of 260 MPa, and strain-to-failure of about 0.6%. The effect of BN powder was to weaken the strength of the matrix, resulting in the shear failure of matrix in the vicinity of the interface prior to the failure of the carbon fibers. The BN powder in matrix also decrease the interlaminate shear strength. The fiber pullout of both HMCF/SiC-BN3 and HSCF/SiC-BN3 was not long, because the surfaces of carbon fibers which were adhered with matrix particles were very rough.

References

1. A. G. Evans and F. W. Zok, *J. Mater. Sci.* **29** (1994) 3857.
2. M. D. Thouless, O. Sbaizero, L. S. Sigl, and A. G. Evans, *J. Am. Ceram. Soc.*, **72** (1989) 525.
3. G. N. Morscher, *J. Am. Ceram. Soc.*, **80** (1997) 2029.
4. E. Y. Sun, S. R. Nutt and J. J. Brennan, *J. Am. Ceram. Soc.*, **79** (1996) 1521.
5. J.-K. Kim and Y.-W. Mai, in "Materials Science and Technology: vol.13 Structure and Properties of Composites" (VCH, Germany, 1993), p. 239.
6. M. Y. He, and J. W. Hutchinson, Int. J. Solids Struct. 25 (1988) 1.
7. P. D. Jero, and R. J. Kerans, *J. Am. Ceram. Soc.*, **74** (1991) 2793.

Chapter 7 Summary

Carbon fiber reinforced SiC composites (CF/SiC) were originally developed for applications in the fields of space, military, etc. where the cost of the materials was not a problem. Because of their excellent properties at high temperatures, the increasing interest to develop CF/SiC for non-military applications has been noted in last decade. The main problems that have to be solved in the development of CF/SiC are the high cost of the materials, and how to tailor the interface between fiber and matrix. The high cost makes CF/SiC incompetent with other materials. Tailoring interface characteristics is critical to obtain high-performance CF/SiC composites. The researches on CF/SiC were mainly focused on CVI process and fiber surface coating, both of which were high cost in essence. In recent years, the process of polymer impregnation-pyrolysis has been gaining increasing interest. However, many issues on this process, especially the interface, are not understood yet.

In the present research, some basic behaviors of polycarbosilane impregnation-pyrolysis process were investigated. The mechanical behavior of the CF/SiC was controlled through modifying the structure of reinforcing carbon fibers and matrix.

Chapter 1 summarizes the current state of the researches on CF/SiC composites. The advantages and shortcomings of various fabrication methods of CF/SiC were reviewed. Backgrounds and objectives of the present research were introduced.

In Chapter 2, four types of carbon fibers, PAN-based HSCF and pitch-based HMCF which had low graphitization degree, and pitch-based CF50 and CF70 which had a high graphitization degree, were used to prepare carbon fiber reinforced SiC composites by polycarbosilane impregnation-pyrolysis method. The microstructure of the matrix, the infiltration behavior of PCS and the flexural behavior of the composites were investigated. It was found that pyrolytic product of polycarbosilane at 1200°C in N_2 consisted of nearly amorphous β-SiC and some impurity oxygen. It took 9 times for HSCF/SiC and HMCF/SiC, and 12 times for CF50/SiC and CF70/SiC to achieve high density. CF70/SiC exhibited different impregnation behavior of polycarbosilane from HSCF/SiC and HMCF/SiC. During pyrolysis, matrix shrank away from the fiber in

CF70/SiC, and the following impregnation allowed polycarbosilane infiltrate into the space between fiber and matrix. Matrices in HSCF/SiC and HMCF/SiC strongly bonded with the fibers, polycarbosilane infiltrated the space between matrix particles at the following impregnation.

Among the four types unidirectional CF/SiCs, CF50/SiC and CF70/SiC showed non-brittle fracture behavior with multiple matrix cracking and extensive fibre pullout, while HSCF/SiC and HMCF/SiC exhibited brittle fracture behavior, by four-point bending tests. The graphitized carbon fibres (CF50 and CF70) were more adequate to be used as reinforcement of the CF/PCS-derived-SiC than the carbon fibres (HSCF and HMCF) treated below 1500°C. CF70/SiC exhibited high flexural strength of approximately 967 MPa which was about 75% of predicted strength. On the other hand, the flexural strength of CF50/SiC was 624 MPa, which was about 38% of predicted strength, because CF50/SiC failed in a shear way during bending tests.

Although CF70 shows high crystallinity, the skin of CF70 showed relatively poor crystallinity. However, the high crystallinity of CF70 and CF50 still resulted in a weaker interface bonding than HSCF and HMCF.

In Chapter 3, microstructures and mechanical behavior of HSCF/SiC and HMCF/SiC after heat treatment were investigated. Thermal stability of CF/SiC composites is important for their application. With heat-treatment at 1400°C, the crystallite size of the PCS-derived SiC matrix increased from 1.9 nm to 3 nm, although the weight loss was hardly observed. With heat-treatment at 1600°C and 1800°C, the crystallite size of the matrix markedly increased to 12 nm and 19.5 nm, respectively, accompanied by significant weight loss, due to the reactions in the matrix.

Despite the weight loss, HSCF/SiC showed no significant change in the mechanical properties. But HMCF/SiC showed somewhat degradation in the mechanical properties. The formation of SiC whiskers was also observed in HSCF/SiC at 1600°C and 1800°C. It can be said that CF/SiC was stable at 1400°C, but unstable at temperatures above 1600°C.

In Chapter 4, modification of interface between fiber and matrix by heat-treatment of the carbon fibers at the temperatures ranged from 1400°C to 2000°C was performed to

control the mechanical behavior of HSCF/SiC and HMCF/SiC composites. It was found that the tensile strength of pitch-based HMCF increased slightly with increasing heat treatment temperature. The elastic modulus of the carbon fibers increased slightly below 1600°C and significantly above 1600°C, which was consistent with the trend of the crystallinity of the carbon fibers with HTT. The HMCF/SiC composites with carbon fibers heat-treated below 1400°C showed a low strength and brittle fracture behavior. On the other hand, the HMCF/SiC composites with carbon fibers heat-treated above 1500°C possessed 3 times higher strength and non-brittle fracture behavior with extensive fiber pullout. This was attributed to the weakening of the interface bonding by the heat treatment of the carbon fibers. When the HTT of the HMCF was higher than 1500°C, the fiber pullout length of the HMCF/SiC composites decreased and the interface sliding stress between the fibers and the matrix increased with HTT, which was considered to be due to enhanced surface roughness of the carbon fibers with increasing HTT.

The PAN-based HSCF exhibited highest strength when heat-treated at 1400°C, 1500°C and 1600°C, and the strength decreased when the fiber was heat-treated at higher temperatures. The elastic modulus of HSCF increased slightly with HTT, and the tendency was consistent with that of the crystallinity of HSCF with HTT. The HSCF/SiC composites whose carbon fibers were heat-treated below 1400°C showed low strength and completely brittle fracture behavior. With the increase of HTT to 1800℃, the HSCF/SiC composites showed increased ultimate tensile load and long fiber pullout length, because of decreased interface bonding. For the carbon fibers heat-treated at 2000℃, the HSCF/SiC composite showed lower ultimate tensile load and shorter fiber pullout than HSCF16/SiC and HSCF18/SiC. It might be due to the increase of the interface sliding stress caused by the surface roughening of the carbon fibers.

Therefore, the mechanical properties of the composites could be controlled by heat treatment of the reinforcing carbon fibers. HMCF/SiC exhibited longer fiber pullout, thus had a higher toughness than HSCF/SiC.

In Chapter 5, modification of the interface between fiber and matrix by boron addition and oxidation resistance of CF/SiC-B composites were investigated. Although

boron addition to HSCF/SiC slightly increased the flexural strength, it did not have an obvious effect on the brittle fracture mode of HSCF/SiC. Boron addition to HMCF/SiC increased the flexural strength of HMCF/SiC by 2.5 times, and changed the brittle fracture mode to non-brittle mode. Boron addition to CF70/SiC decreased slightly the flexural strength of CF70/SiC without changing non-brittle fracture mode.

The main effect of boron addition was to decrease the interfacial bonding strength. It was believed that the B/SiC interlayer played a main role in weakening interface bonding. The formation of BN from the reaction of B and N_2 was thought to cause the weakening of interface bonding.

Boron addition to the carbon fiber/polycarbosilane-derived-SiC composites improved their oxidation resistance, especially for the carbon fibers with small diameter, because the formation of boron oxide sealed the pores in the composites. The additional B/SiC coating on the samples helped cover the cross sections of the carbon fibers in CF/SiC composites, thus resulted in much better oxidation-resistance.

In Chapter 6, modification of the interface between fiber and matrix by BN addition was investigated. BN powder was distributed in PCS-derived SiC matrix through the slurry impregnation technique to tailor the interface between the carbon fiber and the matrix. BN powder exhibited a significant effect on the mechanical properties of the composites when the BN was incorporated by using the slurry with highest concentration of BN, i.e. the slurry consisting of BN, PCS and toluene with the ratio of 20:10:100. The HMCF/SiC-BN3 exhibited an average bending strength of 580 MPa, tensile strength of 300 MPa and strain-to-failure of 0.4-0.5%. And the HSCF/SiC-BN3 possessed an average bending strength of 570 MPa, tensile strength of 260 MPa, and strain-to-failure of about 0.6%. The effect of BN powder was to weaken the strength of the matrix, resulting in the shear failure of matrix in the vicinity of the interface prior to the failure of the carbon fibers. The BN powder in matrix also decrease the interlaminate shear strength. The fiber pullout of both HMCF/SiC-BN3 and HSCF/SiC-BN3 was not long, because the surfaces of carbon fibers that were adhered with matrix particles were very rough.

In summary, polycarbosilane impregnation-pyrolysis method can be used to fabricate

simply CF/SiC composites with high properties. The mechanical properties of CF/SiC can be changed markedly by using different types of carbon fibers, or carbon fibers with different heat-treatment conditions. It suggests that optimal properties of CF/SiC can be achieved by controlling the structure of carbon fibers. The mechanical properties of CF/SiC can also be changed significantly by boron or BN addition in matrix. Moreover, the addition was helpful to improve the oxidation resistance of CF/SiC composites.

Acknowledgement

This thesis research was accomplished at the Advanced Materials Laboratory in the Faculty of Engineering, Nagasaki University under the supervision of Professor Kazuo Kobayashi and Professor Makoto Egashira.

I wish to express my profound thanks to Professor Kazuo Kobayashi, my supervisor. He offered me an opportunity to carry out researches in this laboratory. He always encouraged me when I had a new idea, even a minor idea, and guided me to right direction when I had problems with my researches. He revised meticulously the manuscript and allowed no ambiguous expressions. I benefited from his training me to be an independent researcher.

I also wish to express my gratitude to Professor Makoto Egashira who is my supervior in the last year for his invaluable suggestions to this research.

I wish to express my sincere regards and appreciation to Professor S. Kagawa, Professor M. Hasaka and Professor M. Furukawa for their constructive criticisms and advice to this thesis.

I wish to express my thanks to Associate Professor Uchiyama for his numerous suggestions and criticisms to this research. Many of his good suggestions had been taken into this thesis.

I wish to express thanks to Dr. Sano for his kind help and cooperation in laboratory. I benefited a lot from numerous discussions with Dr. Sano. He helped me to accustom the laboratory quickly when I came to Japan.

I wish to express my gratitude to Associate Professor Kunio Suzuki for helping me all the TEM observation in this research and many suggestions to this research.

I wish to express my thanks to Professor Hui-Ming Cheng of Institute of Metal Research, Chinese Academy of Sciences, for many helpful suggestions.

I wish to acknowledge Japan government for financial support from Oct. 1994 to March 1999.

I wish to express thanks to the friends and students in the laboratory for their kind help and cooperation.